Aalto University
School of Engineering

AALTO UNIVERSITY
School of Engineering
Department of Engineering Design and Production

Jere Lehtinen

Nonlinear Lateral Dynamic Behavior of a High Capacity Transport Vehicle

Master's Thesis

Thesis submitted in partial fulfillment of the requirements for the degree of Master of Science in Technology

Espoo 26.11.2015

Thesis supervisor: Professor Matti Pietola
Thesis advisor: Ari Tuononen, D.Sc. (Tech.)

Aalto University
School of Engineering

Aalto University, P.O. BOX 11000, 00076
AALTO
www.aalto.fi

Abstract of master's thesis

Author Jere Lehtinen

Title of thesis Nonlinear Lateral Dynamic Behavior of a High Capacity Transport Vehicle

Degree programme Mechanical Engineering

Major Machine Design **Code** K3001

Thesis supervisor Prof. Matti Pietola

Thesis advisor Ari Tuononen, D.Sc. (Tech.)

Date 26.11.2015 **Number of pages** 94+2 **Language** English

Abstract

In order to improve the productivity of freight transport the high capacity transport (HCT) vehicle combinations have been introduced in the traffic circulation. These vehicle combinations are longer in longitudinal dimension and/or greater in mass than the national traffic legislation allows. This kind of vehicle combination is not considered as a special transport, but it requires derogations of law restrictions. An HCT vehicle combination is restricted to drive in good weather conditions and on predefined routes. The lateral dynamic behavior of HCT vehicle combinations have not been examined on low road friction surfaces.

The purpose of this thesis is to examine the nonlinear lateral dynamic behavior of a Double-A HCT vehicle combination on low road friction surface. The vehicle combination consists of four different vehicle units, three articulations, multiple axles and multiple wheels. The vehicle units are tractor, semi-trailer, dolly and semi-trailer units. An analytical simulation model is designed based on the single-track model. The single-track model is extended to a multi-wheel model, which includes nonlinear tire characteristics and wheel load transfers. The nonlinear tire model being used is the Magic Formula tire model. Relevant theory and parameters are gathered from literature and industry.

The analytical simulation model simulates two different open-loop simulation types at a forward velocity of 80km/h on low road friction surface. A double lane change maneuver based on the ISO 3888 standard and a phase plane simulation method are introduced. The phase plane simulation method is a phase portrait analysis of a specific vehicle unit of the vehicle combination. This kind of phase plane analysis is new for a heavy vehicle combination. This study provides novel results regarding the lateral stability of heavy vehicle combinations on low road friction situations. A sensitivity analysis regarding the lateral stability of the vehicle combination is performed with the two different simulation types. The sensitivity parameters are the length of the dolly unit drawbar and the semi-trailer single or twin wheel parameter. Additionally, a comparison of the lateral stability of the vehicle combination between high and low road friction surfaces is performed.

The study indicates that the examined vehicle combination is relatively unstable with high vehicle forward velocities on low road friction surfaces with any kind of sensitivity analysis settings in a double lane change maneuver and with specific state deviations in the phase plane analysis. The phase plane analysis along with the double lane change maneuver, however, indicate that twin wheels on semi-trailer rear axles and longer dolly drawbar promote stable behavior and increase the lateral stability of the vehicle combination significantly on low road friction surface.

Keywords hct, heavy vehicle, lateral dynamics, nonlinear, phase plane, low friction

Aalto-yliopisto
Insinööritieteiden korkeakoulu

Aalto-yliopisto, PL 11000, 00076 AALTO
www.aalto.fi
Diplomityön tiivistelmä

Tekijä Jere Lehtinen

Työn nimi Ylisuuren raskaan kaluston ajoneuvoyhdistelmän epälineaarinen sivuttaisdynamiikka

Koulutusohjelma Konetekniikka

Pääaine Koneensuunnittelu **Koodi** K3001

Työn valvoja Prof. Matti Pietola

Työn ohjaaja TkT Ari Tuononen

Päivämäärä 26.11.2015 **Sivumäärä** 94+2 **Kieli** Englanti

Tiivistelmä

Tavarankuljetuksen tuottavuuden parantamiseksi on aloitettu ylisuurten raskaan kaluston (HCT) ajoneuvoyhdistelmien kokeilut tieliikenteessä. Tällainen ajoneuvoyhdistelmä on pidempi ja/tai painavampi, kuin kansallinen tieliikennelainsäädäntö sallii. Tätä ajoneuvoyhdistelmää ei luokitella erikoiskuljetukseksi, mutta se tarvitsee poikkeusluvan. HCT ajoneuvoyhdistelmä saa liikennöidä hyvissä keliolosuhteissa ja vain poikkeusluvassa määrätyillä reiteillä. Tällaisen ajoneuvoyhdistelmän sivuttaista liikedynamiikkaa ei ole tutkittu liukkaissa olosuhteissa.

Tämän diplomityön tarkoituksena on tutkia Double-A HCT ajoneuvoyhdistelmän epälineaarista sivuttaisdynamiikkaa liukkaissa olosuhteissa. Ajoneuvoyhdistelmä koostuu neljästä ajoneuvoyksiköstä, jotka ovat vetoauto, puoliperävaunu, etuteli ja puoliperävaunu. Ajoneuvot ovat nivelletty toisiinsa kolmella nivelellä ja ajoneuvoyksiköt sisältävät useita akseleita ja pyöriä. Analyyttinen simulaatiomalli suunniteltiin perustuen kaksipyörämalliin. Kaksipyörämalli laajennettiin monipyörä malliin, joka sisältää epälineaariset rengasominaisuudet ja sivuttaiset painonsiirrot. Epälineaariset rengasominaisuudet perustuvat Magic Formula rengasmalliin. Olennainen teoria ja malliparametrit ovat kerätty kirjallisuudesta ja teollisuudesta.

Analyyttinen simulaatio malli simuloi kahta avoimen silmukan simulaatiota ajonopeudella 80km/h liukkaalla tien pinnalla. Ensimmäinen simulaatio on kaksoiskaistanvaihto perustuen ISO 3888 standardiin. Toisessa simulaatiotyypissä suoritetaan vaihetason analyysi tietylle ajoneuvoyhdistelmän ajoneuvoyksikölle. Tällaista vaihetaso analyysiä ei ole aikaisemmin tehty raskaille ajoneuvoyhdistelmille rakenteen ja dynamiikan monimutkaisuuden vuoksi. Tämä tutkimustyö sisältää uusia tuloksia liittyen raskaiden ajoneuvoyhdistelmien sivuttaisdynamiikan analysointiin liukkaissa olosuhteissa. Ajoneuvoyhdistelmän sivuttaisdynaamista herkkyyttä analysoidaan näillä kahdella simulaatiotyypillä. Herkkyysanalyysin parametrit ovat etutelin aisan pituus ja puoliperävaunujen rengastus asetus. Lisäksi vertaillaan liukkaan ja kuivan olosuhteen välistä vaikutusta sivuttaisdynamiikkaan.

Tämä diplomityö osoittaa, että tutkittu ajoneuvoyhdistelmä on suhteellisen epästabiili korkeilla ajonopeuksilla liukkaissa olosuhteissa kaikilla herkkyysanalyysin asetuksilla kaksoiskaistanvaihdossa ja vaihetason analyysissä tietyillä poikkeutuksilla. Vaihetason analyysi ja kaksoiskaistanvaihto osoittavat kuitenkin, että puoliperävaunujen paripyörät ja etutelin pitkä aisa kiinnitettynä lähelle edessä olevan ajoneuvoyksikön taka-akseleita edistävät sivuttaisdynaamista stabiilisuutta huomattavasti myös liukkaissa olosuhteissa.

Avainsanat hct, raskas ajoneuvo, sivuttaisdynamiikka, epälineaarinen, matala kitka

Acknowledgements

This master's thesis was done in the Aalto University School of Engineering in Finland. I would like to thank my thesis advisor D.Sc. Ari Tuononen for giving me the opportunity and framework for this thesis subject and valuable guidance.

My warmest thanks go to Pekka Rahkola for valuable guidance and knowledge sharing to the matter and previous work on the subject. Thanks are extended to Otto Lahti and Tuomo Vallas for creating the opportunity to see the vehicle combination under examination and for giving the necessary vehicle specifications. I also want to thank my thesis supervisor Professor Matti Pietola for important comments in finishing this thesis.

Special thanks go to the Traffic Safety Committee of Insurance Companies (TSCIC) and Laboratory of Automotive Engineering in Aalto University for providing the thesis scholarship. I want to thank my coworkers for worthwhile peer support. Finally, a shout out to #hapannaamat!

My sincerest appreciation goes to my family and especially to my beloved Nigina Khodjaeva for supporting and encouraging me throughout the studies.

Espoo 26.11.2015

Jere Lehtinen

Table of Contents

Table of Symbols

α	Tire slip angle
β	Vehicle slip angle
γ	MF camber coefficient
δ	Steering angle
ε	Angle between longitudinal and resultant velocities
θ	Pitch
κ	Longitudinal slip
λ	Eigenvalue
λ	MF scaling factor
μ	Friction coefficient
σ	Second articulation angle
$\dot{\sigma}$	Time derivative of second articulation angle
φ	First articulation angle
$\dot{\varphi}$	Time derivative of first articulation angle
φ	Roll
ψ	Third articulation angle
$\dot{\psi}$	Time derivative of third articulation angle
ψ	Yaw
ω	Angular velocity
A	System matrix or Dynamic matrix
a_x	Longitudinal acceleration
a_y	Lateral acceleration
a_i	Distance between CoG and front articulation point
a	Real part of eigenvalues
B	Input matrix
B_y	MF stiffness factor
b	Imaginary part of eigenvalues
b_i	Distance between the CoG and rear articulation point
C_α	Cornering stiffness
C	Coefficient matrix
C_y	MF shape factor
C_u	Unit matrix
D	Impact matrix
D_y	MF peak value
d	Index of dynamic wheel load term
df_z	MF relative change of vertical load
E_y	MF graph curvature and horizontal location factor
F_x	Longitudinal force
F_y	Lateral force
F_z	Vertical force
F	Front wheel index

g	Gravitational constant
h	Height of the CoG
I	Moment of inertia
i	Vehicle unit index
j	Axle index
j	Complex number
k	Tire index
K	Steering matrix
K	Steering gradient
$K_{y\alpha}$	MF slope factor
l	Vehicle length
l	Left axle side index
l_{ij}	Distance between the CoG and a wheel
M	Mass matrix
M_x	Overturning couple
M_y	Rolling resistance
M_z	Aligning moment
m	Vehicle mass
N_k	Vertical load
p_{Cy1}	MF shape factor C_y for lateral forces
p_{Dy1}	MF lateral friction coefficient μ
p_{Dy2}	MF variation of friction coefficient μ with load
p_{Dy3}	MF variation of friction coefficient μ with squared camber
p_{Ey1}	MF lateral curvature E_y at F_{z0}
p_{Ey2}	MF variation of curvature E_y with load
p_{Ey3}	MF zero order camber dependency of curvature E_y
p_{Ey4}	MF variation of curvature E_y with camber
p_{Ey5}	MF camber curvature E_y
p_{Hy1}	MF horizontal shift S_{Hy} at F_{z0}
p_{Hy2}	MF variation of shift S_{Hy} with load
p_{Hy3}	MF variation of shift S_{Hy} with camber
p_{Ky1}	MF maximum value of stiffness $K_{y\alpha}/F_{z0}$
p_{Ky2}	MF load at which $K_{y\alpha}$ reaches maximum value
p_{Ky3}	MF variation of $K_{y\alpha}/F_{z0}$ with camber
p_{Ky4}	MF peak stiffness variation with camber squared
p_{Ky5}	MF lateral stiffness dependency with camber
p_{Ky6}	MF camber stiffness factor
p_{Vy1}	MF vertical shift in S_{Vy}/F_z at F_{z0}
p_{Vy2}	MF variation of shift S_{Vy}/F_z with load
p_{Vy3}	MF variation of shift S_{Vy}/F_z with camber
p_{Vy4}	MF variation of shift S_{Vy}/F_z with camber and load
R	Rear wheel index

R	Cornering radius
r	Right axle side index
r_i	Yaw velocity
$\dot{r}_i$	Yaw acceleration
S_{Hy}	MF horizontal shift
S_{Vy}	MF vertical shift
s	Index of static wheel load term
t_{ij}	Axle width
t	Time
u	Longitudinal velocity
v_i	Lateral velocity
$\dot{v}_i$	Time derivative of lateral velocity
w	Vertical velocity
$\bar{x}$	State vector
$\dot{\bar{x}}$	Time derivative of state vector
$\dot{x}$	Differential system of equations
x_i	MF general input variable
x_m	MF distance factor
y_a	MF distance factor
$\bar{y}$	MF starting parameter vector

Abbreviations

ABS	Anti-lock Braking System
CoG	Center of Gravity
DoF	Degree(s) of Freedom
Ecocombi's	Eco combinations
EU	European Union
HCT	High Capacity Transport
HVC	Heavy Vehicle Combination
MF	Magic Formula
MTAHV	Multi-Trailer Articulated Heavy Vehicle
PBS	Performance Based Standard
RA	Rearward Amplification
TSCIS	Traffic Safety Committee of Insurance Companies
VTI	Swedish National Road and Transport Research Institute

1 Introduction

The road safety and handling behavior of heavy vehicle combinations (HVC) in extreme situations are continuously topical. The increase in weight and size even over the current legislations has created the need for further research of HVC dynamics. The increasing of dimensions has also drawn the media's attention, which has resulted in negative reputation for the heavy vehicle fleet (Torkkeli & Lindström 2015). An HVC is a vehicle, which has one or more articulations between different axles or axle groups. A traditional HVC is usually a combination of truck and full trailer, tractor and semitrailer or truck-center axle trailer (Luijten 2010). Eco combinations (Ecocombi's) are larger than the traditional combinations and high capacity transport vehicles (HCT) are oversized HVCs. They consist of a truck or a tractor and one or more different trailer type (Karlsson et al. 2015; Luijten 2010).

Handling characteristics and stability of an HVC may become problematic, because of the load, vehicle dimensions, driver behavior and road and weather conditions (Rahkola 2006). These problems are especially present in HCT vehicles and on low road friction situations. The loss of stability and handling is one of the most common reasons for HVC accidents. These accidents generally cause significant personnel and economical damage by nature.

The heavy vehicle combination size and weight legislations are generally nationwide, but for example European Union (EU) sets restrictions for the member states. Despite of restrictions, EU has provided circumstances where derogations to the maximum dimensions can be granted (European Commision 2012). Member states Finland and Sweden have oversized HVCs in circulation and several member states are considering their introduction (Christidis & Leduc 2009). The abbreviation HCT is an internationally established term for an HVC, which is longer in longitudinal dimension and/or greater in mass than the national legislation allows and it is not categorized as a special transport (Trafi 2015).

1.1 Background

Heavy vehicle combinations have been studied widely past decades. The studies focus mainly on vehicle and driving dynamics, performance and productivity. Research has been done especially in Northern and Middle Europe, North America and Australia. The vehicle dynamics research focuses mainly on lateral dynamics, whereas longitudinal and vertical dynamics have been studied less. The research on driving dynamics and performance of HVCs studies the influence of driver input to safety, vehicle handling and vehicle performance. The HVC productivity studies address the advantages of heavy vehicle fleet as a transport method. In addition some HVC tire research has been conducted.

The lateral dynamics research addresses the problems related to the handling characteristics and overall stability of the vehicle. The stability and handling has been studied by creating analytical models, which include linear or nonlinear characteristics. The analytical model simulations can usually be compared to real life test drives. In Netherlands M.F.J. Luijten has developed linear lateral dynamic computer models for

articulated commercial vehicles (Luijten 2010). Luijten's research focuses on the rearward amplification and directional stability of HVCs. P. Rahkola in Finland developed a semi-linear and linear analytical models to study the vehicle dynamics of a multi-trailer HVC (Rahkola 2006). His thesis work compares the analytical model results to real life tests with the same HVC in a double lane change maneuver. M. Lehessaari studied the development stability of HVCs with ADAMS/Car simulation program based on the modular concepts by tires (Lehessaari 2007). His thesis focuses on the possibility of improving the stability of HVCs with different tire configurations. A different tire configuration in the thesis means using different kind of tires, new and worn on separate axles. His study concluded that using new tires on the rear axles of every vehicle unit in an HVC decreases the trailer swinging and improves lateral stability.

Oulu and Aalto Universities of Finland have studied the stability, safety and braking performance and the passing situations of HCT combinations. Specifically, in Oulu University, the stability of an HCT vehicle has been studied in an ISO-standard double lane change. The biggest concerns are the stability of HCT combinations in low road friction surfaces and the capability of fitting in size and weight in the existing infrastructure, including older bridges. However, the circulation of HVCs in Finland has showed that the HCT combinations improve both fuel and monetary economics as well as the productivity of transportation. In addition, Volvo Sweden has studied the lateral dynamics of a Double-B HCT combination with a MATLAB simulation model. The Double-B combination has truck, semi-trailer, dolly and link-trailer vehicle units. The B-double was simulated in a double lane change maneuver and the rearward amplifications of lateral accelerations and yaw velocities were examined. (Raatikainen 2015; Venäläinen & Korpilahti 2015)

J. Aurell in Sweden has studied the handling characteristics of HVCs from the 80's (Aurell & Edlund 1989). Aurell's research focuses on the lateral dynamic behavior of HVCs with multiple steering axles. University of Michigan Transportation Research institute developed an electronic braking system for an HCT vehicle to control the lateral motions (Fancher et al. 1998). The electronic braking system was based on Fancher's previous work. Paul Fancher started the research on directional dynamics of multi axle heavy vehicles in the 80's (Fancher 1989). The electronic braking system model was a nonlinear analytical simulation model for a vehicle with three articulations. The model indicates that a dynamic braking system suppresses rearward amplification and improves lateral stability. (Fancher et al. 1998).

The heavy vehicle roll dynamics and roll-over has been studied in Cambridge and Glasgow universities in United Kingdom. In the University of Glasgow, R. Kamnik et al. developed a nonlinear lateral load transfer estimator employing sensors in order to predict heavy vehicle roll-over. It is based on the lateral dynamics of the vehicle combination. In Cambridge University, D. J. M. Sampson et al. developed a yaw-roll behavior simulation model, which analyzed the controllability and limitations of load transfers, roll and yaw motions with active roll control systems. The study indicates that an active roll control system improves the roll stability of a heavy vehicle by 30 to 40 percent. This leads into a significant increase in handling performance. (Kamnik et al. 2003a; Sampson & Cebon 2005)

In the Swedish National Road and Transport Research Institute (VTI), Karlsson et al. proposed performance based regulations for HVC and especially HCT vehicles and their access to the road network (Karlsson et al. 2015). The study analyses the existing

regulations, literature and performance based standard (PBS) approaches. The PBSs addresses all the three domains of safety, infrastructure and environment, but the focus is mainly on the safety. The VTI also conducted a study in the advanced moving-base driving simulator (Sandin & Nilsson 2013). The driver's maneuverability skill was assessed driving a similar A-Double HCT vehicle with and without full automation. The simulation results showed that the driver has a great influence on the vehicle safety and performance. In addition, the drivers' experience was crucial for the safety.

The VTI has done research for about 40 years on heavy vehicle dynamics related to braking, steering and tires. O. Nordström concluded 20 years of work on dynamic stability of heavy vehicles with ABS in different vehicle handling situations (Nordström 1989). The research addressed specifically winter conditions and low road friction surfaces. Nordström concluded that ABS improves maneuverability, handling and both the active and passive safety of an HVC. In Germany Mercedes-Benz AG has studied the impact of different ABS-philosophies in HVCs. The research indicates that different kind of ABS control systems have different impacts on the directional behavior of HVCs (Göhring et al. 1989). The general conclusion is that all types of ABSs promote active and passive safety of an HVC.

Kati et al in Chalmers University of Technology, Sweden studied the influence of a smart dolly vehicle unit to HCT performance (Kati et al. 2013). The dolly vehicle unit is equipped with integrated propulsion, steering and braking systems (Kati et al. 2013). The results showed the increase of performance in startability, gradeability, rearward amplification and yaw damping. M. Islam designed a parallel optimization of multi-trailer articulated heavy vehicle with active safety systems in Canada (Islam 2013). According to M. Islam (2013), "the research indicates that the PDO method is effective for identifying desired design variables and predicting performance envelopes in the early design stages of MTAHV with active safety systems".

The high capacity transport productivity and commercial benefits has been studied widely in Australia. A. Bucko et al. studied the AB-triple HCT vehicles (Bucko et al. 2013). In the study the powertrain and freight types were the main concern related to the stability and maneuverability. The study indicated that the productivity and economy is increased in certain road networks without decreasing safety. In addition Welsh et al. compared the safety benefits of HCT vehicles and conventional HVCs (Welsh et al. 2013). The study was performed comparing insurance companies' empirical data about road accidents that involved different HCT and HVC vehicles. The study also included public administration and industry data about accidents and road operations. The study indicates that the number of serious and major accidents of HCT vehicles in Australia is much less than of the conventional HVCs (Welsh et al. 2013).

1.2 Thesis objectives & structure

In this thesis an analytical simulation model in MATLAB environment is designed for an HCT vehicle. The vehicle combination consists of tractor, semi-trailer, dolly and semi-trailer vehicle units and it is known as the A-Double combination. The analytical model includes nonlinear tire characteristics, which are essential on low road friction surface. The simulation model is based on the lateral dynamics of the vehicle combination. The required vehicle and model parameters are gathered from literature and industry. The

model simulates different directional responses (driving inputs) over time on low road friction surface. The two chosen simulation types for this thesis are a double lane change maneuver and a phase plane analysis method. According to my best knowledge, the phase plane method for any kind of HVC has never been done before, so this thesis provides novel results. The simulations measure the directional stability, handling characteristics and maneuverability of the vehicle combination by examining the lateral accelerations, yaw velocities, slip angles and their rearward amplifications. A sensitivity analysis for the vehicle combination is performed with two different parameters in the two chosen simulation types. The chosen sensitivity analysis parameters are the twin or single wheel settings on semi-trailer rear axles and the drawbar length of the dolly vehicle unit. In addition, a comparison between high and low road friction surfaces for the vehicle combination is performed. The problematic situations on low road friction surface can be determined from the analysis. The state of the vehicle combination in the problematic situations is analyzed more in depth and indicators for the stability are searched. Parameters are searched for the distance of instability in the double lane change maneuver. The phase plane method determines the stability and recovering capability of the vehicle from the problematic situations in the phase portrait of slip angle and yaw velocity. Some of the simulations imitate situations, where the vehicle combination is mathematically stable, but the movements are broad and therefore not acceptable by a real vehicle. This kind of situation can develop, when a semi-trailer starts oscillating between the roadsides. The sensitivity analysis provides implications and conclusions regarding how to improve the lateral stability of the vehicle combination.

Based on the literature review and existing studies, this research is essential in order to examine the lateral dynamic behavior of HCT vehicles on low road friction situations. The lateral dynamic behavior of HCT vehicles has not been studied in slippery circumstances, as in low road friction surfaces. Additionally, the new lateral dynamic examination method of phase plane analysis for HVCs is introduced, which provides novel results. If more EU member states and other states around the world want to implement HCT vehicles permanently or temporary in their vehicle fleet, this research is essential. The results of this research are important, because HCT vehicles are already driven around the world in slippery circumstances with derogations of law restrictions and their lateral dynamic behavior in slippery conditions has not been studied yet. This research provides novel results academically and is useful for nations, which have winter conditions.

The structure of this thesis is as follows. The second chapter addresses the general vehicle and tire dynamics, which are essential when studying vehicle behavior. The general vehicle dynamics definitions are first presented. Based on the general vehicle dynamics, a single-track vehicle model is presented for a single vehicle unit. The second subject addresses the general tire dynamics, tire models and linear and nonlinear tire characteristics. After the tire dynamics, the single-track model is extended with linear and nonlinear tire characteristics. In the later subheadings, the single-track vehicle model is extended to a dynamic model of an articulated vehicle. Based on the extensive vehicle dynamics theory, the dynamics and simulation model of the Double-A combination with linear and nonlinear characteristics is derived in the third chapter. The sensitivity analysis parameters and the simulation types are addressed in depth in the fourth chapter. The fifth chapter presents the simulation and sensitivity analysis results with very comprehensive discussion and error analysis. The last chapter concludes the results and discussion in appropriate findings and suggestions.

2 Vehicle dynamics

Vehicle dynamics are divided into longitudinal, lateral and vertical dynamics. Longitudinal dynamics are linked to the concept of vehicle performance, such as aerodynamics, gradeability, engine power and acceleration. Lateral dynamics are linked to the concept of vehicle handling, stability and maneuverability. The vertical dynamics are usually linked to the vehicle comfort, but they also affect the longitudinal and lateral dynamics via vehicle suspension and wheel load transfer. (Tuononen & Koisaari 2014)

This thesis focuses on the lateral dynamics and the lateral dynamic behavior of the vehicle combination, which include vehicle handling, maneuverability and safety of the vehicle combination.

The vehicle handling addresses the response of the vehicle to different motions of the steering wheel and the response of the vehicle to different impulses caused by the external driving conditions. The vehicle handling is divided into two main categories, directional behavior and directional stability. The directional behavior addresses the maneuverability of the vehicle on a desired path. The directional stability addresses the directional stability of the vehicle against external interferences. (Wong 2001)

On the other hand, the vehicle handling can be perceived as the vehicle characteristics that indicate the position and state of the vehicle to the driver. When only the characteristics of the vehicle are examined, the open-loop examination is at issue. Vehicle characteristics can be considered to assist the driver to handle and control the vehicle. In that case, the target of the examination is a closed-loop of driver-vehicle-combination behavior. In practice this means that the driver detects the position and state of the vehicle and fixes it towards a desired state. (Gillespie 1992)

The global vehicle coordinate system is a standard three dimensional right-handed Cartesian coordinate system. Positive X-axle points to the driving direction, positive Y-axle points to right in perpendicular to X-axle and positive Z-axle points downwards and is parallel to the direction of gravity. The corresponding vehicle velocities are u, v and w, but in substitution subscripted velocity symbols v_x, v_y and v_z are also being used. Angular movement around X-axle is called roll φ, around Y-axle pitch θ and around Z-axle yaw ψ. The positive angular movement directions follow the right hand notation. These three velocities and angles are the degrees of freedom of a rigid body vehicle, which is presented in figure 1. (Wong 2001)

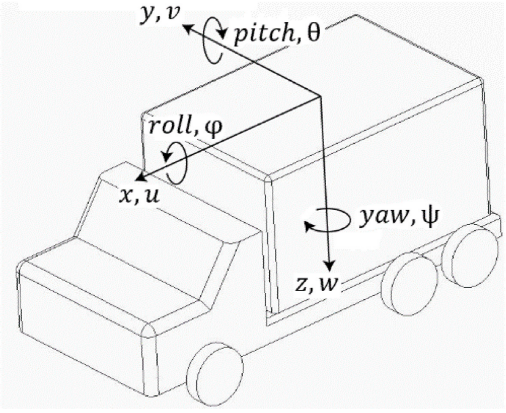

Figure 1. Vehicle coordinate system

The vehicle handling can be examined with two different types of inputs. In steady state response the input stays constant over time. In steady state examination, the vehicle is driving with a constant velocity either a straight path or a steady-state cornering. The examination occurs with different velocities and cornering radiuses. In transient state response, the input is varying over time. In the transient response examination, the behavior of the vehicle before it reaches the steady state is at issue. In this examination the distance from stability and the recovery time required after the transient response to get back to stable state are in question. The transient response examination is also called the dynamic state examination. (Dukkipati et al. 2008)

The vehicle stability means the capability of the vehicle to attain stable state during or after an input. The vehicle stability can be divided according to the vehicle coordination system to yaw, roll and pitch stability. However, in the examination of lateral dynamic behavior the yaw and roll stability are specifically at issue. The yaw and roll stability are dependent on the lateral acceleration. The yaw motion produces lateral acceleration which furthermore, causes roll motion. The loss of lateral stability can occur, if the tires of the vehicle can't produce enough lateral force to steer the vehicle to desired path. In an understeering cornering situation the front tires of the vehicle produce too little or the rear tires too much lateral force as the lateral acceleration increases. This phenomenon requires that the steering angle is increased as the lateral acceleration increases in order to stay on the same cornering radius. In an oversteering cornering situation the front tires of the vehicle produce too much or the rear tires too little lateral force as the lateral acceleration increases. This phenomenon requires that the steering angle is decreased as the lateral acceleration increases in order to stay on the same cornering radius. The possible prolonged over- and understeering situations may develop into a vehicle spin. However, if the tires can produce enough lateral force, but the lateral acceleration exceeds its stable maximum, the vehicle tends to roll-over its side instead of spinning over the Z-axis as a result of excessive yaw movement. The locking of either front or rear tires in braking situations can also lead to these unstable conditions. The loss of stability usually occurs in high vehicle speeds. The loss of roll stability occurs more often in normal road conditions, whereas the loss of yaw stability is more essential in worse road conditions, such as on low road friction surfaces. (Aurell & Edlund 1989; Fancher 1985; Tuononen & Koisaari 2014)

In addition, the vehicle stability is divided into static and dynamic stability. A system is statically stable, if the vehicle is deviated from the position of equilibrium and it tries to return towards the same position of equilibrium over time. A system is also dynamically stable if the vehicle which is deviated from the equilibrium state reaches and restores the same previous position of equilibrium at least asymptotically. This restoring motion is usually through a damped oscillation. The system is dynamically unstable if it doesn't reach the previous position of equilibrium, this is usually because a divergent oscillation occurs. It is also defined that the dynamic stability is neutral when an undamped oscillation occurs. (Genta 1997)

2.1 Single-track model

The single-track model represents a two degree of freedom (2-DoF) model for a road vehicle unit. The single-track model is also known as the bicycle model. The term bicycle

comes from the fact that the vehicle is modelled with two wheels, one front wheel and one rear wheel. The bicycle model combines the lateral dynamic properties of one axle and its wheels to form one effective wheel (Bosch 2011). The single-track model can be extended to four-wheel model, if necessary.

The single-track model is the most commonly used model for the study of lateral dynamic behavior of a vehicle. H. Pacejka has been studying vehicle dynamics and bicycle model (Pacejka 2006) for decades. The single-track model represents the essential lateral dynamic phenomena accurately with linear or nonlinear characteristics. It is most commonly used for steady state examination, however it can also be used for dynamic driving situations (Tuononen & Koisaari 2014).

The single-track model has several general limitations and assumptions:

- The road surface is flat and level
- The tires on the same axle have the same slip angle
- Pitch effects are not included
- Resisting forces are considered small
- The effect of longitudinal force on lateral force and aligning torque is ignored
- The vehicle structure is rigid, including the suspension system
- The steering system is rigid or either ignored
- Steering and slip angles are small
- Vehicle driving speed is constant
- The vehicle position is fixed (Bosch 2011; Dukkipati et al. 2008; Milliken & Milliken 1995).

The single-track model has many more limitations and assumptions related to the vehicle geometrics and linear or nonlinear tire characteristics. These limitations and assumptions are presented in the bicycle model formula derivations and under the linear and nonlinear tire characteristics subheadings.

The bicycle model is traditionally observed with regular mechanics (Genta 1997; Gillespie 1992). However, it is also possible to derive the formula with the principle of virtual work (Luijten 2010; Pacejka 2006). This thesis focuses on the regular mechanics and Newton's laws of motion, because they are more intuitive to understand.

The free body diagram of a passenger car in single-track model is presented in figure 2.

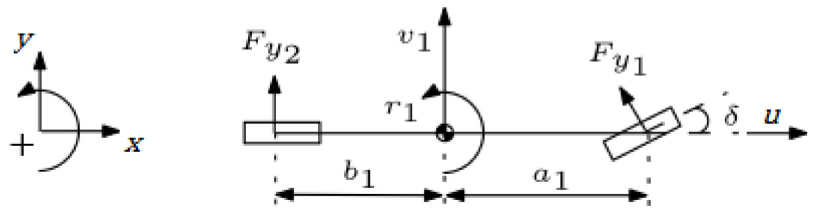

Figure 2. Free body diagram of a passenger car in single-track model (Luijten 2010)

The passenger car is in a fixed position of a cornering situation. It can be assumed that the wheelbase is short compared to the turn radius. Consequently, it can be assumed that the lateral forces F_{y1} and F_{y2} are parallel and point to the direction of positive Y-axle. Due to the assumptions, the front axle can be considered as a one system, which has a

resultant lateral force from two wheels, aligning torque and an axle wide slip angle (Pauwelussen 2015). Respectively, a similar system holds for the rear wheels. The Newton's equations of motions read (Dukkipati et al. 2008; Pauwelussen 2015):

$$\sum F_x = 0, \tag{1}$$

$$\sum F_y = m_1 a_y = F_{y1} + F_{y2}, \tag{2}$$

$$\sum M_z = I_1 \dot{r}_1 = F_{y1} a_1 - F_{y2} b_1. \tag{3}$$

The lateral acceleration a_y is considered more in depth. The trajectory of the vehicle in a circular orbit is presented in figure 3.

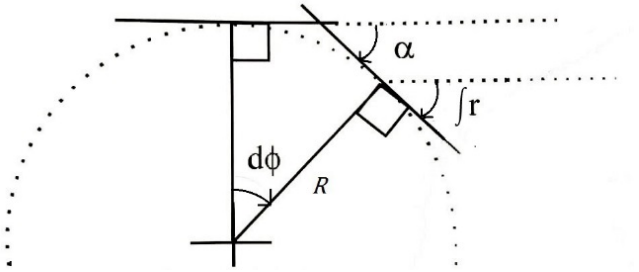

Figure 3. The yaw of the Vehicle is equal to the central angle in circular orbit (Tuononen & Koisaari 2014)

A vehicle with a constant velocity travels an angle of $d\phi$ in circular orbit. The angle α is equal to ϕ, because the sides of the angles are perpendicular to each other. The yaw of the vehicle $\int r$ is equal to the angle α, because they are corresponding angles. Consequently, the angles ϕ and $\int r$ are equal of value and therefore the angular velocities $\frac{d\phi}{dt}$ and r are equal. (Tuononen & Koisaari 2014)

Based on the geometrical rules, the yaw velocity and angular velocity can be written as follows:

$$\omega = \frac{d\phi}{dt} = \frac{u}{R} = r. \tag{4}$$

Now the lateral acceleration a_y can be written as:

$$a_y = \dot{v} + ur. \tag{5}$$

Now the equation (2) can be written as:

$$\sum F_y = m_1(\dot{v}_1 + ur_1) = F_{y1} + F_{y2}. \tag{6}$$

The single-track model is not yet considering the lateral forces F_{y1} and F_{y2} precisely. The exact linear and nonlinear characteristics for lateral forces are considered in the next subheading. This consideration of linear and nonlinear tire characteristics allows the precise single-track model formula solution. In addition, the derivation into the matrix format of the dynamic state examination is presented, because it is often used in the research of lateral dynamic behavior of a vehicle in state space.

2.2 Tire dynamics

Tire dynamics are modelled with different tire models, which are based on different tire characteristics. The tire dynamic models can be divided into several categories. Some general divisions are empirical and physical, quasi-static and momentary and linear and nonlinear models (Tuononen & Koisaari 2014). The mechanical characteristics of a tire are essential for vehicle stability and handling, because the tires generate all the required forces and moments to steer the vehicle (Rahkola 2006). The combination of the different tire characteristics results in the performance of a tire as a force and moment generating structure (Pacejka 2006). The generated moments and forces of a tire are essential when considering tire as a part of a vehicle. Different tires have different mechanical characteristics. The most common tire for a road vehicle is a radial ply-tire, which has replaced the cross-ply tire almost entirely (Tuononen & Koisaari 2014). The radial ply-tire fills the most important criteria of a tire, such as: carry and divide vertical load, produce longitudinal and lateral force, adjust to the prevailing road and dampen interferences. A tire generates forces and moments in every coordinate direction. The general coordinate system of a tire follows the right hand notation such as the general vehicle coordination, it is presented in figure 4.

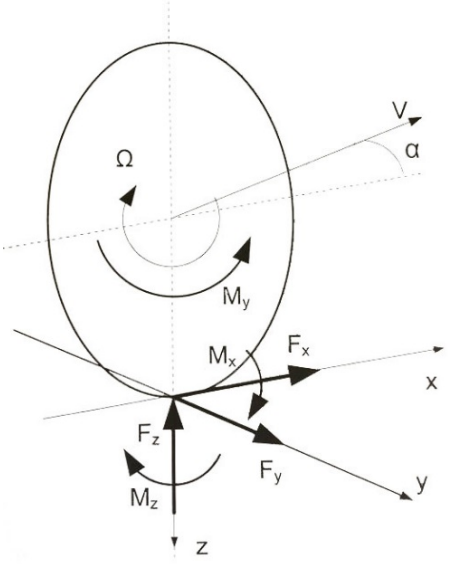

Figure 4. Tire coordinate system (Tuononen & Koisaari 2014)

The vertical force F_z is the vertical load of the wheel and the moment M_z is the self-aligning moment. The longitudinal force F_x is the braking and accelerating force and the moment M_x is the overturning couple. The lateral force F_y is the lateral force and the moment M_y is the rolling resistance moment. These forces and moments are considered as the outputs of a tire. The corresponding inputs are different angles and velocities, of which the most important in the examination of lateral dynamics is the lateral slip angle.

In the research of lateral dynamic behavior the aligning moment M_z and the lateral force F_y are the most important outputs of a tire. The vertical load F_z is also essential in the lateral dynamic analysis. They directly affect the handling characteristics and driving response. Particularly, the aligning moment is significant for the driver in order to steer and maneuver the vehicle to desired path correctly. An extreme case example can be

found, where the tire is completely sliding due to very large slip angle. In this case, the lateral force distribution of the tire is symmetrically and equally distributed over the wheel spin axis. Consequently, the resultant lateral force F_y is located at the origin. Therefore the pneumatic trail $t = 0$, which is the distance between the point of application of the resultant lateral force and the origin. This means that no aligning moment is present and the driving response is completely different and more difficult to control.

The rubber friction has an important effect on the tire input quantities, specifically on the molecular level. However the rubber friction is not self-explanatory. The traditional Coulomb model is not valid for a tire, because of the viscoelastic nature and incompressibility. The tire rubber friction is traditionally divided into hysteresis and adhesion. Hysteresis is the result of rolling resistance and adhesion is developed, because of the Van Der Waals forces between two surfaces. The total amount of friction is the sum of these two factors. The proportions of the factors are dependent on the road surface, rubber characteristics and temperature. A high surface roughness contains many roughness peaks, which allow good hysteresis conditions, but at the same time the contact area is low and therefore the adhesion is low. Respectively, low surface roughness has only few and low roughness peaks, therefore the contact area is large, which results in low hysteresis and high adhesion. (Pacejka 2006; Tuononen & Koisaari 2014)

The different tire models explain different phenomena and characteristics of a tire. There is no one model that explains all the different phenomena and characteristics, because the tire is a complicated structure. That is why different models are being used for different studies, dependent on the study object. In the nonlinear lateral vehicle dynamics the most common tire model is the Magic Formula (MF) tire model, which gives accurate results and explains the prevalent phenomena well, specifically on low road friction surfaces. The MF explains how the longitudinal and lateral forces and moments are developed in a tire. The used tire model in this thesis is the MF tire model. The MF tire model is explained thoroughly in the end of this subheading.

2.2.1 Linear tire characteristics

In the linear tire formula, the lateral forces are functions of the respective slip angles (Pacejka 2006). The slip angles are multiplied with the respective cornering stiffnesses in order to gain the lateral force of a tire. The cornering stiffness acts as the slope of the linear part of the lateral force graph. In other words, the cornering stiffness defines the developing lateral force per slip angle unit (Tuononen & Koisaari 2014).

In linear bicycle model the cornering stiffnesses and lateral forces are axle specific. It is assumed that the cornering stiffness stays constant and this holds with small slip and steering angles. Additionally, it is determined that a cornering stiffness stays constant in good road surface and with a lateral acceleration less than $4\frac{m}{s^2}$ (Milliken & Milliken 1995). The linear lateral force reads (Genta 1997):

$$F_{yi} = C_i \alpha_i. \tag{7}$$

The cornering stiffnesses are usually calculated from practical driving tests and found in literature for specific tires and vehicles. In the Bosch automotive handbook the cornering

stiffness is addressed more in depth. The lateral force of a freely rolling truck wheel is presented in figure 5.

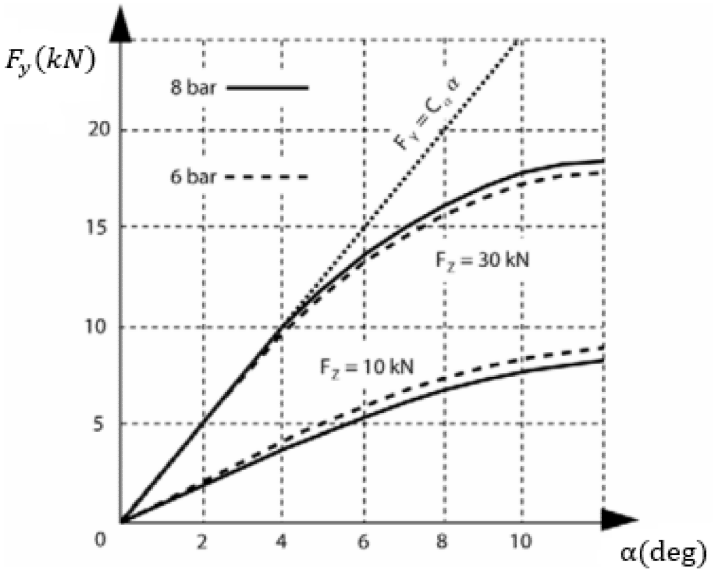

Figure 5. The lateral force of a truck wheel as a function of slip angle (Bosch 2004)

As seen in the figure 5, the lateral force stays linear almost up to slip angle of 6 degrees with a vertical load of 10 kN. It is notable from the figure 5 that with higher vertical loads and tire pressures, the lateral force linearity suffers, because the linearity is only valid with small slip angle and vertical wheel load values (Aurell & Edlund 1989; Bosch 2011). However, the slope changes if the vertical load or tire pressure changes. The cornering stiffness value can be replaced with a more general variable $C_{F\alpha i}$, which also takes into account the camber and aligning stiffnesses (Pacejka 2006).

The earlier mentioned limitations and assumptions for the single-track model still hold. The slip angle is the angle between the direction of tire heading and the direction of travel or the angle between the centerline of the tire and the resultant velocity vector. The development of the slip angle is presented in figure 6.

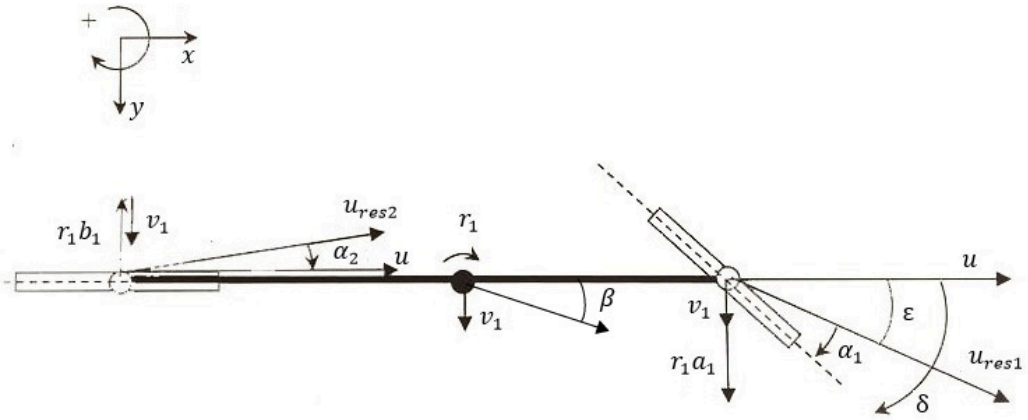

Figure 6. The relation between the slip and steering angle of a vehicle (Tuononen & Koisaari 2014)

The wheelbase is short compared to the turn radius and the slip and steering angles are small. Therefore, following geometrical approximations hold:

$$\sin\alpha \approx 0, \cos\alpha \approx 1 \text{ and } \tan\alpha \approx \alpha. \quad (8)$$

The longitudinal velocity u is constant and of equal value in every point of the vehicle. The total lateral velocity consists of two factors, lateral velocity at the center of gravity (CoG) v_1 and a portion of the yaw velocity r_1 multiplied with the corresponding distance from the CoG (Tuononen & Koisaari 2014). Consequently, the vehicle slip angle β and angle ε can be solved from the CoG and contact point of the front wheel with geometry:

$$\beta \approx \tan\beta = \frac{v_1}{u}, \qquad \varepsilon \approx \tan\varepsilon = \frac{v_1 + r_1 a_1}{u}. \quad (9)$$

The slip angle of the front wheel is therefore:

$$\alpha_1 = \delta - \varepsilon = \delta - \frac{v_1 + r_1 a_1}{u}. \quad (10)$$

The slip angle of the rear wheel can be calculated similarly:

$$\alpha_2 = \frac{r_1 b_1 - v_1}{u}. \quad (11)$$

In the steady state examination, the steering properties of the vehicle are most commonly examined. The kinematic steering theory was created by Rudolph Ackermann. The kinematic steering can be examined in steady state cornering, where:

$$\dot{v_1} = \dot{r_1} = 0. \quad (12)$$

The Ackermann angle can be derived from the slip angle and single-track model formula. By eliminating the velocity v_1 from the slip angle equations (10)-(11) and including $l = a_1 + b_1$ and conditions from equations (4) and (7):

$$\frac{l}{R} = \delta - \alpha_1 + \alpha_2 = \delta - \frac{F_{y1}}{C_1} + \frac{F_{y2}}{C_2}. \quad (13)$$

From the Newton's equations of motions (2)-(3), the lateral forces can be solved as follows:

$$F_{y1} = \frac{b_1 m_1 u^2}{lR}, \quad (14)$$

$$F_{y2} = \frac{a_1 m_1 u^2}{lR}. \quad (15)$$

Now the Ackermann angle can be determined from the equation (13) by including the lateral force equations (14)-(15):

$$\delta = \frac{l}{R} + \frac{m_1 u^2}{R}\left(\frac{C_2 b_2 - C_1 a_1}{l C_1 C_2}\right). \quad (16)$$

According to the kinematic theory, the Ackermann angle determines the steering characteristics of a vehicle (Dukkipati et al. 2008). From the equation (16), the steering gradient K can be separated as follows:

$$K = \left(\frac{C_2 b_2 - C_1 a_1}{l C_1 C_2}\right). \quad (17)$$

The steering gradient determines the vehicles maneuverability in cornering. If the steering gradient $K < 0$, the vehicle is understeering. In an understeering situation the vehicle drifts off of the path of the constant-radius turn as the centripetal acceleration increases. When the $K = 0$, the vehicle is neutral steering. In a neutral steering situation, the vehicle

stays at the same steady state cornering roadway, as the centripetal acceleration increases. In oversteering situation the $K > 0$. Consequently, as the centripetal acceleration increases, the vehicle is driven off of the inner edge of the path of a constant-radius turn. (Milliken & Milliken 1995; Pacejka 2006)

The understeer level can be quantified by a parameter of characteristic speed. At the characteristic speed, the yaw velocity gain of the vehicle reaches its maximum value. At the characteristic speed the required steering angle to perform the steady state turn is twice the Ackermann angle. Respectively, an oversteering vehicle has a parameter of critical speed. The critical speed can be found from the point where the initial steering angle has become zero in order to stay on the same turn radius. When the critical speed is surpassed, the oversteering vehicle becomes unstable. (Dukkipati et al. 2008; Gillespie 1992)

The different steering gradients, characteristic speed and critical speed are presented in figure 7.

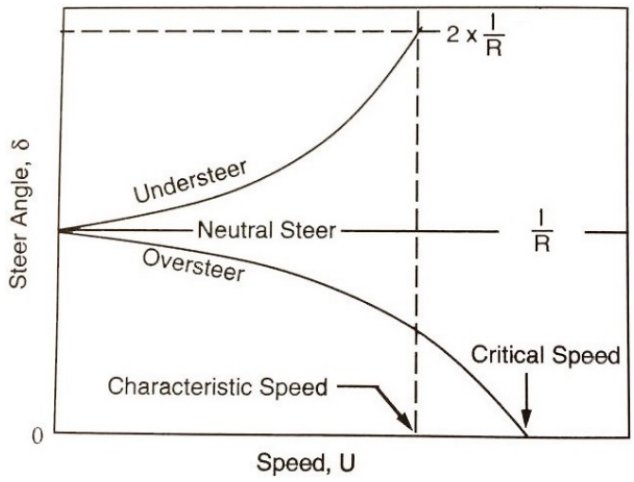

Figure 7. The steering gradients, characteristic speed and critical speed (Gillespie 1992)

The Ackermann angle can be found in neutral steer point as $\frac{l}{R}$. The characteristic speed and critical speed can be derived from the Newton's equations of motions (2)-(3) by including the lateral force equation (7) (Genta 1997):

$$u_{characteristic} = \sqrt{\frac{l^2 C_1 C_2}{m_1(b_1 C_2 - a_1 C_1}} = \sqrt{\frac{l}{K}}, \tag{18}$$

$$u_{critical} = \sqrt{\frac{l^2 C_1 C_2}{m_1(a_1 C_1 - b_1 C_2}} = \sqrt{-\frac{l}{K}}. \tag{19}$$

The single-track model is also used for dynamic state examination. In the dynamic state, the state of the vehicle changes over time continuously. The current state is dependent on the previous state and the next state is dependent on the current state. In this state, all the time derivatives of the variables are not zero. The dynamic state of the vehicle can be examined in state space, which is often used in linear vehicle dynamics. The state space assumes linear conditions. It can be seen from the Newton's equations of motions that variables such as cornering stiffnesses, vehicle mass and dimensions are constant variables. The steering angle is considered as an input parameter controlled by the driver. However, lateral velocity and yaw velocity are output parameters that are the responses to the driver's behavior. (Pacejka 2006)

The Newton's equations of motions of the bicycle model are solved in terms of the chosen state parameters. Traditionally the first-order derivatives of lateral velocity v_1 and yaw velocity r_1 are chosen, because these parameters are suitable to describe the lateral behavior of a vehicle. In addition, by choosing these parameters, the equations reduce into more simple form. The differential equations describing bicycle model are linear in terms of the state variables (Tuononen & Koisaari 2014). This means, that the variables can be collected in different vectors and parameters in different matrices. The standard matrix notation for a single vehicle in single-track model becomes (Pacejka 2006; Pauwelussen 2015):

$$\begin{cases} \dot{\bar{x}} = A\bar{x} + Bu \\ \bar{y} = C_u\bar{x} + Du \end{cases}, \tag{20}$$

where vector $\dot{\bar{x}}$ contains the state parameters, u input parameters and $\bar{y}$ starting parameters. The A matrix is called as the system or dynamic matrix, B input matrix, C_u starting matrix and D impact matrix. The starting matrix C_u is a unit matrix and the impact matrix D is often a zero matrix. In the vehicle dynamics a different matrix notation is often used for state space, because of the complexity of different vehicle combinations. This matrix notation reads (Aurell & Edlund 1989):

$$M\dot{\bar{x}} = C\bar{x} + K\delta, \tag{21}$$

where $\dot{\bar{x}}$ is the state vector, M is the mass matrix, C is the coefficient matrix and K is the steering matrix. A connection between these two matrix notations can be derived:

$$A = M^{-1}C, \tag{22}$$

$$B = M^{-1}K. \tag{23}$$

Generally the latter matrix notation is easier to solve from the Newton's equations of motions in complex vehicle combinations. The derivation of the latter matrix notation begins from the Newton's equations of motions (2)-(5) by including the linear lateral forces (7) and slip angle equations (10)-(11):

$$\sum F_y = m_1(\dot{v}_1 + ur_1) = C_1\left(\delta - \frac{v_1 + r_1 a_1}{u}\right) + C_2\left(\frac{r_1 b_1 - v_1}{u}\right), \tag{24}$$

$$\sum M_z = I_1\dot{r}_1 = C_1 a_1\left(\delta - \frac{v_1 + r_1 a_1}{u}\right) - C_2 b_1\left(\frac{r_1 b_1 - v_1}{u}\right). \tag{25}$$

Now the matrix notation can be formed from the equations (24)-(25):

$$\begin{pmatrix} m_1 & 0 \\ 0 & I_1 \end{pmatrix}\begin{pmatrix} \dot{v}_1 \\ \dot{r}_1 \end{pmatrix} = \begin{pmatrix} -\frac{C_1 + C_2}{u} & \frac{C_2 b_1 - C_1 a_1}{u} - m_1 u \\ \frac{C_2 b_1 - C_1 a_1}{u} & -\frac{C_1 a_1^2 + C_2 b_1^2}{u} \end{pmatrix}\begin{pmatrix} v_1 \\ r_1 \end{pmatrix} + \begin{pmatrix} C_1 \\ C_1 a_1 \end{pmatrix}\delta. \tag{26}$$

For a single vehicle unit, which has 2 degrees of freedom (DoF), the matrices are 2x2 matrices and the number of state variables is equal to the number of DoF. The lateral dynamic behavior of the vehicle can be evaluated from the state parameters with different transient or steady state responses. Usually the lateral velocity, lateral acceleration, vehicle slip angles and yaw velocity are the matter of investigation. These state variables describe the stability and handling characteristics of the vehicle well, as earlier mentioned. The stability, instability, maneuverability, handling characteristics and safety

of the vehicle can be estimated from the simulation results. Various research results indicate that this analytical model is accurate and close to real life results for different kinds of vehicles in normal driving and road surface conditions (Rahkola 2006; Luijten 2010). In addition, the bicycle model describes the lateral dynamic phenomena of a vehicle relatively accurately.

2.2.2 Nonlinear tire characteristics

The advantage of nonlinear tire characteristics is that they are not limited by slip angle, state variables, road friction or wheel load (Genta 1997). As was indicated, the linear tire characteristics are very limited by these conditions so they are not suitable in the evaluation of vehicle dynamic behavior on low road friction surfaces or in extreme situations. Consequently, nonlinear tire characteristics are much more suitable for evaluating lateral dynamic behavior of a vehicle in extreme conditions and on low road friction surfaces. In these extreme conditions the problematic situations of the vehicle become more effective and the vehicle specific problematic phenomena can be found and evaluated. The problematic phenomena can be high lateral velocity, high lateral acceleration, high yaw velocity or large slip angle. High yaw and lateral velocity or acceleration can bring the vehicle into an unstable state, which can result into the loss of control of the vehicle, particularly on a low road friction surface (Pacejka 2006). Additionally, large vehicle slip angles are extremely dangerous, because of the incapability of producing enough lateral force to steer the vehicle towards the desired path, which tends to result in a vehicle spin or roll-over. Nonlinear tire characteristics are specifically used in the research of vehicle behavior on low road friction surfaces, which is essential during wintertime or in places where the road conditions are worse and slippery (Aurell & Edlund 1989).

In vehicle lateral dynamic research, the MF is a commonly used nonlinear tire model. The MF is an empirical tire model. However, some of its parameters have a physical background, therefore it is also called a semi-empirical tire model (Tuononen & Koisaari 2014). The basis of the MF was created by Bakker and Pacejka and later on, Pacejka created an extended version of the model (Smakman 2000).

The extended model includes a set of formulas describing the longitudinal and lateral forces and the self-aligning moment comprehensively with the same form (Dukkipati et al. 2008). The MF has been shown to suitably match the experimental data of the dynamic tire characteristics (Dukkipati et al. 2008). In addition, the model is based on trigonometric functions, which come from the similarity method. The similarity method means that the formula graph has similar shape as the lateral force graphs of different tire models (Pacejka 2006). The MF is fit into experimental data of lateral force and slip angle with non-dimensional quantities. The non-dimensional quantities and parameters are gathered and stored, once the formula parametrization is accurate. The MF is always set up for specific friction coefficient, tire and loads and different combinations can be found from the literature (Pauwelussen 2015).

There are different versions and definitions of MF and its parameters. The general form of MF is often used, however, in the examination of lateral force and lateral dynamics, the pure side slip formula is used (Pacejka 2006):

$$F_{y0} = D_y \sin[C_y \arctan\{B_y\alpha_y - E_y(B_y\alpha_y - \arctan(B_y\alpha_y))\}] + \mathrm{S_{Vy}}, \quad (27)$$

$$\alpha_y = \alpha + S_{Hy}, \quad (28)$$

$$S_{vy} = F_z\left(p_{Vy1} + p_{Vy2}df_z + \left(p_{Vy3} + p_{Vy4}df_z\right)\gamma\right), S_{Hy} = \left(p_{Hy1} + p_{Hy2}df_z\right)\lambda_{Hy}. \quad (29)$$

In the formula, the output variable $F_{y0}$is the lateral force F_y. The input variable α_y is the tire slip angle. S_{Vy} is the vertical shift factor, S_{Hy} is the horizontal shift factor. The different coefficients $B_y, C_y, D_y, E_y, S_{Vy}, S_{Hy}, y_a$ and x_m can be calculated with auxiliary parameters or read from the curve. The MF graph is presented in figure 8.

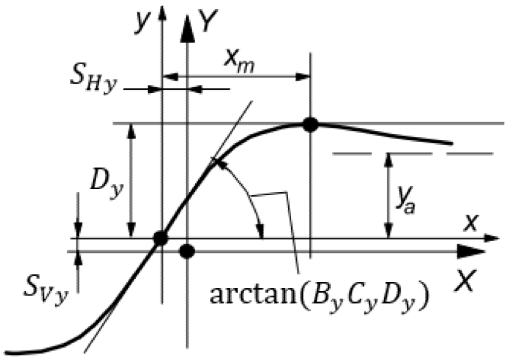

Figure 8. Curve produced by Magic Formula and curve parameters (Pacejka 2006)

The formula coefficients read (Pacejka 2006): B_y parameter is called the stiffness factor, C_y is called the shape factor, D_y represents the peak value of the curve, E_y is the bend factor, S_{Vy} is the vertical shift factor, S_{Hy} is the horizontal shift factor, y_a is the distance of the decline part of the graph from the x-axle and x_m is the distance of the peak value from y-axle. The coefficients are defined in the following way. The slope of the linear part is defined as (Pacejka 2006):

$$K_{y\alpha} = B_yC_yD_y. \quad (30)$$

The coefficients y_a, x_m and D_y can be read from the graph. The coefficient C_y and also D_y can be solved as (Pauwelussen 2015; Pacejka 2006; Genta 1997):

$$C_y = p_{cy1}, \quad D_y = \mu_y \cdot F_z, \ \mu_y = \left\{\frac{p_{Dy1}+p_{Dy2}df_z}{1+p_{Dy3}\gamma^2}\right\}\lambda_{\mu y}, \ df_z = \frac{F_z - F_{z0}}{F_{z0}}. \quad (31)$$

The shape coefficient C_y describes how much the graph declines after the peak value. A typical value for lateral force is around 1.3 (Tuononen & Koisaari 2014). The coefficient df_z is the relative change of the vertical load F_z calculated from the nominal load F_{z0}. The coefficient $K_{y\alpha}$ can be solved as (Dukkipati et al. 2008; Pacejka 2006):

$$K_{y\alpha} = p_{Ky1}F_{z0}\sin\frac{\left(p_{Ky4}\arctan\left[\frac{F_z}{\left(p_{Ky2}+p_{Ky5}\gamma^2\right)F_{z0}}\right]\right)}{1+p_{Ky3}\gamma^2}. \quad (32)$$

The E_y coefficient defines the curvature and horizontal location of the peak point of the curve (Pacejka 2006; Tuononen & Koisaari 2014):

$$E_y = \left(p_{Ey1} + p_{Ey2}df_z\right)\left\{1 + p_{Ey5}\gamma^2 - \left(p_{Ey3} + p_{Ey4}\gamma^2\right)sgn\left(\alpha_y\right)\right\}\lambda_{Ey} \quad (33)$$

The offsets due to ply steer, camber, king pin, caster or conicity are incorporated in the shift terms S_{Vy} and S_{Hy} (Smakman 2000). The shift coefficients S_{Vy} and S_{Hy} are non-dimensional quantities and they are manually set to fit the curve precisely. The different p_y auxiliary coefficients are presented in the appendices A1-A2 and the offset phenomena are also incorporated in these auxiliary coefficients. The MF fits accurately different setups and it provides accurate and fast results in simulations. However, in order to receive accurate results, the measurements for coefficients and parameters need to be performed for the prevailing tire, vehicle and road base. These measurements require sophisticated test equipment, which make the testing procedure difficult and even impractical for some organizations (Dukkipati et al. 2008). Another option is to find precise parameters from literature, if the measurements have already been done for the particular setup. It is said that the MF describes the vehicle behavior accurately enough in snow and ice surfaces (Aurell & Edlund 1989). On the other hand, it is also said that the MF model is not well suited to parametric studies of the impacts of snow- and ice-induced changes in the surface friction (Dukkipati et al. 2008). This contradiction means that the MF gives sufficiently accurate results in low road friction surfaces, yet it doesn't correctly describe the snow and ice surface phenomena.

The tendency of the vehicle to roll is the result of lateral acceleration. The handling characteristics suffer when the vehicle rolls strongly. During a cornering situation, the wheel loads transfer from inner wheels to outer wheels. With a small amount of wheel load transfer, the transferred load stays on the linear region of lateral force graph and the sum production of lateral force stays unchangeable. However, if the wheel loads transfer strongly, the outer wheels exceed their linear region and are incapable of producing more lateral force linearly. As a result, the total lateral force decreases, because the outer wheels can't completely carry the dynamic load transfer from the inner wheels and produce enough lateral force to compensate the load transfer. This is because of the nonlinear correlation between lateral force and vertical load or slip angle, where additionally, the slope of the lateral force graph decreases significantly. On the other hand, in the linear bicycle model as the lateral forces of single tires are summed to axle effective forces, the resultant force is the same. This is the result of the assumption that the tires can produce lateral force linearly as a function of slip angle without a nominal maximal value, therefore the load transfers can be compensated completely. Consequently, the phenomena is insignificant in linear tire model and it is therefore often ignored in linear single-track model. As opposite to linear tire characteristics, in the nonlinear tire characteristics the wheel load transfers are usually included, because then the phenomenon is of significance in the nonlinear single-track model. In the nonlinear tire characteristics the lateral force of a single tire has a maximal nominal value and it acts nonlinearly as seen in the figure 8. This effect of load transfer on lateral force is demonstrated in figure 9. (Dukkipati et al. 2008; Rahkola 2006)

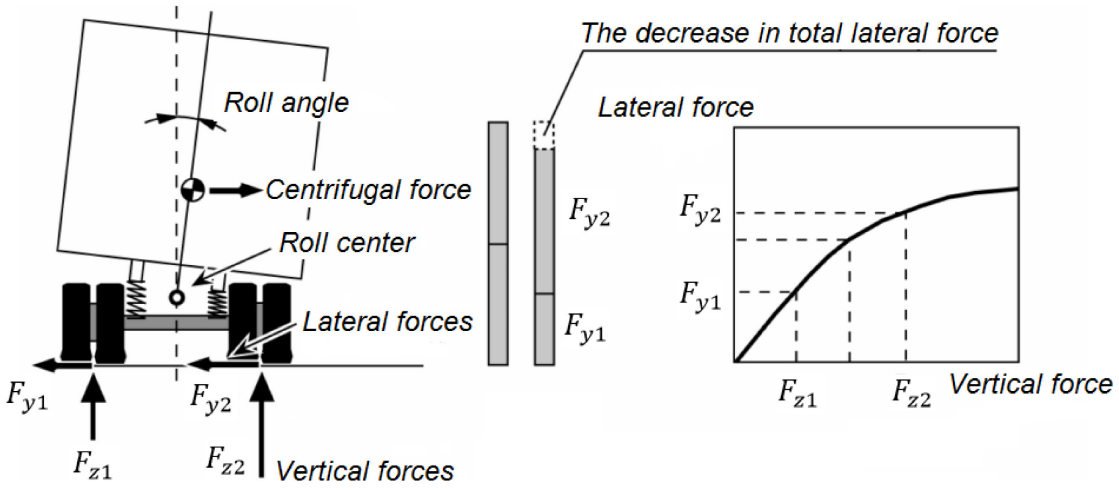

Figure 9. The effect of wheel load transfers on lateral force (Rahkola 2006)

The wheel load transfer effect is emphasized in single-track model, if the particular vehicle is driven into extreme conditions. In extreme conditions the wheels can exceed the linear lateral force region even with low lateral accelerations. This is the result of the prevailing low road friction, which disallows large slip angles and high vertical forces and the nonlinear region of the lateral force graph starts earlier due to the slippery road conditions. When a tire acts strongly in the nonlinear region, even beyond the maximal nominal value, the wheel can lose its capability to carry the vertical load and produce lateral force. Consequently, the other wheels try to carry the load and produce lateral force to compensate the lost wheel. However, this can't be done completely as it was indicated in the last paragraph. This usually leads in an unstable state and loss of control of the vehicle. With low CoG vehicles such loss of control usually results in a vehicle spin. High CoG vehicles tend more to roll over, since the position of CoG surpasses the fulcrum point before the vehicle starts to spin. On high road friction surfaces the wheels can carry more vertical load and produce higher lateral forces. Consequently, it is highly improbable for the vehicle to spin and it tends more to roll over. Respectively, on low road friction surfaces the vehicle tends to spin. It is notable that an aggressive spinning usually leads to a vehicle roll-over. (Pacejka 2006; Tuononen & Koisaari 2014)

The wheel load distribution in a vehicle can be evaluated by splitting up the load at a certain wheel into various components (Smakman 2000):

- Static wheel load due to vehicle weight
- Wheel load transfer due to vehicle longitudinal and lateral accelerations
- Dynamic wheel load due to vertical motion of the vehicle body or wheel
- Wheel load due to external forces.

The following assumptions and simplifications are made. In this analysis, the vehicle will be limited to driving on a flat surface. The dynamic wheel load due to vertical motion will be neglected, because the vehicle structure is assumed rigid, including the suspension system. Moreover the vertical motion has only slight impact on the total wheel load transfer. The external forces, such as rolling, powertrain and aerodynamic resistances are also neglected due to the low impact on normal vehicle speeds (Dukkipati et al. 2008). The importance of external forces is emphasized on higher vehicle velocities, but in this analysis they are considered out of scope (Pacejka 2006; Smakman 2000). Additionally,

in the examination of lateral dynamic behavior the longitudinal wheel load transfers are considered beyond scope as the simulations are performed on a flat surface with a constant driving velocity.

The xy-projection of a vehicle is presented in figure 10.

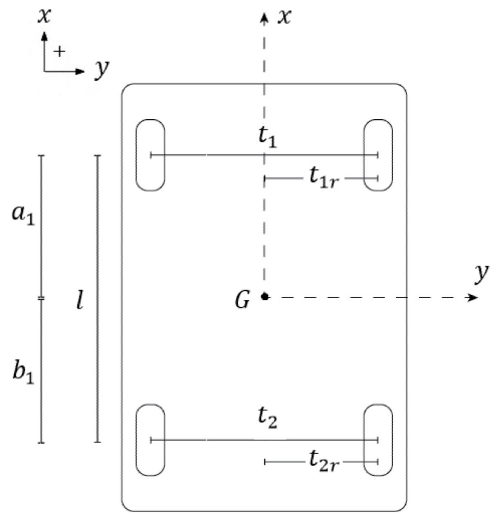

Figure 10. The xy-projection of a vehicle

The static wheel loads for each wheel can be calculated as follows (Pauwelussen 2015; Smakman 2000):

$$F_{z1l} = \frac{b_1}{l} m_1 g \frac{t_{1r}}{t_1},\ F_{z1r} = \frac{b_1}{l} m_1 g \frac{t_{1l}}{t_1}, \tag{34}$$

$$F_{z2l} = \frac{a_1}{l} m_1 g \frac{t_{2r}}{t_2},\ F_{z2r} = \frac{a_1}{l} m_1 g \frac{t_{2l}}{t_2}. \tag{35}$$

The index 1 represents front axle and respectively the index 2 represents rear axle. The indexes l and r represent the left and right sides. The total axle static load is the sum of the static wheel loads of both the left and right wheels on an axle:

$$F_{z1} = F_{z1l} + F_{z1r} = m_1 g \frac{b_1}{l}, \tag{36}$$

$$F_{z2} = F_{z2l} + F_{z2r} = m_1 g \frac{a_1}{l}. \tag{37}$$

The effect of lateral acceleration is considered.

In cornering state, the wheel load transfers from the inner wheels to the outer wheels in respect of lateral acceleration. A rear perspective of a front axle of a vehicle in steady state cornering is presented in figure 11.

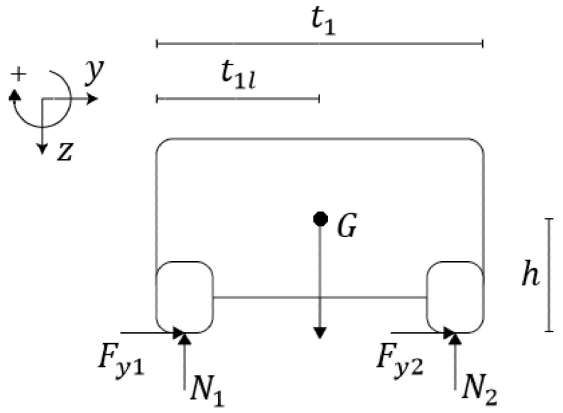

Figure 11. The front axle of a vehicle from rear perspective

Newton's equations of motion read (Pacejka 2006; Pauwelussen 2015):

$$\sum F_y = m_1 \frac{b_1}{l} a_y = F_{y1} + F_{y2}, \tag{38}$$

$$\sum F_z = G - N_1 - N_2 = 0, \tag{39}$$

$$\sum M_x = -h\left(F_{y1} + F_{y2}\right) - t_{1r} N_2 + t_{1l} N_1 = 0, \tag{40}$$

where $G = m_1 g \frac{b_1}{l}$. By substituting equations (38)-(39) to equation (40), the vertical load N_2 reads:

$$-h m_1 \frac{b_1}{l} a_y - t_{1r} N_2 + t_{1l}(G - N_2) = 0, \tag{41}$$

$$N_2 = -\frac{h m_1 \frac{b_1}{l} a_y - t_{1l} m_1 g \frac{b_1}{l}}{t_1}. \tag{42}$$

Respectively, the vertical load N_1 can be evaluated:

$$N_1 = \frac{h m_1 \frac{b_1}{l} a_y + t_{1r} m_1 g \frac{b_1}{l}}{t_1}. \tag{43}$$

According to the exact same principles, the wheel load transfers of the rear axle in lateral direction can be evaluated:

$$N_3 = \frac{h m_1 \frac{a_1}{l} a_y + t_{2r} m_1 g \frac{a_1}{l}}{t_2}, \tag{44}$$

$$N_4 = -\frac{h m_1 \frac{a_1}{l} a_y - t_{2l} m_1 g \frac{a_1}{l}}{t_2}. \tag{45}$$

Although the static wheel load terms were already derived separately, it can be seen that the vertical loads contain both the lateral dynamic wheel load and static wheel load terms. It is notable that the respective mass m_1 must be multiplied with the lever ratio in order to get the respective axle mass. In this coordinate system, with a positive lateral acceleration, the wheel loads transfer from right side to the left side, and with negative lateral acceleration vice versa.

Now the total amount of vertical load and wheel load transfers can be written by combining the static wheel load and lateral wheel load transfer. The vertical loads read:

$$N_1 = \frac{b_1}{l} m_1 g \frac{t_{1r}}{t_1} + \frac{h}{t_1} m_1 \frac{b_1}{l} a_y, \quad (46)$$

$$N_2 = \frac{b_1}{l} m_1 g \frac{t_{1l}}{t_1} - \frac{h}{t_1} m_1 \frac{b_1}{l} a_y, \quad (47)$$

$$N_3 = \frac{a_1}{l} m_1 g \frac{t_{2r}}{t_2} + \frac{h}{t_2} m_1 \frac{a_1}{l} a_y \quad (48)$$

$$N_4 = \frac{a_1}{l} m_1 g \frac{t_{2l}}{t_2} - \frac{h}{t_2} m_1 \frac{a_1}{l} a_y. \quad (49)$$

In the evaluation of lateral dynamic behavior of a vehicle, the effect of longitudinal force is often assumed minimal and ignored. Moreover, the test drives and simulations in lateral dynamic observation are performed in flat surfaces and usually with constant driving velocities. Therefore, the longitudinal acceleration is often negligible or zero. Under these circumstances, the longitudinal wheel load transfers along with the external forces are not essential and they are often neglected in lateral dynamic observation. Generally, the total wheel load in lateral dynamics evaluation consists of the static wheel load term and lateral dynamic wheel load term.

Combining the bicycle model with nonlinear tire characteristics results in a nonlinear vehicle model (Genta 1997). The term nonlinear here means that only the tires include nonlinear characteristics. In addition, the wheel load transfers can be included in order to extend the bicycle model to four-wheel model. However, the equations of motion and lateral and longitudinal dynamic behavior are still linearized. Consequently, as mentioned earlier, the nonlinear model enables the observation of lateral dynamic behavior of a vehicle in extreme situations. The extreme conditions allow the large variation of slip angle, friction coefficient and state variables.

The nonlinear model differs from the linear model only by the calculation of tire forces. The separation of longitudinal and lateral motion and the evaluation of tire forces are still possible. However, it is not possible to examine the stability and lateral dynamic behavior of a vehicle in the state space by the same principles as in the linear model. This is the result of the nonlinear tire components. For the nonlinear model, the same Newton's equations of motion for a vehicle still apply. The tire forces are calculated with the MF model. The axle effective lateral force now reads:

$$F_{yi} = y(x_i, F_{zi}, \mu). \quad (50)$$

The input variable x_i of the MF is the corresponding tire slip angle α_i in the case of lateral force. In order to extend the nonlinear bicycle model to nonlinear four-wheel model, the vertical loads and wheel load transfers must be taken into account. The lateral force of a single tire in four-wheel model reads:

$$F_{yij} = y\big(x_i, F_{zij}, \mu\big), \quad (51)$$

Where the vertical wheel force F_{zij} is the opposite force of the vertical load N_n. The lateral force of a single tire is the MF lateral force function of the corresponding slip angle, vertical load including wheel load transfers and surface friction coefficient. It is notable that the axle effective lateral force in four-wheel model is the sum of the single tire forces of the axle. The effective axle lateral force in four-wheel model reads:

$$F_{yi} = F_{yij} + F_{yij+1} = y\big(x_i, F_{zij}, \mu\big) + y\big(x_i, F_{zij+1}, \mu\big). \quad (52)$$

The lateral forces have the same slip angle input variable, because it was assumed that the tires on the same axle have the same slip angles. Now the index i represents the axle and the index j represents the wheel of the axle. In the single-track model the axle effective lateral force is essential. Both the equation (50) and (51) result into the same effective axle force in normal road conditions. If the target of the research is to examine the lateral dynamic behavior of a vehicle, the equation (50) is sufficient in normal conditions. However, if one is interested to examine the single tire forces or the lateral dynamic behavior of a vehicle in extreme conditions, then the equation (52) is essential to describe the results and phenomena more accurately. Now the nonlinear model for a passenger vehicle in the figure 2 can be evaluated. The lateral forces of the passenger vehicle read:

$$F_{y1} = y(\alpha_1, F_{z1}, \mu) = F_{y11} + F_{y12} = y(\alpha_1, F_{z11}, \mu) + y(\alpha_1, F_{z12}, \mu), \quad (53)$$

$$F_{y2} = y(\alpha_2, F_{z2}, \mu) = F_{y21} + F_{y22} = y(\alpha_2, F_{z21}, \mu) + y(\alpha_2, F_{z22}, \mu). \quad (54)$$

The exact same equations of motion can be written for the vehicle as in the linear model by replacing the linear lateral tire forces with the nonlinear MF forces. The Newton's equations of motion read:

$$m_1(\dot{v}_1 + ur_1) = y(\alpha_1, F_{z11}, \mu) + y(\alpha_1, F_{z12}, \mu) + y(\alpha_2, F_{z21}, \mu) + y(\alpha_2, F_{z22}, \mu), \quad (55)$$

$$I_1\dot{r}_1 = a_1\big(y(\alpha_1, F_{z11}, \mu) + y(\alpha_1, F_{z12}, \mu)\big) - b_1\big(y(\alpha_2, F_{z21}, \mu) + y(\alpha_2, F_{z22}, \mu)\big). \quad (56)$$

The nonlinear solution is possible to derive by substituting the slip angle (10)-(11), MF (27) and vertical load equations (46)-(49) to the Newton's equations of motion (55)-(56). The equations of motion form a nonlinear first-order differential algebraic system of equations. The differential algebraic system of equations is in the form of:

$$\dot{x} = f(t, x), \quad (57)$$

where x is the same state vector as in the corresponding linear model $\bar{x} = [v_1\ r_1]^T$. The differential algebraic system of equations can be solved in a time domain simulation as a numeric integral.

2.3 Articulated vehicle dynamics

An articulated vehicle is a vehicle combination, where two or more vehicle units are connected together with articulations. The stability of articulated vehicles can become problematic in many driving situations and conditions. The vehicle combination stability is traditionally divided into lateral or yaw stability and roll stability, which are dependent on each other by the lateral acceleration (Aurell & Edlund 1989). In general, the height of the CoG is high compared to the length of the axles. In normal road conditions this may cause the loss of roll stability before yaw stability. Consequently, the vehicle may roll-over and fall on its side. In worse or slippery road conditions, such as on low road friction surface the loss of yaw stability usually occurs before the roll stability. This results in the loss of lateral stability. When the lateral stability is lost, the vehicle unit and moreover combination usually spins, drives off of the roadway and then rolls over, depending on the situation. (Rahkola 2006)

The loss of lateral stability of articulated vehicles can be divided into three common cases, which are presented in figure 12. In the tractor jackknife situation the rear tires of the tractor or truck unit can't produce enough lateral force to steer the vehicle to desired path. In this case the tractor unit also oversteers, which can be the result of the locking of rear tires in braking situation or engine braking. In addition, there is a possibility in low road friction surfaces that the trailer pushes the tractor in cornering situation. Oversteering for a short tractor or truck vehicle can be problematic, because the tractor jackknife occurs fast. The two other cases are related to the trailer unit. The trailer jackknife and trailer swing usually occur as the result of locking of tires in braking situation. Consequently, the tires lose their capability to produce lateral force. After the tires are freed from the tire locking, the trailer unit usually stabilizes itself fast. In the trailer jackknife the front wheels of the trailer unit are not responding to the steering and the vehicle unit tries to drive and push itself off of the roadway. It is notable that in the trailer jackknife the yaw direction of the trailer is opposite to the yaw direction of the tractor unit. In the trailer swing the rear wheels of the trailer unit are not responding to the steering and the trailer swings to the roadside. In the trailer swing case the yaw direction of the trailer unit is the same as the yaw direction of the tractor unit. It is also possible that the trailer swing develops to an oscillation motion between roadsides. The instability of the trailer unit can also be a result of high lateral acceleration. In higher lateral accelerations the tires of the trailer unit can't produce enough lateral force to steer the vehicle to desired path due to the excessive rearward amplification of different state variables. This instability occurs with higher vehicle velocities and is extremely dangerous, because it's hard to control. (Aurell & Edlund 1989; Lehessaari 2007; Rahkola 2006)

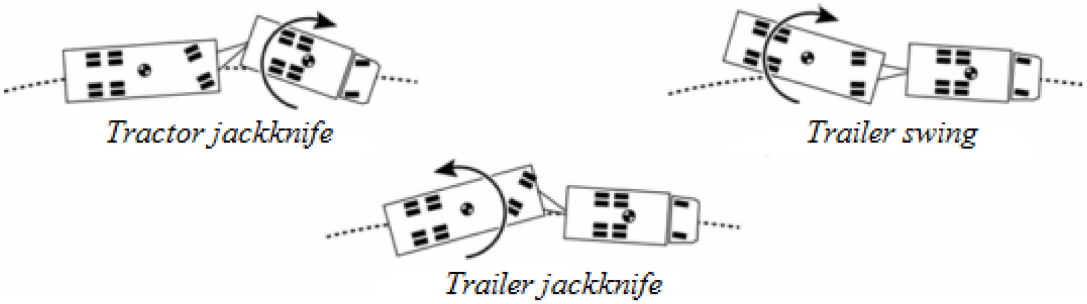

Figure 12. The instability of a tractor-trailer-combination (Rahkola 2006)

The roll stability of an HVC is of significance on good road friction surface, such as normal driving conditions in regular life. The roll-over lateral acceleration limits for most HVCs are between $0.3g$ and $0.7g$ on normal driving conditions (Kamnik et al. 2003a; Sampson & Cebon 2005). The roll stiffness and roll damping are significant factors affecting the vehicle roll stability. Particularly the stiffness differences between the vehicle units of the vehicle combination affect the total roll stability. Traditionally the trailer units have the highest stiffness in vehicle combinations and the lowest stiffness is on the steering axle of the tractor unit (Sampson & Cebon 2005). In general, the heavier latter vehicle units and particularly rear axles have the highest stiffnesses compared to lighter vehicle units or front axles. Usually the trailer units have over two times the stiffness of the tractor unit (Tabatabaei Oreh et al. 2014). This improves the roll and overall stability of the vehicle combination, as most of the load transfers occur in the lighter vehicle units and the heavier vehicle units act more gradual (Kamnik et al. 2003a; Sampson & Cebon 2005).

The developed simulation model in this thesis particularly simulates different test-drives on low road friction surfaces. Consequently, the possibility for the vehicle combination to reach such roll-over lateral acceleration limits is unrealistic, because the vehicle combination tends to spin before it reaches this lateral acceleration range. The lateral acceleration spin limit of an HVC on a low road friction surface can be as low as $0.2g$, therefore the roll stability in these simulations are not significant. Additionally, large vehicle slip angles on low road friction surfaces with higher vehicle forward velocities are considered dangerous. A vehicle unit slip angle of 2.5° is considered as the limit, where the tires of the vehicle unit may surpass the linear region of the lateral force on low road friction surfaces (figures 5 and 8). This is emphasized later in the simulation chapter, where the MF parameters for the simulations of this thesis are addressed more in depth (figures 26 and 27). The tire slip angle was not only dependent on the lateral velocity, but the yaw velocity as well. A vehicle unit travelling at a forward velocity of 80 km/h with a vehicle unit slip angle of 2.5° has over 1 m/s lateral velocity. This may promote the instability of the vehicle combination as a form of excessive sliding, when the tires are very close to the nonlinear region of the lateral force. However, simulations on a better road friction surface are performed in order to compare the effect of roll stability versus yaw stability for heavy vehicles and the effect of different road friction surfaces. (Giangiulio 2005b; Kamnik et al. 2003b; Sampson & Cebon 2005)

For vehicles with multiple articulations, other types of instability has been found. An articulated vehicle travels in a straight line and the front tires of the tractor unit lock. The motion itself is mathematically stable, however, the driver loses control. An articulated vehicle travels in a straight line and the tires of the trailer unit lock. This results in a large articulation angle at the dolly unit. It is also possible for the trailer unit of a vehicle combination to start oscillate between the roadsides. This motion is mathematically stable, although, the movements are broad and uncontrollable by the driver. Theoretically more types of instability exist, but they have not been encountered. (Luijten 2010)

A vehicle combinations stability and handling are often analyzed with two performance measures (Luijten 2010):

- The maneuverability and required space for a vehicle combination to fit in the existing infrastructure.
- Directional stability and roll-over to evaluate lateral dynamic behavior

The first performance measure includes the swept-path, high and low-speed off-tracking and out-swing of the vehicle combination. The second performance measure includes static roll-over threshold, dynamic load transfer ratio, yaw damping ratio and rearward amplification.

The rearward amplification (RA) quantifies the dynamic lateral acceleration, yaw acceleration, yaw velocity, lateral velocity or any other state variable amplification from the towing unit to the other vehicle units. The RA can be defined in two following ways (Fancher 1985; Luijten et al. 2012):

$$RA_t = \frac{\max|i_n|}{\max|i_{towing}|}, \tag{58}$$

$$RA_f = \max\left|\frac{H_{i_{n,\delta}}(\omega)}{H_{i_{towing,\delta}}(\omega)}\right| = \max\left|H_{i_n,i_{towing}}(\omega)\right|. \tag{59}$$

In the first definition (58), the RA is calculated using time histories of the measured variable. This means, that the absolute maximal values of the n^{th} unit and the tractor unit are divided. In the second definition (59), the RA is defined as the maximum gain between two frequency response functions. The frequency response function between the measured variable gain of the n^{th} unit to the steering angle of the front axle of the towing unit $H_{i_{n,\delta}}(\omega)$, and the measured variable of the towing unit to the steering angle of the front axle of the towing unit $H_{i_{tractor,\delta}}(\omega)$. Figure 13 shows that the two different definitions can give different RA results in a same single sine wave input simulation.

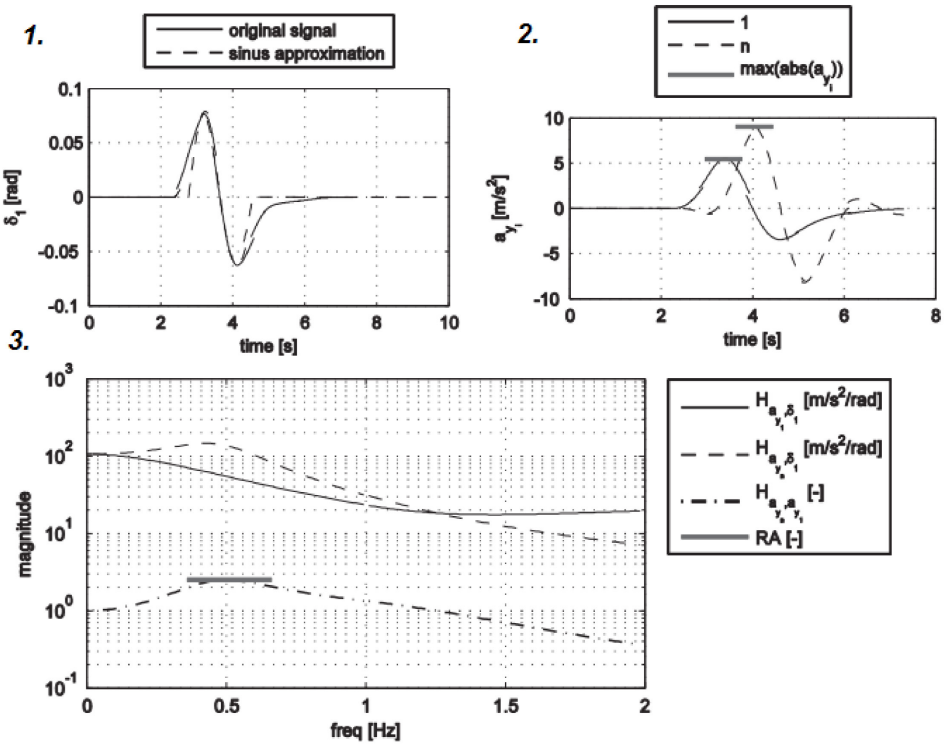

Figure 13. RAs in different definitions, with $u = 25$ m/s (Luijten et al. 2012)

The graph 13.1 represents the steering input of the front axle of the towing unit. The different RA-values can be read from the graph 13.2 for the time domain definition $RA_t = \frac{9.0}{5.5} = 1.6$ and from the graph 13.3 for the frequency response function definition $RA_f = 2.5$. Generally, the RA-values of different state variables over 1.5 are considered dangerous and they may cause the loss of control of the vehicle combination. The calculation approach is different between these two RA definitions. In the time domain, the absolute maximal values are divided, whereas in the frequency domain the gains are divided first and then the maximal value is calculated. In the time domain approach, the phase information is lost. Usually the phase difference is observed afterwards from the time domain approach simply as the time and motion delay between the vehicle units. The phase difference intuitively indicates the time delay for motions in a vehicle combination, which is of interest when evaluating performance measures and safety. (Luijten et al. 2012)

The dynamic stability of an articulated vehicle combination or a single vehicle unit can be evaluated also from the matrix notation of the linear model in steady state or transient state response. In the linear model, the dynamic stability is a characteristic for the system and it holds in the entire state space. The eigenvalues of the dynamic matrix A can be

solved. The eigenvalues λ_i for dynamic matrix $A = M^{-1}C$ are complex numbers and they can be expressed in the form of (Rahkola 2006):

$$\lambda_i = a_i + \boldsymbol{j} b_i. \tag{60}$$

The sign of the real part a_i determines the stability. If the real part is negative, the vehicle combination is stable and if the real part is positive, the vehicle combination is unstable. However, the imaginary part b_i determines the behavior of the vehicle. When the imaginary part is nonzero, the behavior is periodic oscillatory. While the imaginary part is zero, the behavior is aperiodic oscillatory. (Genta 1997)

The principle effect of different eigenvalues λ_i on the state variables x_i over time are presented in figure 14.

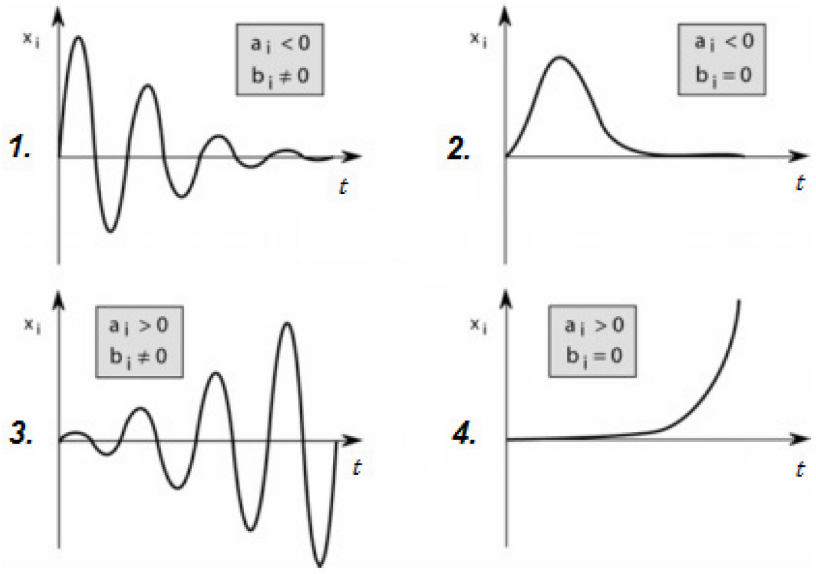

Figure 14. The principle of eigenvalue solutions (Rahkola 2006)

In graphs 14.1 and 14.2 the oscillation is damping and asymptotically approaching the equilibrium, because the real part is less than zero. The difference between the graphs can be seen in the sign of the imaginary part. In the graph 14.1 the oscillation is periodic where as in the graph 14.2 it is aperiodic. In graphs 14.3 and 14.4 the oscillation is diverging and unstable, because the real part is greater than zero. The imaginary part determines the nature, in graph 14.3 the oscillation is periodically diverging and in graph 14.4 the oscillation is aperiodically diverging. (Genta 1997; Rahkola 2006)

The vehicle dimensioning and structural parameters are of significance to vehicle stability, particularly, to the stability of vehicle combinations. The following overview is a list of various parameters and dimensions that have significant effect on the stability boundaries of a vehicle with articulations (Fancher & Mathew 1987; Hac et al. 2008):

- Axle and vehicle dimensions
- Location of center of gravity
- Drawbar length
- Vehicle wheelbases
- Types of coupling
- Coupling rear overhang

- Number of articulations
- Number and distance of axles on a vehicle unit
- Number of wheels on an axle

The vehicle dimensions and the location of CoG affect the stability. Long and wide vehicle combinations are more stable, but their swept-path, off-tracking and out-swing suffer. A low CoG increases stability, whereas high CoG decreases. The CoG should be located near axles and articulation points, this improves the overall stability of the vehicle. A long drawbar reduces RA, but the swept-path, off-tracking and out-swing of the vehicle combination suffer. A short wheelbase of a trailer unit results in a low trailer yaw damping, which leads to higher RA-values. However, long wheelbases also increase the swept-path, off-tracking and out-swing of a vehicle combination. A rigid body and stiff structure components increase stability, as the dynamic load transfers decrease, which moreover increase the roll and yaw stability as was indicated earlier. (Fancher & Mathew 1987; Luijten 2010)

Two main types of coupling are A and B type couplings. The A-type coupling is a towing hitch with drawbar connection. This type is not favorable for dynamic stability, but it has a better swept-path compared to B-type coupling. The A-type coupling is also called the rear hang coupling. The B-type coupling is a fifth wheel connection and it is favorable for dynamic vehicle behavior. The B-type coupling is also called the overhang coupling. The number of articulations affect the RA, more articulation joints increase it towards the end of the vehicle combination. The distance between the coupling point and the rear axle of towing unit has a large effect on stability. The dynamic stability of a vehicle combination suffers, if the coupling point is far away from the rear axles of the towing unit. (Hac et al. 2008; Luijten 2010)

During turning and cornering situations the amount of load transfer from side to side is considered large for heavy fleet vehicles, because of the overall mass and location of CoG of heavy fleet vehicles. There are national and international legislations and restrictions for the axle loads of heavy vehicles. Consequently, multiple wheels and axles are introduced. The number of axles and wheels on an axle affect the vertical wheel load distribution. The greater number of axles and wheels improves the stability, as the vertical load of a single wheel is decreased. Therefore, a single tire performs better in the linear region, as was shown in the figure 5. As the vertical load of a single wheel doesn't exceed the linear region, the production of lateral force in a single tire is possible linearly further and thus the production of overall axle effective lateral force increases. Consequently, the effect of wheel load transfer also decreases significantly, as the multiple wheels and axles share the static and dynamic load transfer and the vehicle unit becomes more stable. In addition, the multiple rear axles stabilize the vehicle, as the multiple axles introduce yaw moments which resist the total yaw motion of the vehicle. This phenomena can be visualized by thinking of an equivalent wheelbase. The effect of a dual axle or a twin wheel is presented in figure 15. (Aurell & Edlund 1989; Fancher 1989)

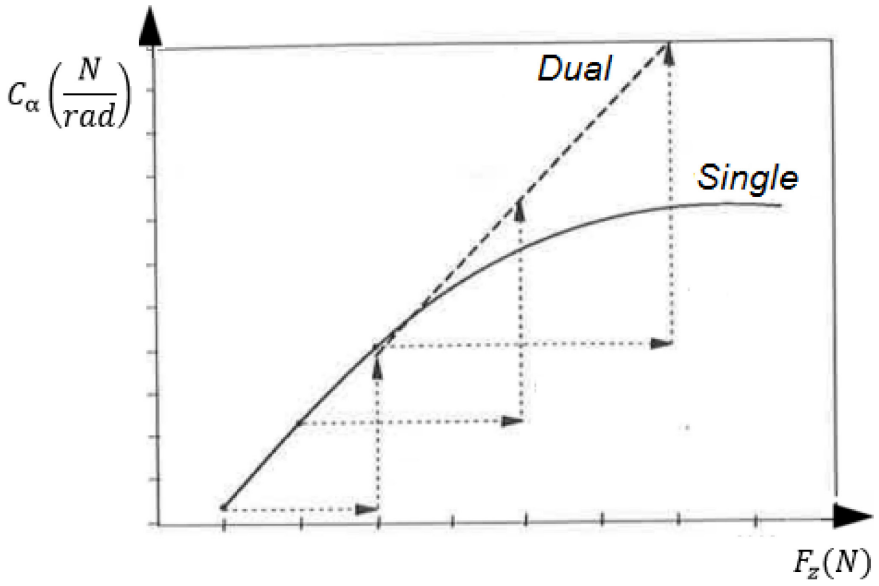

Figure 15. The effect of dual axle or twin wheel on the axle effective cornering stiffness versus vertical force characteristics (Fancher 1989)

The tires of heavy fleet vehicles differ from regular vehicle tires. Particularly the form of the cornering stiffness characteristics of a heavy fleet tire differs from that of a passenger car tire in one important aspect. Specifically, the relationship between cornering stiffness and vertical load increases monotonically up to much higher vertical loads. Consequently, these heavy fleet tires are considered to be almost completely linear in regular road transport due to these tire characteristics. This means that as the load on an axle increases, the ratio of load divided by cornering stiffness, the "cornering compliance", tends to stay constant to very high vertical loads. Therefore, it is said that a tire feature of a heavy fleet vehicle has a built-in mechanism for load sensing proportioning of the lateral force characteristics of each tire over the wide range of loads. However, if the nominal load carrying capacity is surpassed, the tire becomes nonlinear. In addition, the level of tire wear has a great impact on cornering stiffness. The linearity of cornering stiffness of a worn tire and vertical load carrying capability suffers compared to new tire. This effect of wear and the relationship between cornering stiffness and vertical load are presented in figures 16 and 17. (Fancher 1989)

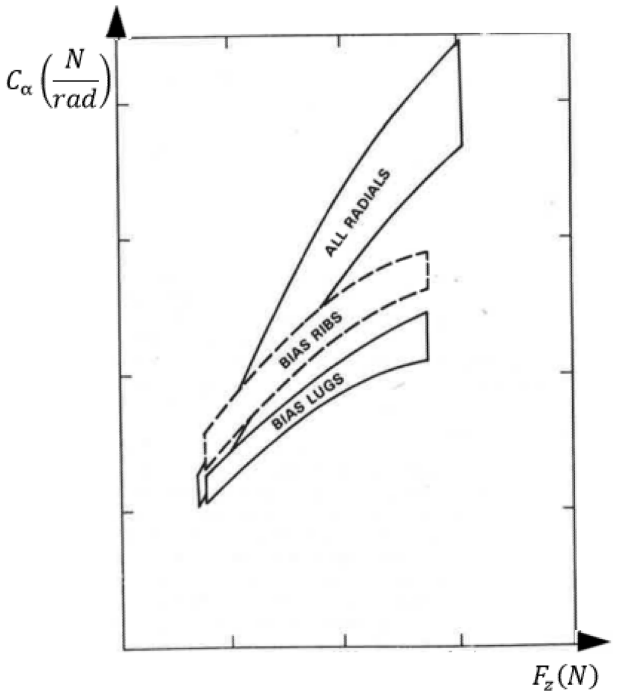

Figure 16. The relationship between cornering stiffness and vertical force on different tires (Fancher 1989)

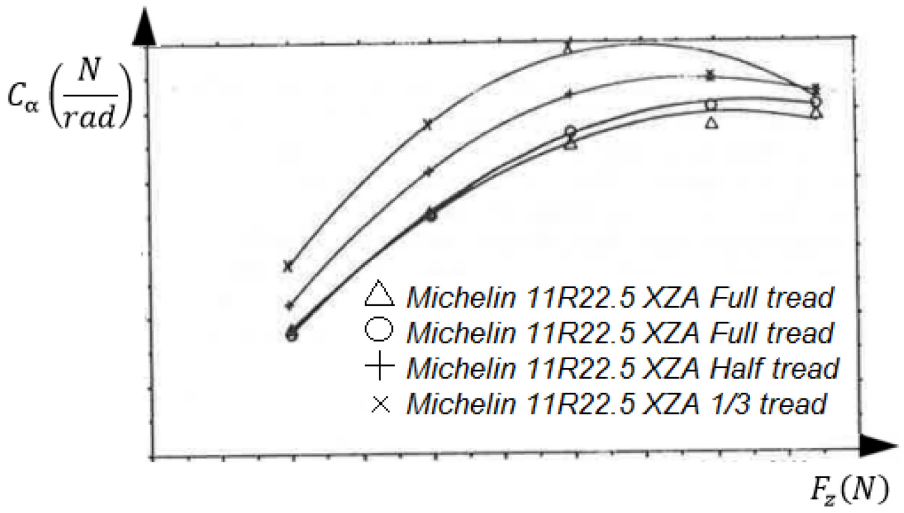

Figure 17. The impact of wear on a tire (Fancher 1989)

A truck and semi-trailer combination, a vehicle with one articulation is particularly now under examination. A truck plus semi-trailer are the first two vehicle units of the Double-A combination. Pacejka and Genta has studied the dynamics of a vehicle with one articulation, specifically passenger car and trailer combination (Genta 1997; Pacejka 2006). In addition, Pauwelussen has done research on the car plus trailer combination, particularly on the maneuverability and required space for a vehicle combination to fit in the existing infrastructure (Pauwelussen 2015). Furthermore, the dynamics of multiple articulated vehicles has been studied widely in Sweden, Finland and Netherlands (Aurell & Edlund 1989; Lehessaari 2007; Luijten 2010; Rahkola 2006). Additionally, Paul Fancher has studied multi-articulated vehicles in Michigan (Fancher 1989).

The dynamics of a vehicle with one articulation follow the exact same principles as a single vehicle unit in the bicycle model. Although, the vehicle consists of two vehicle units. The combination is modelled as two single rigid bodies articulated to each other. The rigid body assumption is based on the implication of cylindrical articulation which has an axis perpendicular to the road. The articulation link acts as a kinematic constraint between the vehicle units and produces a force of constraint. However, it transmits the dynamic forces and phenomena between the vehicles and acts as a back coupling link. Practically the vehicle units have both three degrees of freedom (3-DoF). By introducing the two equations for the constraint due to the articulation, the degrees of freedom can be reduced from six possible DoFs to four by eliminating excess equations and variables. In general, a vehicle combination with one articulation is a four degree of freedom (4-DoF) vehicle. (Genta 1997; Pacejka 2006)

Similarly, the exact same assumptions and restrictions for a vehicle with one articulation hold as for the single vehicle unit in single-track model. If any new assumptions or restrictions appear, they will be introduced and derived. The model is similarly derived with regular mechanics, however, it is possible to use the Lagrange equations of motions and the principle of virtual work. Both the linear and nonlinear tire characteristics as well as the matrix notation are derived for the vehicle combination. The free body diagram of a tractor plus semi-trailer combination with multiple axles and wheels is presented in figure 18.

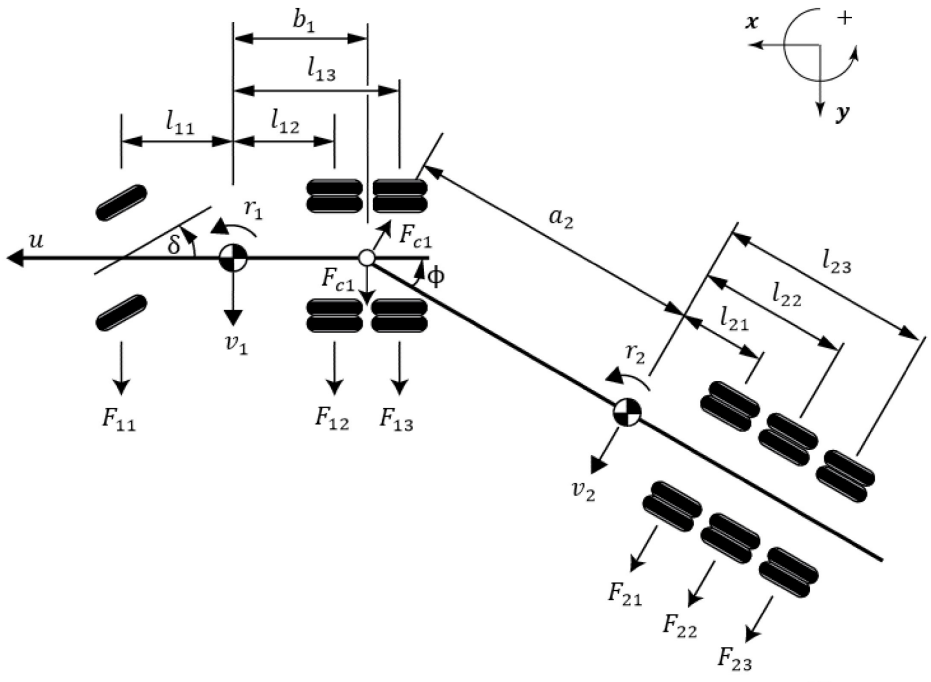

Figure 18. A free body diagram of a tractor plus semi-trailer combination

The vehicle combination is in a fixed position of a cornering situation with a constant steering angle δ and velocity u. The Newton's equations of motion are written separately for each vehicle unit. The longitudinal direction x is considered insignificant in the examination of lateral dynamics. By including the lateral acceleration equation (5), the Newton's equations of motions read (Pacejka 2006):

$$\sum F_{x1} = 0, \tag{61}$$

$$\sum F_{y1} = m_1 a_{y1} = m_1(\dot{v}_1 + u r_1) = F_{11} + F_{12} + F_{13} + F_{c1}, \tag{62}$$

$$\sum M_{z1} = I_1 \dot{r}_1 = F_{11} l_{11} - F_{12} l_{12} - F_{13} l_{13} - F_{c1} b_1, \tag{63}$$

$$\sum F_{x2} = 0, \tag{64}$$

$$\sum F_{y2} = m_2 a_{y2} = m_2(\dot{v}_2 + u r_2) = F_{21} + F_{22} + F_{23} - F_{c1}, \tag{65}$$

$$\sum M_{z2} = I_2 \dot{r}_2 = -F_{21} l_{21} - F_{22} l_{22} - F_{23} l_{23} - F_{c1} a_2. \tag{66}$$

The force of constraint acting between the vehicle units is the articulation force F_{c1}. The articulation force is based on the Newton's third law. The two additional equations for the constraint force can be written as (Fancher 1989; Genta 1997):

$$\dot{\phi} = r_1 - r_2, \tag{67}$$

$$v_2 = v_1 - b_1 r_1 - a_2 r_2 + u\phi, \tag{68}$$

In addition, the time derivative of the lateral velocity v_2 is required:

$$\dot{v}_2 = \dot{v}_1 - b_1 \dot{r}_1 - a_2 \dot{r}_2 + u\dot{\phi}. \tag{69}$$

The articulation dynamics are relatively complex. The lateral velocity of the 2nd vehicle unit is dependent on the other velocities of the system. They either increase or decrease it from a distance of a point of application based on the coordinate system. The equations (67) and (68) are formed, when the free body diagram of the articulation point is under examination. Furthermore, the equation (69) is simply the derivative in respect of time of the equation (68). (Aurell & Edlund 1989; Fancher 1989)

Four equations are required for a 4-DoF system. The equations are solved and chosen in a way that the desired state variables are left in the equations. Lateral velocities, yaw velocities and articulation angles are traditionally the most suitable variables for describing the lateral dynamic behavior of an articulated vehicle. Moreover, the vehicle unit slip angles can be calculated from these state variables easily afterwards. In this case the chosen state variables are $\overline{x} = [v_1\ r_1\ r_2\ \phi]^T$. The dynamic system can be solved in a form that the examination of vehicle dynamics is possible, however, the linear or nonlinear characteristics of the tire forces are not yet considered.

In the linear equations, the axle effective lateral forces are considered. In addition, the twin wheels are considered as a single equivalent wheel. The effect of multiple axles is taken into account in the equations of motions. The linear tire characteristics and slip angles can be derived similarly to single vehicle unit model. The slip angles and linear lateral forces are based on the same geometrical assumptions and equations as in the single vehicle unit. The general slip angle and lateral force for non-steered axles can be derived from the equations (7) and (11):

$$\alpha_{ij} = \frac{r_i l_{ij} - v_i}{u}, \tag{70}$$

$$F_{ij} = C_{ij}\alpha_{ij} = C_{ij}\left(\frac{r_i l_{ij} - v_i}{u}\right), \tag{71}$$

where the index i represents the vehicle unit and the index j represents the axle of the vehicle unit. Respectively, the front axle of the towing vehicle is the steering axle.

Consequently, the lateral force and slip angle for the first axle is derived similarly as in the equation (10):

$$F_{11} = C_{11}\alpha_{11} = C_{11}\left(\delta - \frac{r_1 l_{11} + v_1}{u}\right). \quad (72)$$

It is possible that the rear vehicle units have steered axles or front axles. In these cases, the derivation of slip angles and lateral forces is according to the same geometrical principles and assumptions as in the case of the front axle of a single vehicle or a towing vehicle. However, in this case, the introduction is considered beyond scope.

The linear lateral dynamic behavior of a vehicle combination can be modelled similarly in state space as a feedback control system with the matrix notation. The matrix notation can be solved from the system of equations, by eliminating every excess variable. The matrix notation can be solved either in the matrix form of the equation (20) or equation (21). The size of the matrices correlate with the number of DoF. In general, it can be derived that for an n-DoF dynamic system, the number of state variables is equal to the number of DoF. In addition, the matrices of the n-DoF system are n-square or n-column matrices. Although, it is possible to include extra state variables for a vehicle combination if desired. In that case, more equations are required, but no extra DoFs.

The nonlinear tire characteristics and wheel load transfers can be derived exactly by the same principles as for a single vehicle unit. The vehicle units are considered one at a time individually, but due to the two equations for the constraint force the dynamic connection is formed.

The Magic Formula is considered similarly for a single wheel. The vertical load for a single wheel isn't self-explanatory. For the simplicity, the twin wheels can first be considered as a single equivalent wheel if necessary. The wheel load transfers and static vertical loads are considered more in depth. The vertical load distribution is greatly dependent on the coupling type. If the coupling type is a B-type overhang coupling, then a portion of the mass of the latter unit is distributed to the vehicle unit in front of that unit. Respectively, if the coupling type is an A-type rear hang coupling, the static and dynamic load transfers between vehicle units are negligible and therefore usually considered zero. In the case of multiple axles, the vertical load distribution is derived by considering an equivalent axle first. Furthermore, the vertical load of an equivalent axle is distributed equally among the real axles. This method gives accurate enough results in terms of analytical model. The consideration of vertical load distribution begins from the last vehicle unit. Finally, the static vertical loads for a tractor plus semi-trailer combination in figure 18 can be derived.

It is assumed for the sake of simplicity that all the axles exist equally in the center line of the vehicle unit. This means that the left and right side lengths are equal for all the axles in the same vehicle unit.

$$t_{11l} = t_{11r}, \quad t_{12l} = t_{12r} \ldots t_{ijl} = t_{ijr}. \quad (73)$$

The load of the rear equivalent axle of the semi-trailer and the load of the front side of the semi-trailer read:

$$F_{zs2F} = \frac{l_{22}}{a_2 + l_{22}} m_2 g, \quad (74)$$

$$F_{zs2R} = \frac{a_2}{a_2 + l_{22}} m_2 g. \quad (75)$$

The index s represents the static wheel load term. Furthermore, the rear axle equivalent load is divided equally for the three axles:

$$F_{z21} = F_{z22} = F_{z23} = \frac{1}{3}F_{zs2R} = \frac{1}{3}\frac{a_2}{a_2+l_{22}}m_2 g. \tag{76}$$

Now the vertical load of a single wheel on the rear axles is dependent on the number of wheels on the axle. If all the wheels are considered, there are 4 wheels per a rear axle, 2 at each side. Consequently, the single wheel static vertical load of the semi-trailer rear axle read:

$$F_{zs211} = F_{zs212} = F_{zs213} \ldots F_{zs2jk} = \frac{1}{4}\cdot\frac{1}{3}F_{zs2R} = \frac{1}{12}\frac{a_2}{a_2+l_{22}}m_2 g, \tag{77}$$

where the index k represents the number of wheel on the axle. The vertical load of the front side of the CoG of the semi-trailer is distributed for the truck vehicle unit and the mass is located at the coupling point. Respectively, the rear axles of the tractor unit are considered as an equivalent axle first, so the front axle load of the semi-trailer can be distributed:

$$F_{zs1F,2} = \frac{\frac{(l_{13}+l_{12})}{2}-b_1}{l_{11}+\frac{(l_{13}+l_{12})}{2}}F_{zs2F}, \tag{78}$$

$$F_{zs1R,2} = \frac{l_{11}+b_1}{l_{11}+\frac{(l_{13}+l_{12})}{2}}F_{zs2F}. \tag{79}$$

It is also possible that in some cases the overhang coupling point is located after the rear axles or equivalent rear axle. In these cases the rear axles carry all the vertical load from the latter vehicle unit and it is usually divided equally between the rear axles. However, if desired, it is possible to calculate the exact distribution for the rear axles. Respectively, the own mass of the tractor unit is distributed between the axles:

$$F_{zs1F,1} = \frac{\frac{(l_{13}+l_{12})}{2}}{l_{11}+\frac{(l_{13}+l_{12})}{2}}m_1 g, \tag{80}$$

$$F_{zs1R,1} = \frac{l_{11}}{l_{11}+\frac{(l_{13}+l_{12})}{2}}m_1 g. \tag{81}$$

Consequently, the total axle masses for the truck unit consists of the own mass of the tractor unit plus the distributed mass from the semi-trailer unit:

$$F_{zs1F} = F_{zs1F,1} + F_{zs1F,2}, \tag{82}$$

$$F_{zs1R} = F_{zs1R,1} + F_{zs1R,2}. \tag{83}$$

Finally, the single wheel loads can be divided similarly from the front axle load and equivalent rear axle load:

$$F_{zs11k} = \frac{1}{2}F_{zs1F}, \tag{84}$$

$$F_{zs12k} = F_{zs13k} = \frac{1}{8}F_{zs1R}. \tag{85}$$

The dynamic wheel load transfers are complicated. However, because of the examination of lateral dynamic behavior, the longitudinal wheel load transfers were considered beyond scope. The lateral wheel load transfers can be derived by the same principles as for the

single vehicle unit. The dynamic wheel load transfer of a single axle can be derived from the respective static axle load. In the case of the twin wheels, an equivalent wheel is similarly to an equivalent axle considered first. Furthermore, the distribution of wheel load transfer is assumed equal between the twin wheels, but exact lever arm dimensions can be used for the single wheels on the twin wheel setting if desired. Although, the difference between the equivalent wheel and the real lever ratio is negligible in terms of wheel load transfer effect on the lateral dynamic behavior. A generic dynamic lateral wheel load transfer formula for a rear equivalent wheel reads:

$$F_{zdijkR} = \frac{2}{wpa_j}\frac{1}{rapv_i}\frac{h_i}{t_{ij}}F_{zsiR}\frac{a_{yi}}{g}, \tag{86}$$

where index d represents the dynamic wheel load transfer, wpa_j represents the number of wheels on the respective axle and $rapv_i$ represents the number of rear axles on the respective vehicle unit. Similarly for the front axles:

$$F_{zdijkF} = \frac{2}{wpa_j}\frac{1}{fapv_i}\frac{h_i}{t_{ij}}F_{zsiF}\frac{a_{yi}}{g}, \tag{87}$$

where $fapv_i$ represents the number of front axles on the respective vehicle unit. As derived earlier, the lateral wheel load transfer terms are similar on the both side of the axle, but the difference is in the sign. The sign is dependent on the prevailing coordinate system. Generally, the wheel loads transfer from inner wheels to outer wheels. Finally, the dynamic wheel load terms for this particular tractor plus semi-trailer vehicle combination:

$$F_{zd111} = -F_{zd112} = \frac{2}{2}\frac{1}{1}\frac{h_1}{t_{11}}F_{zs1F}\frac{a_{y1}}{g} = \frac{h_1}{t_{11}}F_{zs1F}\frac{a_{y1}}{g}, \tag{88}$$

$$F_{zd121} = F_{zd122} = -F_{zd123} = -F_{zd124} = \frac{2}{4}\frac{1}{2}\frac{h_1}{t_{12}}F_{zs1R}\frac{a_{y1}}{g} = \frac{1}{4}\frac{h_1}{t_{12}}F_{zs1R}\frac{a_{y1}}{g}, \tag{89}$$

$$F_{zd131} = F_{zd132} = -F_{zd133} = -F_{zd134} = \frac{2}{4}\frac{1}{2}\frac{h_1}{t_{13}}F_{zs1R}\frac{a_{y1}}{g} = \frac{1}{4}\frac{h_1}{t_{13}}F_{zs1R}\frac{a_{y1}}{g}, \tag{90}$$

$$F_{zd211} = F_{zd212} = -F_{zd213} = -F_{zd214} = \frac{2}{4}\frac{1}{3}\frac{h_2}{t_{21}}F_{zs2R}\frac{a_{y2}}{g} = \frac{1}{6}\frac{h_2}{t_{21}}F_{zs2R}\frac{a_{y2}}{g}, \tag{91}$$

$$F_{zd221} = F_{zd222} = -F_{zd223} = -F_{zd224} = \frac{2}{4}\frac{1}{3}\frac{h_2}{t_{22}}F_{zs2R}\frac{a_{y2}}{g} = \frac{1}{6}\frac{h_2}{t_{22}}F_{zs2R}\frac{a_{y2}}{g}, \tag{92}$$

$$F_{zd231} = F_{zd232} = -F_{zd233} = -F_{zd234} = \frac{2}{4}\frac{1}{3}\frac{h_2}{t_{23}}F_{zs2R}\frac{a_{y2}}{g} = \frac{1}{6}\frac{h_2}{t_{23}}F_{zs2R}\frac{a_{y2}}{g}. \tag{93}$$

The total amount of vertical load for a single wheel consists of the static and dynamic wheel load terms, as earlier derived:

$$F_{zijk} = F_{zsijk} + F_{zdijk}. \tag{94}$$

The nonlinear tire characteristics can be combined from the vertical loads and MF model for each tire, similarly as in the equation (51). This results in a nonlinear model. The MF parameters are found from literature for heavy vehicles or measured in practical tests. The sum of the single lateral tire forces of the axle is similarly the effective lateral force of the axle. The same Newton's equations of motion (61)-(69) still apply for the truck and semi-trailer combination. The nonlinear solution is possible to derive by substituting the nonlinear lateral forces to the Newton's equations of motion and solving the system similarly to the linear model by eliminating excess variables and equations. The equations

of motion form a nonlinear first-order differential algebraic system of equations, similarly to a nonlinear single vehicle. The state vector is the same as in the corresponding linear model $\bar{x} = [v_1\ r_1\ r_2\ \phi]^T$. The differential algebraic system of equations can be solved in a time domain simulation as numeric integral.

3 Lateral dynamics of Double-A

The lateral dynamics of the Double-A vehicle combination are presented and derived in this chapter based on the theory in the chapter 2. Furthermore, a simulation model is implemented and designed based on the lateral dynamics of the Double-A combination. The simulation model is constructed with both linear and nonlinear tire characteristics.

The Double-A vehicle combination is a combination with three articulations. Globally, the combination is known as the Double-A combination, but other names are also found. For example the combination with derogations of law restrictions driven in Finland is commonly known with the name of DUO2 combination. The combination consists of a tractor, semi-trailer, dolly and semi-trailer vehicle units. The combination is 32 meters long and weighs up to 80 000 kilograms. Currently, in Finland these vehicle combinations are driven with derogations of law restrictions. The Double-A combination is presented in figure 19.

Figure 19. The Double-A combination

The tractor unit of the Double-A combination is equipped with twin wheels on all axles except the front steering axle. The semi-trailer units are either single or twin wheel semi-trailer units. The tractor unit has two rear axles and the semi-trailers have three rear axles each. The tractor unit has a tandem drive, a weight of 9 680 kilograms and a total length of 6.615 meters. The semi-trailers are standard three-axle cargo semi-trailers, which have a length of 13.715 meters and a maximum weight of 33 320 kilograms. The dolly unit is a standard twin axle twin wheel dolly vehicle unit with a length of 5.01 meters and weight of 2 500 kilograms. All the vehicle units are 2.5 meters wide and the axle widths are 2 meters. The first and third articulations are overhang coupled and the second articulation is rear hang coupled. The dimensions and parameters for the Double-A combination could be obtained from literature and industry (Kamnik et al. 2003a; Luijten 2010; Otto Lahti (Trafi) 2015; Rahkola 2006).

The Double-A combination is equipped with two safety systems. The first system is a traditional ABS, which is connected by the CAN-channel of the tractor unit between the different vehicle units. This means that the ABS can function individually in a specific vehicle unit if only the wheels of the axles of the specific vehicle unit lock in a braking situation. Additionally, the cargo semi-trailers are equipped with an active roll-over prevention system. The system requirements are regulated in the UNECE E-regulation of ECE-R13. The roll-over prevention system means a function within a vehicle stability function that reacts to an impending roll-over in order to stabilize the vehicle unit during dynamic maneuvers within the physical limits of the vehicle. In practice this means that the vehicle unit brakes certain wheels in a specific way that it creates yaw moments to the

opposite direction of the yaw velocity in order to calm down and stabilize the vehicle unit in the maneuver. (Otto Lahti (Trafi) 2015; United Nations (UNECE) 2008)

Additional observations were obtained from an interview with a logistics company, which had Double-A combinations in circulation with derogations of law restrictions. The number of wheels on the semi-trailer rear axles being used may change. The semi-trailer is equipped with single or twin wheels, dependent on the cargo type and weight being transferred. With a low CoG and weight cargo, only single wheel semi-trailers are being used in order to gain economical savings. With a high CoG and weight cargo it's vice versa. Furthermore, the dolly vehicle unit has a telescope drawbar. This means that the length of the drawbar can be adjusted if desired. With a low CoG and weight cargo the drawbar can be adjusted shorter without too much of stability and maneuverability losses. With a high CoG and weight cargo the drawbar is adjusted longer to increase the stability and maneuverability.

The dynamics of Double-A is based on the same principles and theory as the single vehicle and tractor plus semi-trailer combination. The same assumptions, restrictions and principles hold as for the earlier derived vehicles. If any new assumptions or restrictions appear, they will be introduced and derived. The only difference compared to the earlier derived combinations, is that Double-A has four vehicle units and three articulations. Similarly, the single vehicle units have 3-DoF. By introducing the six equations for the constraint forces due to the three articulations, the degrees of freedom can be reduced to eight from the total of twelve possible DoF by eliminating excess equations and variables. Respectively, a vehicle combination with three articulations and four vehicle units is generally an eight degree of freedom (8-DoF) vehicle combination. The model is similarly derived with regular mechanics, however, it is possible to use the Lagrange equations of motions and the principle of virtual work if desired. Both the linear and nonlinear tire characteristics are derived for the vehicle combination. The free body diagram of the Double-A combination is presented in figure 20.

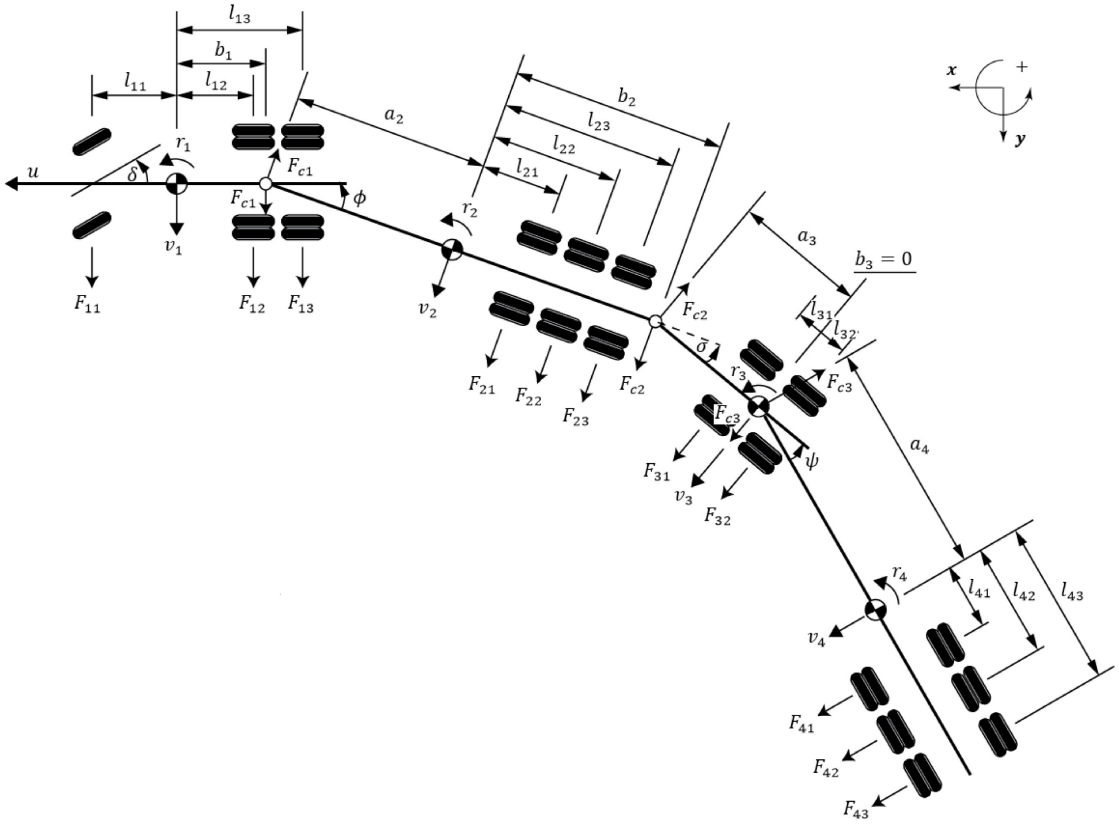

Figure 20. Double-A free body diagram

The Double-A is in a fixed position of a cornering situation with a constant steering angle δ and velocity u. Similarly, the Newton's equations of motion are written separately for each vehicle unit. The Newton's equations of motions read (Luijten 2010; Rahkola 2006):

$$\sum F_{y1} = m_1 a_{y1} = m_1(\dot{v}_1 + u r_1) = F_{11} + F_{12} + F_{13} + F_{c1}, \tag{95}$$

$$\sum M_{z1} = I_1 \dot{r}_1 = F_{11} l_{11} - F_{12} l_{12} - F_{13} l_{13} - F_{c1} b_1, \tag{96}$$

$$\sum F_{y2} = m_2 a_{y2} = m_2(\dot{v}_2 + u r_2) = F_{21} + F_{22} + F_{23} - F_{c1} + F_{c2}, \tag{97}$$

$$\sum M_{z2} = I_2 \dot{r}_2 = -F_{21} l_{21} - F_{22} l_{22} - F_{23} l_{23} - F_{c1} a_2 - F_{c2} b_2, \tag{98}$$

$$\sum F_{y3} = m_3 a_{y3} = m_3(\dot{v}_3 + u r_3) = F_{31} + F_{32} - F_{c2} + F_{c3}, \tag{99}$$

$$\sum M_{z3} = I_3 \dot{r}_3 = F_{31} l_{31} - F_{32} l_{32} - F_{c2} a_3 + F_{c3} b_3. \tag{100}$$

$$\sum F_{y4} = m_4 a_{y4} = m_4(\dot{v}_4 + u r_4) = F_{41} + F_{42} + F_{43} - F_{c3}, \tag{101}$$

$$\sum M_{z4} = I_4 \dot{r}_4 = -F_{41} l_{41} - F_{42} l_{42} - F_{43} l_{43} - F_{c3} a_4. \tag{102}$$

Similarly, the equations for the constraint forces F_{c1}, F_{c2} and F_{c3} can now be written as (Luijten 2010; Rahkola 2006):

$$\dot{\phi} = r_1 - r_2, \tag{103}$$

$$\dot{\sigma} = r_2 - r_3, \tag{104}$$

$$\dot{\psi} = r_3 - r_4, \tag{105}$$

$$v_2 = v_1 - b_1 r_1 - a_2 r_2 + u\phi, \tag{106}$$

$$\dot{v_2} = \dot{v_1} - b_1 \dot{r_1} - a_2 \dot{r_2} + u\dot{\phi}, \tag{107}$$

$$v_3 = v_2 - b_2 r_2 - a_3 r_3 + u\sigma, \tag{108}$$

$$\dot{v_3} = \dot{v_2} - b_2 \dot{r_2} - a_3 \dot{r_3} + u\dot{\sigma}, \tag{109}$$

$$v_4 = v_3 - b_3 r_3 - a_4 r_4 + u\psi, \tag{110}$$

$$\dot{v_4} = \dot{v_3} - b_3 \dot{r_3} - a_4 \dot{r_4} + u\dot{\psi}. \tag{111}$$

Eight equations are required for an 8-DoF system. The equations are solved and chosen in a way that the desired state variables are left in the equations. In this case the chosen state variables are $\overline{x} = [v_1\ v_2\ v_3\ v_4\ r_1\ r_2\ r_3\ r_4]^T$. The dynamic system can be solved in a form that the examination of the vehicle lateral dynamics is possible, however, the linear or nonlinear characteristics of the tire forces are not yet considered.

The linear model could be derived similarly to the single vehicle or the tractor plus semi-trailer combination. The same assumptions, restrictions and principles hold. The slip angle (70), the general linear lateral force (71) and the linear lateral force and slip angle of the steering axle of the towing unit (72) are substituted to the chosen equations of motions. Although, the simulations and examination of the Double-A combination in this thesis is particularly emphasizing the low road friction surfaces. Therefore, the linear model isn't suitable as was earlier indicated and it is not being used in the simulations. The linear model principles are just mainly presented in this chapter for the Double-A, because they function as a basis for the nonlinear characteristics.

It is possible that the rear vehicle units have steered axles or front axles. In these cases, the derivation of slip angles and lateral forces is according to the same geometrical principles and assumptions as in the case of the front axle of a single vehicle or towing vehicle. However, the Double-A combination is not equipped with any of those. The linear lateral dynamic behavior of the Double-A can be modelled in state space as a feedback control system. This can be done similarly to the cases of other vehicles derived earlier in this thesis with the matrix notation, by eliminating every excess variable. The matrix notation can be solved either in the matrix form of the equation (20) or equation (21).

The nonlinear model is formed similarly from the nonlinear tire characteristics and wheel load transfers. The vehicle units are considered one at a time individually. Similarly, due to the equations for the constraint forces the dynamic connection is formed between the vehicle units. The MF is considered for a single wheel one at a time. As earlier mentioned, the vertical loads are dependent on the coupling types. The first and third articulations are B-type overhang coupled, similarly to the articulation between the tractor and semi-trailer units. Therefore, there is load transfer between the first and second vehicle units, as well as between the third and fourth vehicle units. However, the second articulation is an A-type rear hang coupling type. Consequently, the static and dynamic load transfers between the second and third vehicle units are negligible and therefore considered zero. The vertical loads and wheel load transfers are distributed similarly as for the tractor and semi-trailer combination. Equivalent axles and wheels are considered first and then the equivalent loads are distributed among the single wheels. The same assumptions and principles hold as for the tractor and semi-trailer vehicle combination. The calculation of

vertical loads begin from the last vehicle unit. The static wheel loads for the front side of the CoG and the rear wheels of the 2nd semi-trailer unit read:

$$F_{zs4F} = \frac{l_{42}}{a_4+l_{42}} m_4 g, \tag{112}$$

$$F_{zs411} = F_{zs412} = F_{zs413} \ldots F_{zs4jk} = \frac{1}{12}\frac{a_4}{a_4+l_{42}} m_4 g. \tag{113}$$

Respectively, the front side load of the 2nd semi-trailer unit is distributed to the dolly vehicle unit and the mass is located at the coupling point. The dolly unit has only two axles, so the vertical load is distributed:

$$F_{zs3F,2} = \frac{l_{32}\pm b_3}{l_{32}+l_{31}} F_{zs4F}, \tag{114}$$

$$F_{zs3R,2} = \frac{l_{31}\mp b_3}{l_{32}+l_{31}} F_{zs4F}. \tag{115}$$

The signs $\pm$ and $\mp$ in the equations (114)-(115) come from the fact that the sign of the term b_3 is dependent on which axle is closer to the coupling point. It is theoretically also possible, that in some cases the overhang coupling point is not located between the dolly axles. In that case the coupling point is outside the axles and the axle which is closer to the coupling point carries the entire vertical load. The own mass of the dolly unit is distributed among the axles:

$$F_{zs3F,1} = \frac{l_{32}}{l_{32}+l_{31}} m_3 g, \tag{116}$$

$$F_{zs3R,1} = \frac{l_{31}}{l_{32}+l_{31}} m_3 g. \tag{117}$$

Similarly, the total axle masses for the dolly unit consists of the own mass of the dolly unit plus the distributed mass from the 2nd semi-trailer unit. Now the single wheel loads of the dolly unit can be written as:

$$F_{zs31k} = \frac{1}{4}\left(F_{zs3F,1} + F_{zs3F,2}\right) = \frac{1}{4} F_{zs3F}, \tag{118}$$

$$F_{zs32k} = \frac{1}{4}\left(F_{zs3R,1} + F_{zs3R,2}\right)\frac{1}{4} F_{zs3R}. \tag{119}$$

The first and second vehicle units are calculated similarly as in the case of tractor plus semi-trailer. The vertical loads of the first semi-trailer are calculated similarly to the second semi-trailer:

$$F_{zs2F} = \frac{l_{22}}{a_2+l_{22}} m_2 g, \tag{120}$$

$$F_{zs211} = F_{zs212} = F_{zs213} \ldots F_{zs2jk} = \frac{1}{12} F_{zs2R} = \frac{1}{12}\frac{a_2}{a_2+l_{22}} m_2 g. \tag{121}$$

The distributed mass from the 1st semi-trailer to the tractor unit and the own mass of the tractor unit read:

$$F_{zs1F,2} = \frac{\frac{(l_{13}+l_{12})}{2}\mp b_1}{l_{11}+\frac{(l_{13}+l_{12})}{2}} F_{zs2F}, \tag{122}$$

$$F_{zs1R,2} = \frac{l_{11}\pm b_1}{l_{11}+\frac{(l_{13}+l_{12})}{2}} F_{zs2F}, \tag{123}$$

$$F_{zs1F,1} = \frac{\frac{(l_{13}+l_{12})}{2}}{l_{11}+\frac{(l_{13}+l_{12})}{2}} m_1 g, \tag{124}$$

$$F_{zs1R,1} = \frac{l_{11}}{l_{11}+\frac{(l_{13}+l_{12})}{2}} m_1 g. \tag{125}$$

Furthermore, the vertical loads of the single wheels for the tractor unit read:

$$F_{zs11k} = \frac{1}{2}\left(F_{zs1F,1} + F_{zs1F,2}\right) = \frac{1}{2}F_{zs1F}, \tag{126}$$

$$F_{zs12k} = F_{zs13k} = \frac{1}{8}(F_{zs1R,1} + F_{zs1R,2})\frac{1}{8}F_{zs1R}. \tag{127}$$

The lateral wheel load transfers are derived similarly to the tractor and semi-trailer combination with the same equations (86)-(87). Again, the longitudinal wheel load transfers are beyond scope. The lateral wheel load transfers for Double-A combination read:

$$F_{zd111} = -F_{zd112} = \frac{2}{2}\frac{1}{1}\frac{h_1}{t_{11}}F_{zs1F}\frac{a_{y1}}{g} = \frac{h_1}{t_{11}}F_{zs1F}\frac{a_{y1}}{g}, \tag{128}$$

$$F_{zd121} = F_{zd122} = -F_{zd123} = -F_{zd124} = \frac{2}{4}\frac{1}{2}\frac{h_1}{t_{12}}F_{zs1R}\frac{a_{y1}}{g} = \frac{1}{4}\frac{h_1}{t_{12}}F_{zs1R}\frac{a_{y1}}{g}, \tag{129}$$

$$F_{zd131} = F_{zd132} = -F_{zd133} = -F_{zd134} = \frac{2}{4}\frac{1}{2}\frac{h_1}{t_{13}}F_{zs1R}\frac{a_{y1}}{g} = \frac{1}{4}\frac{h_1}{t_{13}}F_{zs1R}\frac{a_{y1}}{g}, \tag{130}$$

$$F_{zd211} = F_{zd212} = -F_{zd213} = -F_{zd214} = \frac{2}{4}\frac{1}{3}\frac{h_2}{t_{21}}F_{zs2R}\frac{a_{y2}}{g} = \frac{1}{6}\frac{h_2}{t_{21}}F_{zs2R}\frac{a_{y2}}{g}, \tag{131}$$

$$F_{zd221} = F_{zd222} = -F_{zd223} = -F_{zd224} = \frac{2}{4}\frac{1}{3}\frac{h_2}{t_{22}}F_{zs2R}\frac{a_{y2}}{g} = \frac{1}{6}\frac{h_2}{t_{22}}F_{zs2R}\frac{a_{y2}}{g}, \tag{132}$$

$$F_{zd231} = F_{zd232} = -F_{zd233} = -F_{zd234} = \frac{2}{4}\frac{1}{3}\frac{h_2}{t_{23}}F_{zs2R}\frac{a_{y2}}{g} = \frac{1}{6}\frac{h_2}{t_{23}}F_{zs2R}\frac{a_{y2}}{g}, \tag{133}$$

$$F_{zd311} = F_{zd312} = -F_{zd313} = -F_{zd314} = \frac{2}{4}\frac{1}{1}\frac{h_3}{t_{31}}F_{zs3F}\frac{a_{y3}}{g} = \frac{1}{2}\frac{h_3}{t_{31}}F_{zs3F}\frac{a_{y3}}{g}, \tag{134}$$

$$F_{zd321} = F_{zd322} = -F_{zd323} = -F_{zd324} = \frac{2}{4}\frac{1}{1}\frac{h_3}{t_{32}}F_{zs3R}\frac{a_{y3}}{g} = \frac{1}{2}\frac{h_3}{t_{32}}F_{zs3R}\frac{a_{y3}}{g}, \tag{135}$$

$$F_{zd411} = F_{zd412} = -F_{zd413} = -F_{zd414} = \frac{2}{4}\frac{1}{3}\frac{h_4}{t_{41}}F_{zs4R}\frac{a_{y4}}{g} = \frac{1}{6}\frac{h_4}{t_{41}}F_{zs4R}\frac{a_{y4}}{g}, \tag{136}$$

$$F_{zd421} = F_{zd422} = -F_{zd423} = -F_{zd424} = \frac{2}{4}\frac{1}{3}\frac{h_4}{t_{42}}F_{zs4R}\frac{a_{y4}}{g} = \frac{1}{6}\frac{h_4}{t_{42}}F_{zs4R}\frac{a_{y4}}{g}, \tag{137}$$

$$F_{zd431} = F_{zd432} = -F_{zd433} = -F_{zd434} = \frac{2}{4}\frac{1}{3}\frac{h_4}{t_{43}}F_{zs4R}\frac{a_{y4}}{g} = \frac{1}{6}\frac{h_4}{t_{43}}F_{zs4R}\frac{a_{y4}}{g}. \tag{138}$$

The total amount of vertical load for a single wheel consists of the static and dynamic wheel load terms, as earlier derived in the equation (94).

Respectively, the nonlinear tire lateral forces can be combined from the vertical wheel loads and MF for each tire with the equation (51). Suitable MF parameters for Double-A combination were found from Volvo Vertec-project HVC tire measurement data, and they are addressed more in depth in the next chapter of simulations. The sum of the single lateral tire forces of the axle is similarly the effective lateral force of the axle. The same Newton's equations of motion (95)-(111) still apply. The nonlinear solution is derived by substituting the nonlinear lateral forces to the Newton's equations of motion and solving

the system by eliminating excess variables and equations. The equations of motion form a nonlinear first-order differential algebraic system of equations. The chosen state vector for the nonlinear dynamic model is the same as earlier mentioned $\bar{x} = [v_1\ v_2\ v_3\ v_4\ r_1\ r_2\ r_3\ r_4]^T$. The differential system of equations is solved in a time domain simulation as a numeric integral.

The Double-A simulation model is based on the above derived dynamics. The linear model can be simulated in MATLAB state-space environment with the matrix notation. The nonlinear model with the nonlinear tire characteristics are simulated in MATLAB as a time domain simulation. In the time domain simulation, the vehicle dynamics script calls for the nonlinear lateral force functions and calculates a linearization of the entire system step by step. This sum of the linearized steps from nonlinear characteristics is called the nonlinear model and it is practically integrated numerically from the equation (57), where the state vector is the one chosen above. The model needs to be given the simulation time and corresponding steering angles as inputs. Additionally, the initial states and their derivatives in respect of time are required. The model simulates the two chosen test-drives of double lane change maneuver and the phase plane analysis method, which function as the simulation inputs. The simulation inputs are explained and reasoned thoroughly in the next chapter.

4 Simulations

Two different simulations were performed for the Double-A vehicle combination with the nonlinear analytical simulation model. The first simulation was an open-loop double lane change, which imitates the ISO 3888 standard double lane change. In the second simulation a phase plane analysis for the dolly unit of the vehicle combination was performed. A sensitivity analysis was performed based on the two different simulations. Several parameters were first tested and based on the parameter iteration tests, the two most suitable parameters were chosen. The chosen parameters also take into account the given derogations of law restrictions and general vehicle legislations. The two chosen parameters for the sensitivity analysis were the number of wheels on a semi-trailer rear axle and the length of the dolly drawbar. A sensitivity analysis was performed by examining the effect of the chosen parameter on the entire system. Meanwhile the other parameters were kept unmodified, because the subject of the examination was on a single parameter effect, not on parameter combinations. The sensitivity analysis was performed with a low road friction coefficient of approximately $\mu = 0.25$. Additionally, simulations were performed with a good road friction coefficient of approximately $\mu = 0.75$ to compare the slippery and dry road circumstances in the two chosen simulation types with the default parameter settings.

The open-loop double lane change simulation was performed with a forward velocity of 80 km/h. The double lane change consists of two 3.5-meter-wide lanes and the vehicle combination changes the lane twice. A sufficient lateral displacement had to be obtained, which was quantified as 3.5 ± 0.5 meters. The total simulation time was 15 seconds, and the lane changes were performed in a time span of 6.67 seconds, which corresponded a translational motion of 150 meters. The simulation consisted of separate steering angle inputs and corresponding time spans, which combined together imitate the ISO 3888 standard double lane change simulation. Similar steering inputs and double lane change maneuver validations could be found from two other studies (Lehessaari 2007; Rahkola 2006). The objective of this simulation was to study the impact of the chosen sensitivity analysis parameters to the RAs of the examined state variables of the vehicle combination, as well as to compare the slippery and dry surfaces. This simulation and the RAs give an insight to the overall lateral stability of the vehicle combination in a low road friction double lane change. All the RA-values were calculated with the time domain approach. The open-loop double lane change simulation is demonstrated in figure 21.

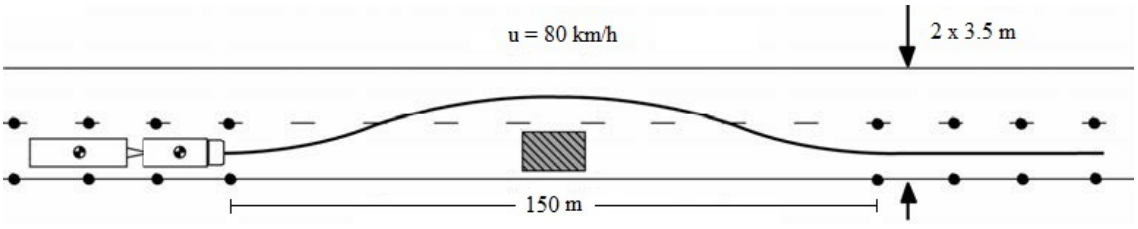

Figure 21. Open-loop double lane change, based on the ISO 3888 standard (Rahkola 2006)

Nonlinear dynamics of vehicle planar motion systems can be examined with a phase plane analysis, which is considered as an open-loop examination. Only very limited research on this has been reported, especially for HVCs. Consequently, this research provides novel results, regarding planar motions and study on lateral stability of HVCs. Nonlinear

systems generally have more than one equilibrium, so the analysis requires a deep insight into the dynamics. Specifically, when the vehicle contains articulations, the complexity of the dynamics increase. A phase plane method was used, which was proposed by Inagaki et al (Inagaki et al. 1994). The phase portrait describes the vehicle sideslip angle and the vehicle yaw rate in a planar diagram to analyze vehicle stability in xy-planar motion. If the sideslip angle or yaw rate increase or decrease up to a certain level, a saddle-node bifurcation occurs and the vehicle loses its stability. Below the certain levels, the system has one stable and two unstable equilibria. The attraction domain diminishes when the sideslip angle or yaw rate increases and enlarges when they decrease towards zero. The phase plane method gives an insight to the vehicle overall lateral stability and addresses the nonlinear system planar motions, recovery time and stability with more than sufficient accuracy, specifically with low road friction coefficients. An example of a phase portrait method for a passenger vehicle is shown in figure 22. (Inagaki et al. 1994; Shen et al. 2007)

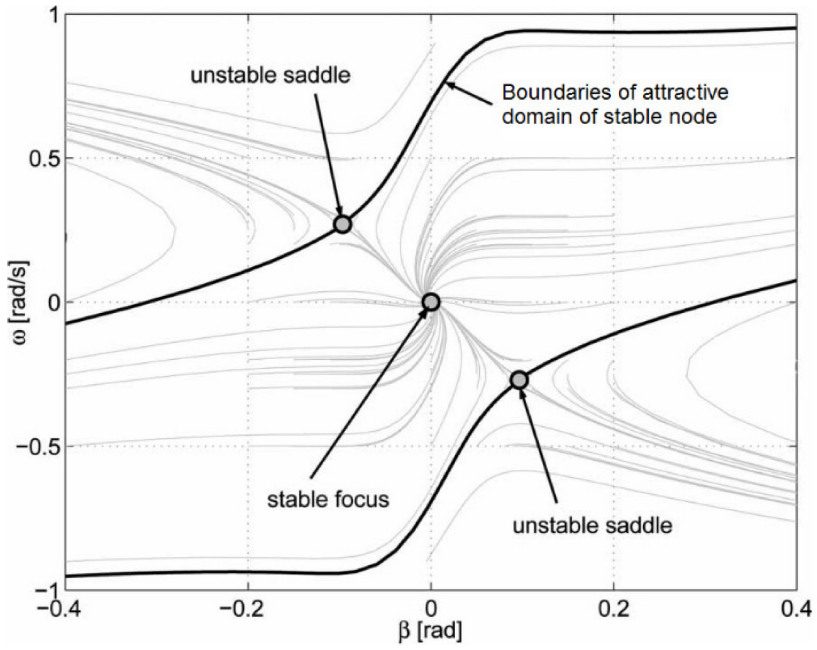

Figure 22. Phase portrait of a passenger vehicle (Shen et al. 2007)

The stable focus is located at the origin (0, 0) and the unstable saddle points are located at (-0.0966, 0.27) and (0.0966, -0.27). The symmetry of the phase portrait seen in the figure 22 is the result of no initial steering commands or the steering command for both the front and rear wheels are equal. The initial vehicle state and steering commands for the rear and front wheels have a key role regarding the phase portrait, the location of the locus and the dynamics of the vehicle planar motion system. If the vehicle under examination has initial steering commands for front and rear wheels and they are unequal, it results in an asymmetric shape of the phase portrait.

The phase-plane analysis used in this thesis addressed the planar motions of the dolly vehicle unit. The dolly vehicle unit is the most sensible vehicle unit regarding vehicle stability. This is due to the light overall mass and size of the vehicle unit combined with the rear hang coupling type in front, which furthermore decreases the stability of the vehicle unit by increasing the RAs of different state variables. It is notable that if the dolly unit loses its stability, the 2nd semi-trailer behind it highly tends to lose its stability as well, because of the coupling types and RAs. In addition, the rear vehicle units of the

vehicle combination are usually uncontrollable by the driver in problematic situations due to the long delay and response time. If the stability of the latter vehicle units are lost, this usually results in the loss of stability of the entire vehicle combination. The loss of stability in the latter vehicle units are usually seen too late by the driver and by that time they are already uncontrollable.

The setup for the phase-plane analysis in this thesis was as follows. The vehicle combination was simulated in a straight line with a forward velocity of 80km/h, the initial steering commands were zero for all the vehicle units. The dolly vehicle unit was deviated from the initial position and state artificially by manipulating the state variables of the dolly unit. In order to simulate problematic situations, the tractor vehicle unit was similarly deviated from its original state and position. The dolly vehicle unit was then given a time span of 6.75 seconds to recover and settle down. The vehicle unit should strive towards the stable focus point, unstable saddle point or possibly escape totally as a result of a vehicle spin or roll-over. This given time span corresponded a translational motion of 150 meters, similarly to the open-loop double lane change simulation. The objective of this simulation was to study the impact of the chosen sensitivity analysis parameters to the size of the stable area of the dolly vehicle unit, as well as to compare the slippery and dry surfaces. The phase portraits were created based on a very dense distribution of deviated states. The stable-unstable boundary values are estimated visually, based on the curves close to the limit and their final state. Estimating criteria for the stability-instability of different states were, what the final state of the vehicle was and how straightforward the curve was. Curves that ended up in the stable focus as straightforward as possible were considered as stable and curves that reached unstable saddle point or didn't have time to settle down even close to the stable focus were considered unstable. In addition, curves that had exceptionally wide oscillation and returned to the stable focus were considered unstable due to the lack of proper evidence regarding the vehicle motion and dynamics in reality. This estimating criteria was based on the dynamic stability theory, which was addressed in the figure 14. Based on the phase portraits, a phase plane analysis was performed. A demonstrative figure of the initial state and the logic of deviated states are presented in figure 23.

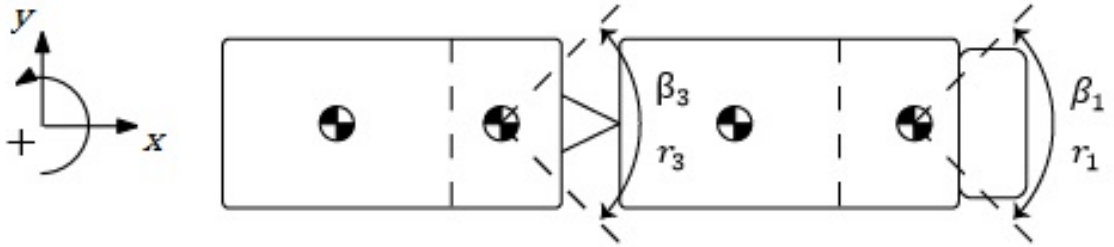

Figure 23. Initial Double-A state and the deviation states

The semi-trailers used in the Double-A combination are standard cargo semi-trailers. They are always 3-axle semi-trailers; however, the number of wheels on a single axle can vary, as was explained in the previous chapter. The axles are either equipped with single wheels or twin wheels, depending on which type of semi-trailer is free to use and what kind of cargo is being transferred. Mixed single and twin wheel settings on the same axle group were considered out of scope. Four different combinations were found and they are presented in the following list.

- Both semi-trailers have twin wheels

- The 1st semi-trailer has single wheels and the 2nd semi-trailer twin wheels
- The 1st semi-trailer has twin wheels and the 2nd semi-trailer single wheels
- Both semi-trailer have single wheels

A demonstrative figure of a single semi-trailer with the two different wheel settings is presented in figure 24.

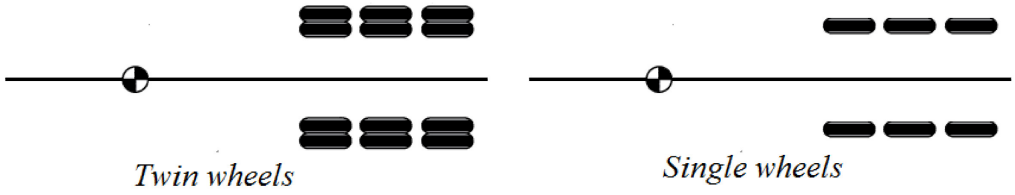

Figure 24. Different wheel settings for a standard 3-axle semi-trailer

The axle loads remain the same on both semi-trailer types, but the single wheel loads change. The above explained simulations were performed with the four different semi-trailer wheel setting combinations.

The dolly vehicle units used in the Double-A combination are standard twin axle twin wheel dolly units. However, the length of the drawbar can be adjusted, as was explained in the previous chapter. The condition for the Double-A combination is that it has to be of the same total length of 32 meters. If the drawbar length is adjusted, the location of the articulation point needs to be modified as well. Three different combinations for the drawbar and articulation point were found for the dolly vehicle unit and they are presented in the list below.

- The default setting: $a_3 = 3.65\ m \quad b_2 = 6.553\ m$
- The minimum setting: $a_3 = 2.535\ m \quad b_2 = 7.668\ m$
- The maximum setting: $a_3 = 4.95\ m \quad b_2 = 5.253\ m$

The minimum and maximum settings came from the total vehicle length restrictions, which were the absolute minimum and maximum settings for the drawbar length and articulation point location. The default setting was given by a logistics company as a dimensioning drawing of Double-A. The three dolly settings are presented in figure 25.

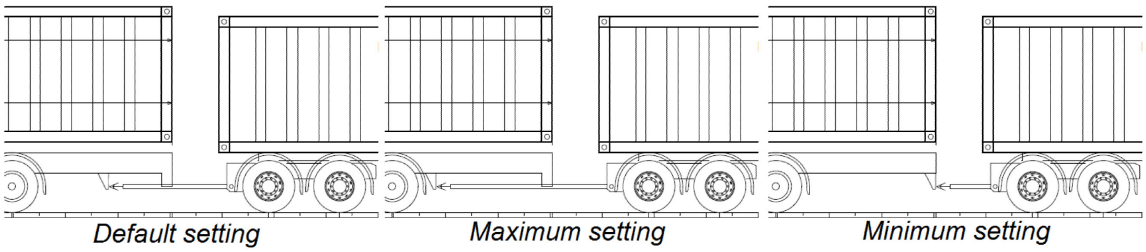

Figure 25. Different dolly unit drawbar and articulation point settings

The above explained simulations were performed with the three different dolly unit settings.

The Magic Formula tire parameters used in the simulations were obtained from the Volvo Vertec-project HVC tire measurements (Giangiulio 2005a; Giangiulio 2005b). The measurements were performed over several months, on different test locations by different test suppliers in the year of 2005. The parameters were measured in practical driving tests on different road conditions. Driving tests included lane changes and steady

state and transient state maneuvers with different constant forward velocities. In addition, braking and accelerating driving tests were performed from different initial velocities. The driving tests were performed with tractor and semi-trailer vehicle units. The different road conditions were dry asphalt, snow, rough ice and smooth ice. The different heavy vehicle tires were from Pirelli manufacturer and they included new and worn tires from tractor front and rear axles and from trailer rear axles. The measured data from different maneuvers were slip angles and vertical and lateral forces. The measured data was fitted to different MF formulas. The most suitable tire parameters were chosen from the rough ice surface and dry asphalt surface test databases for the lateral force of the MF in pure lateral slip direction. The used fitted MF tire parameters were from one of the test suppliers VTI from the Volvo Vertec-project. The tires were new Pirelli ST35 385/65R22.5 tire, new Pirelli FH55 315/80R22.5 tire and new Pirelli TH65 315/80R22.5 tire.

The lateral force graphs as a function of slip angle with different vertical loads on rough ice and dry asphalt road conditions are presented in figures 26-27.

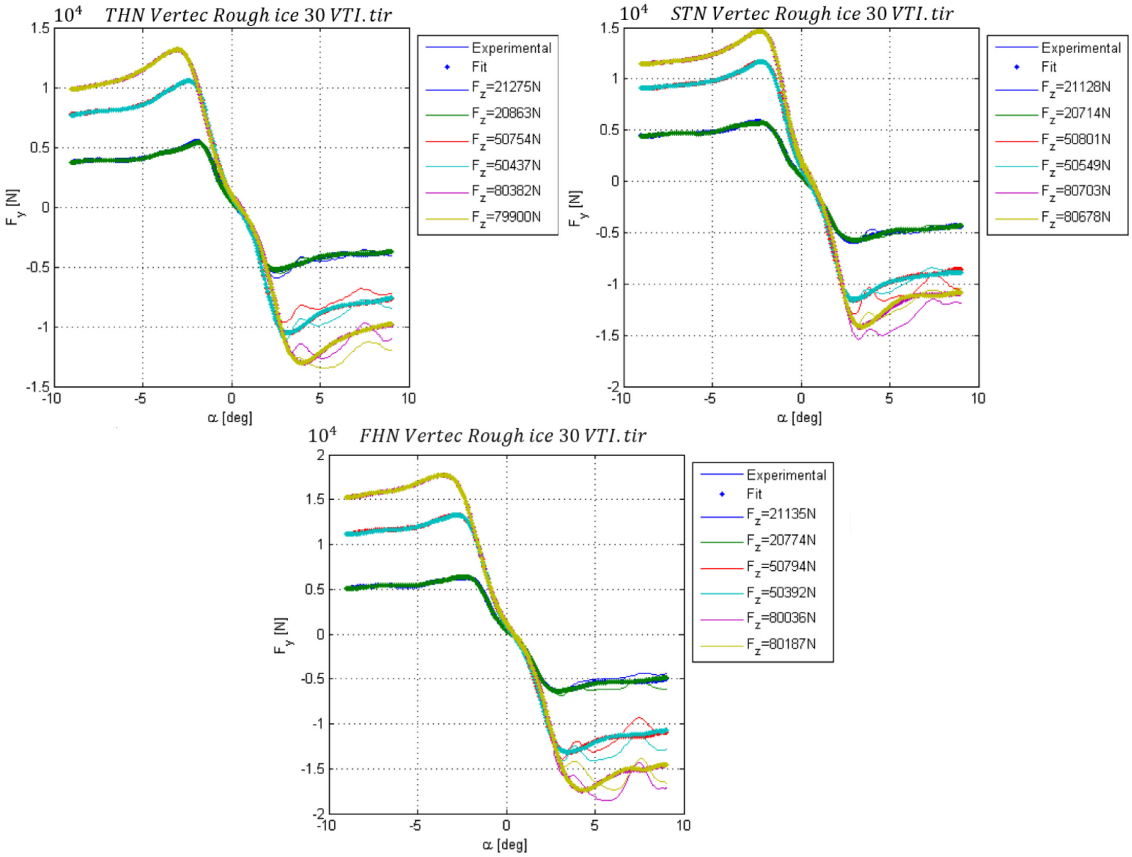

Figure 26. Different Pirelli HVC tire lateral force graphs on rough ice in pure lateral slip with camber $\gamma = 0$ (Giangiulio 2005b)

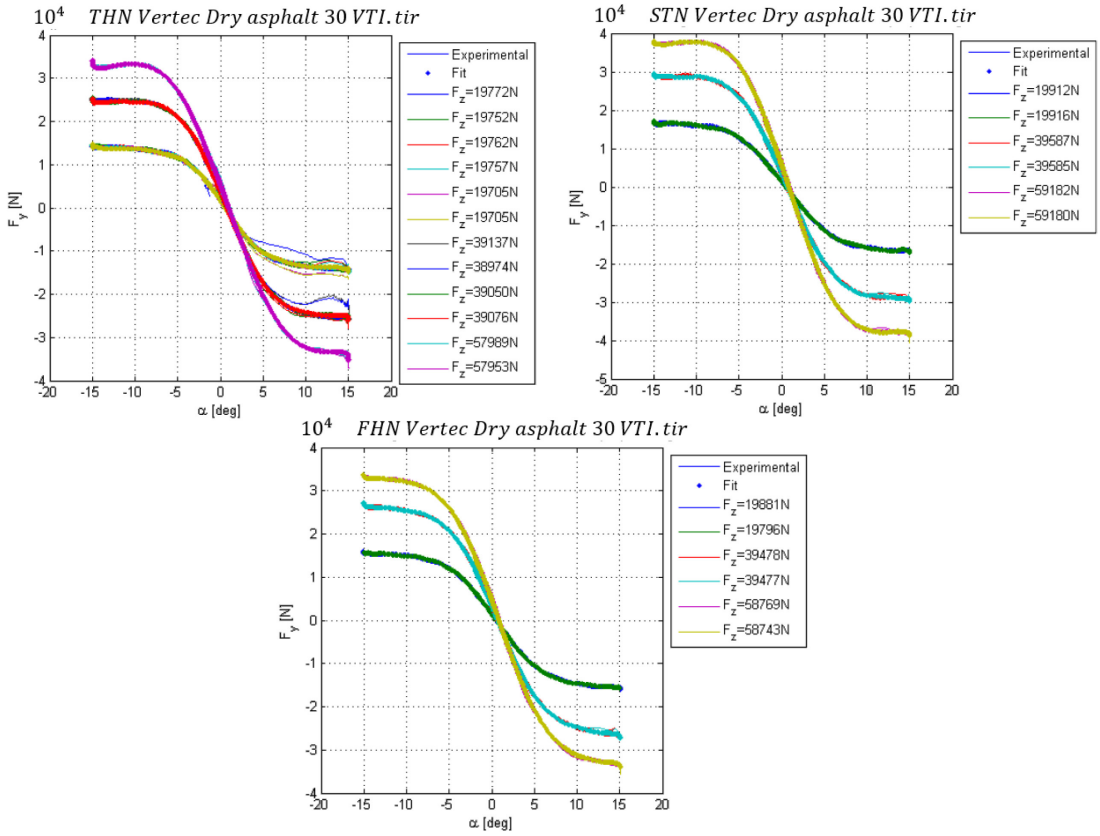

Figure 27. Different Pirelli HVC tire lateral force graphs on dry asphalt in pure lateral slip with camber $\gamma = 0$ (Giangiulio 2005a)

As seen from the figures 26-27, the lateral force production on dry asphalt is more linear and better to larger slip angles. The abbreviations ST, FH and TH stand for the semi-trailer axle tire, tractor front axle tire and tractor rear axle tire. These MF parameters are valid between the slip angles of $\pm 0.4\, rad$ ($\pm 22.9°$) and vertical loads of 0-90 000 N. The linear part of the lateral force graph is only valid approximately between $\pm 2.5°$ on the rough ice surface in the target vertical load area. For the dry asphalt surface the linear part of the lateral force graph is valid approximately between $\pm 5°$ in the target vertical load area. The road friction coefficients in lateral direction were measured and used in the simulation for the rough ice $\mu_{ice} = 0.23 \ldots 0.28$ and for the dry asphalt $\mu_{dry} = 0.67 \ldots 0.75$. The rough ice parameters correspond regular Northern Europe winter road conditions, since the excess snow is usually plowed off of the roadway, which leaves only some snow and rougher ice on the roadway. Parameters for the dolly vehicle unit tires were not measured and couldn't be obtained. However, the above used parameters could be fitted for the dolly vehicle unit, because the tires are similar to trailer tires and the vertical loads could be adjusted according to the parameters based on a reference vertical load. Moreover, the differences between the lateral force graphs between the different vehicle unit tires in the target vertical load area were minuscule, so the dolly parameters were accurate enough. These tire parameters were especially suitable for this nonlinear simulation model and they were measured and validated properly. The MF lateral force parameters used in the simulations are presented in the appendices A1-A2.

5 Results & Discussion

The simulation results for the Double-A vehicle combination are presented in this chapter. The measured quantities are presented in different graphs, from which characteristics for the vehicle combination behavior can be observed and examined. At first, a comparison for the default vehicle combination setting between high road friction (dry asphalt) and low road friction (rough ice) is presented with both simulation type results. This comparison emphasizes the characteristics of slippery circumstances. In the second subheading, the first parameter of the sensitivity analysis is addressed with both simulation type results. Respectively, in the third subheading, the second parameter of the sensitivity analysis is addressed with both simulation type results. The last subheading addresses the error analysis. The results and discussion are concluded in the next chapter.

5.1 Comparison of high and low road friction surfaces

First the double lane change maneuver results are presented. After, the dolly phase plane method results are analyzed. Finally, these two simulation results are connected to each other at the end of the subheading. The lateral accelerations, vehicle trails, yaw velocities and vehicle unit slip angles in a double lane change maneuver on high and low road friction circumstances are presented for the vehicle combination in figures 28 to 31.

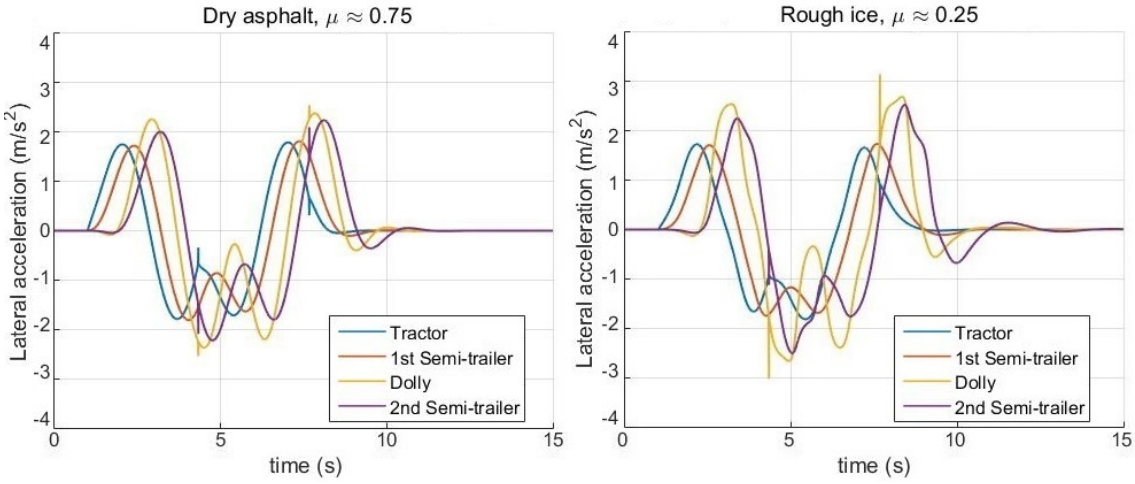

Figure 28. Vehicle unit lateral acceleration comparison between dry asphalt and rough ice surface simulations in a double lane change maneuver with a forward velocity of 80km/h

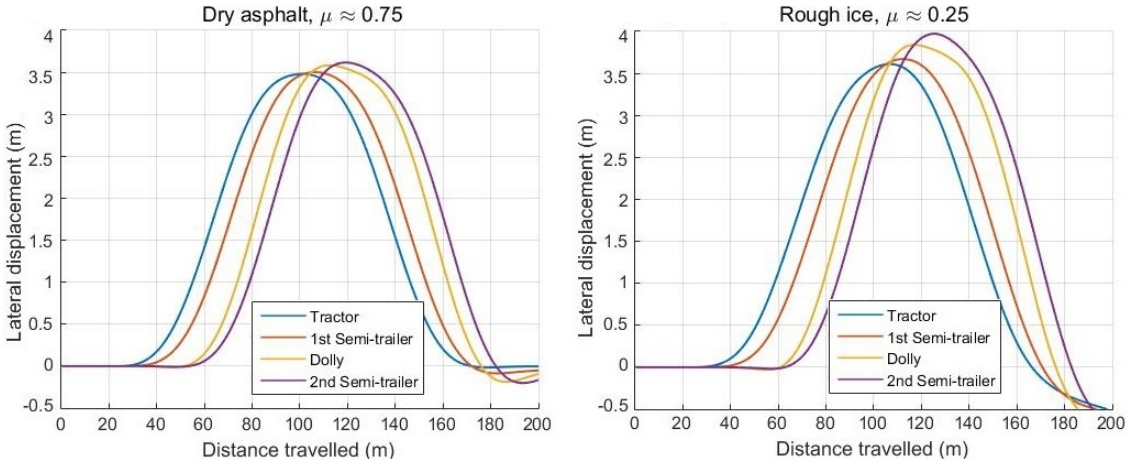

Figure 29. Vehicle unit trail comparison between dry asphalt and rough ice surface simulations in a double lane change maneuver with a forward velocity of 80km/h

The highest lateral acceleration RA from the tractor unit to the dolly unit in dry asphalt simulation is approximately $RA_{dry} = \frac{2.383}{1.792} = 1.33$ and it occurs approximately at time $t = 7.5$. The highest lateral acceleration RA from the tractor unit to the dolly unit in rough ice surface simulation is approximately $RA_{icy} = \frac{2.697}{1.66} = 1.62$ and it occurs approximately at time $t = 7.5$. The motion delay from the tractor unit to the dolly unit for the dry surface vehicle combination is approximately 0.85 seconds, whereas for the rough ice surface vehicle combination it is approximately 1.15 seconds.

The RA-values of the dry surface simulation are relatively high, but they are not considered to be over the dangerous limit of 1.5. The RA-values of the rough ice surface simulation, however, exceed the dangerous limit of 1.5, so the vehicle shows evidence of unstable behavior and it may be uncontrollable by the driver. The increased time delay in the rough ice surface simulation might be due to the slippery road surface, which causes the wheels of the dolly and 2nd semi-trailer units to slide excessively in lateral direction, which furthermore increases the delays. The peak values for the lateral accelerations are presented in the table 1 below.

Table 1. Peak values of lateral accelerations in dry asphalt and rough ice surface simulations

	Dry tractor	**Dry 1st semi-trailer**	**Dry Dolly**	**Dry 2nd semi-trailer**	**Rough Ice tractor**	**Rough Ice 1st semi-trailer**	**Rough Ice Dolly**	**Rough Ice 2nd semi-trailer**
$Peak\ value\left(\frac{m}{s^2}\right)$	1.792	1.813	2.383	2.242	1.82	1.740	2.697	2.533
$Peak\ value\ (g)$	0.183	0.185	0.243	0.228	0.186	0.177	0.275	0.258
$Time\ (s)$	7.0	7.4	7.85	8.10	5.45	7.5	8.35	8.40

The peak values for the lateral accelerations are generally higher for the rough ice surface simulation, but some exceptions are found. The tractor and 1st semi-trailer units have slightly higher lateral acceleration peak values in the dry surface simulation. On the other hand, the peak values of the dolly and 2nd semi-trailer units are clearly higher in the rough ice surface simulation. The trail graphs show that the dolly unit and the 2nd semi-trailer in

the rough ice surface simulation has approximately 0.5 meters more lateral displacement in the maneuver than the tractor and 1st semi-trailer units. In addition, the returning maneuver in the rough ice conditions seem to go approximately 0.5 meters off target. An observation is done regarding the recovery time. The recovery time on the dry surface is approximately 11 seconds, whereas on the slippery surface it is approximately 14 seconds.

Any of the lateral acceleration peak values don't reach the dangerously considered roll-over limits of 0.3 g - 0.7 g as described earlier. However, the lateral acceleration peak values of the rough ice surface dolly and 2nd semi-trailer units exceed 0.2 g. It was said earlier that an HVC may spin or slide excessively in slippery conditions with higher lateral acceleration values than 0.2 g, so the vehicle combination in this rough ice simulation may be in unstable state. Due to the irregularity of the rough ice surface lateral acceleration curves, it can be observed visually that the vehicle is not as stable as the vehicle on dry surface. The vehicle might be close to sliding out of the driveway and its RA-values are continuously clearly higher during the maneuver than the ones in the dry surface simulation. The difference in trail graphs is the result of excessive vehicle sliding in lateral direction, which furthermore is the result of excess RA of the examined state variables in the slippery road conditions. However, the dolly and 2nd semi-trailer units stay on the standard lane, because they had ± 0.5 meters tolerance. This kind of phenomenon is not present in the dry surface simulation. The difference in recovery time is also the result of the slippery circumstances, where the wheels may slide excessively in lateral direction due to the lack of proper lateral force, which furthermore causes more unstable events.

The lateral accelerations are quite similar between the dry asphalt and rough ice surface simulations. In the dry surface simulation, the shape of the curves is much smoother and calmer than in the rough ice surface simulation. The lateral acceleration values, delays, recovery time and RAs are smaller in the dry surface simulation. The rough ice surface vehicle combination is clearly more unstable than the dry surface vehicle combination and it seems to show clear evidence of unstable behavior. The dry surface simulation doesn't seem to show any immediate evidence of unstable behavior.

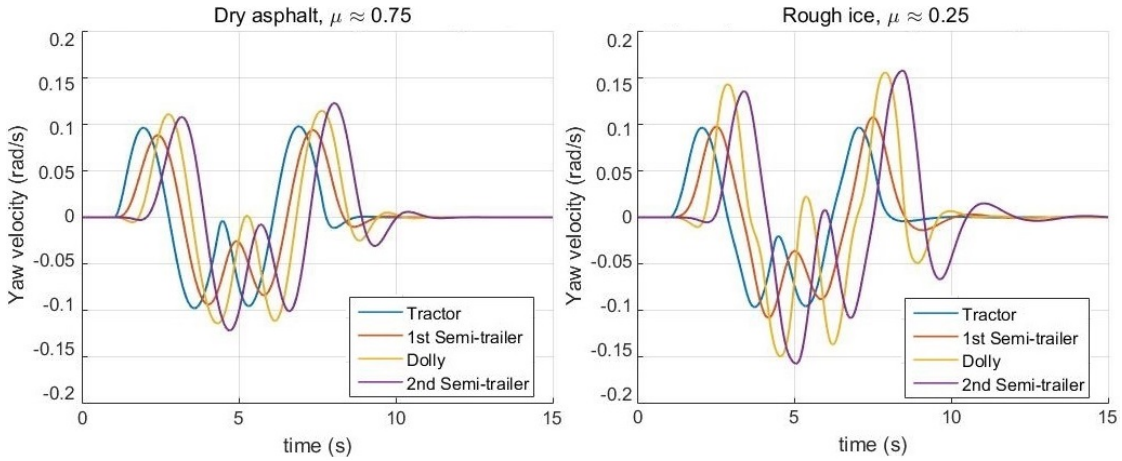

Figure 30. Vehicle unit yaw velocity comparison between dry and rough ice surface in a double lane change maneuver with a forward velocity of 80km/h

The yaw velocities show similarity to the lateral accelerations. The highest yaw velocity RAs are found for both simulations from the tractor unit to the 2nd semi-trailer unit approximately at time $t = 7.5$. In dry surface simulation $RA_{dry} = \frac{0.123}{0.098} = 1.26$ and in rough ice surface simulation $RA_{icy} = \frac{0.158}{0.097} = 1.63$. The motion and time delay from the tractor unit to the 2nd semi-trailer is for the dry surface simulation approximately 1.15 seconds and for the rough ice surface simulation approximately 1.4 seconds. The shape of the curves in both simulations are similar to each other, curves are smooth and calm.

The RA-values of the dry simulation don't exceed the dangerously considered limit of 1.5, however, the RA-values of the rough ice surface simulation exceed this limit. The RA-values of yaw velocity in rough ice surface simulation show evidence of unstable behavior, which may lead in the loss of control of the vehicle combination. Additionally, the yaw velocity peak values over 0.15 rad/s are relatively high and may indicate some unstable behavior and tendency to excess wheel and vehicle unit sliding at the peak value times. The increased time delay in the rough ice surface simulation is due to the slippery road surface, which causes the wheels of the dolly and 2nd semi-trailer units to slide excessively in lateral direction, which furthermore increases the delays. The peak values of the yaw velocities are presented in the table 2 below.

Table 2. Peak values of yaw velocities in dry and slippery surface simulations

	Dry tractor	**Dry 1st semi-trailer**	**Dry Dolly**	**Dry 2nd semi-trailer**	**Rough Ice tractor**	**Rough Ice 1st semi-trailer**	**Rough Ice Dolly**	**Rough Ice 2nd semi-trailer**
$Peak\ value\left(\frac{rad}{s}\right)$	0.098	0.094	0.115	0.123	0.097	0.108	0.156	0.158
$Time\ (s)$	6.9	7.35	7.65	8.0	7.05	7.5	7.9	8.40

The peak values of yaw velocity are generally higher for the rough ice surface simulation. The peak value of the tractor is slightly higher in the dry surface simulation, but the dolly and 2nd semi-trailer yaw velocities are much higher in the rough ice surface simulation. The recovery time for the dry surface vehicle combination is approximately 11 seconds, whereas for the rough ice surface vehicle combination it is approximately 14 seconds.

The higher peak values in rough ice road simulation indicate that the vehicle units are trying to spin more and excessive wheel sliding can be implied. The recovery time difference could be the result of slippery circumstances, where the wheels in rough ice surface may slide excessively in lateral direction. The yaw velocity values, delays, recovery time and RA-values are generally smaller in the dry surface simulation. The yaw velocity graphs alone don't show as clear evidence of unstable behavior in rough ice simulation as the lateral accelerations graphs, but some implications can be done.

The vehicle slip angles are of interest in the dry and rough ice surface comparison. The vehicle slip angles in double lane change are presented in figure 31.

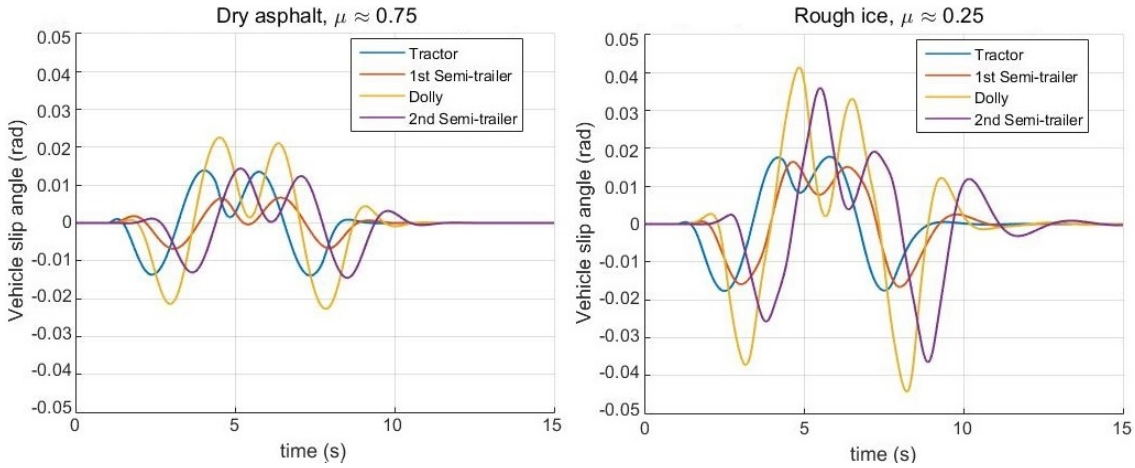

Figure 31. Vehicle unit slip angle comparison between dry and rough ice surface in a double lane change maneuver with a forward velocity of 80km/h

The RA-values of the slip angles are highest from the tractor unit to the dolly unit. The RA-values are for the dry surface simulation $RA_{dry} = \frac{0.023}{0.014} = 1.64$ at $t = 4.25$ and for the rough ice simulation $RA_{ice} = \frac{0.044}{0.018} = 2.44$ at $t = 7.5$. The peak values of the vehicle slip angle are presented in the table 3 below. The time for the total recovery for the vehicle combination is approximately 11 seconds for the dry surface vehicle and 14 seconds or the slippery surface vehicle.

Table 3. Peak values of vehicle slip angles in dry and rough ice surface simulations

	Dry tractor	Dry 1st semi-trailer	Dry Dolly	Dry 2nd semi-trailer	Rough Ice tractor	Rough Ice 1st semi-trailer	Rough Ice Dolly	Rough Ice 2nd semi-trailer
$Peak\ value(rad)$	0.014	0.007	0.023	0.015	0.018	0.016	0.044	0.036
$Peak\ value\ (°)$	0.802	0.401	1.261	0.859	1.031	0.917	2.521	2.063
$Time\ (s)$	4.0	4.55	4.5	8.5	4.15	4.65	8.2	8.9

The RA-value of a slip angle indicates that the latter vehicle unit is turned more than the towing unit. The vehicle slip angles in rough ice surface simulation are larger and approximately twice the values of the dry surface simulation. The slippery conditions in rough ice surface promote excessive wheel and vehicle sliding, which results in larger vehicle slip angles. The rough ice surface vehicle peak slip angles of tractor and 1st semi-trailer units are approximately 1°, which is moderate for a vehicle unit at this forward velocity. This indicates, that these front vehicle units should be controllable. The peak values of vehicle slip angles in dry surface simulation are generally under 1°, which promotes stable behavior. The slip angles, which are between 1° and 2° at this forward velocity indicate that the tires are still probably functioning in the linear region. The dolly and 2nd semi-trailer slip angles in the rough ice surface simulation are over 2°, which are considered larger at this forward velocity. Particularly, the peak value of the dolly unit in rough ice surface simulation exceeds the limit of 2.5° at this forward velocity. This may indicate some unstable behavior, as the tire lateral forces are close to nonlinear region.

The recovery time difference is again promoting the same evidence of excess wheel and vehicle sliding as in the yaw velocity and lateral acceleration graphs. The vehicle slip angles along with the lateral acceleration and yaw velocity graphs indicate that the rough ice surface vehicle combination is much more unstable than the vehicle combination on the dry surface. However, both vehicle combinations succeeded the double lane change maneuver by doing the sufficient lateral displacement and returning to the lane. Furthermore, the graphs indicate that the rough ice surface simulation vehicle is more or less in unstable state and experiences some unstable behavior. The vehicle on slippery surface is possibly uncontrollable by the driver or at least the dolly and 2nd semi-trailer units could be and they might act as a sledge by just following the tractor unit.

An important observation was done regarding the steering input. Generally, the steering input frequency, and magnitude play a key role regarding the RAs (results not shown in figures). Calmer, smoother and nonaggressive inputs tend to decrease RAs and vice versa. The steering input in the dry surface simulation is more aggressive than in the rough ice surface simulation. This is due to the slippery circumstances. In order to achieve the same lateral displacement, a calmer, smoother and overall less aggressive steering wheel input is needed in rough ice surface simulation, or otherwise the vehicle combination is driven off of the roadway due to excessive sliding and vehicle unit spinning. This observation furthermore promotes, that higher RA-values and general values of the state variables are achieved even with less aggressive steering input in rough ice road conditions, which clearly indicates unstable behavior. In addition, the nature of the graphs and curves in rough ice road simulation promote more unstable behavior than in the dry surface simulation.

The last observation towards the stability in double lane change is regarding the 2nd articulation type. The coupling in front of dolly vehicle unit is a back coupling type which, as said earlier increases the RAs and instability. This explains the general phenomena in both of the dry asphalt and rough ice simulation graphs that the dolly and 2nd semi-trailer unit have higher values in general than the tractor and 1st semi-trailer units.

The dolly vehicle unit phase portraits for dry asphalt and rough ice surface simulations are presented in figures 32 and 33.

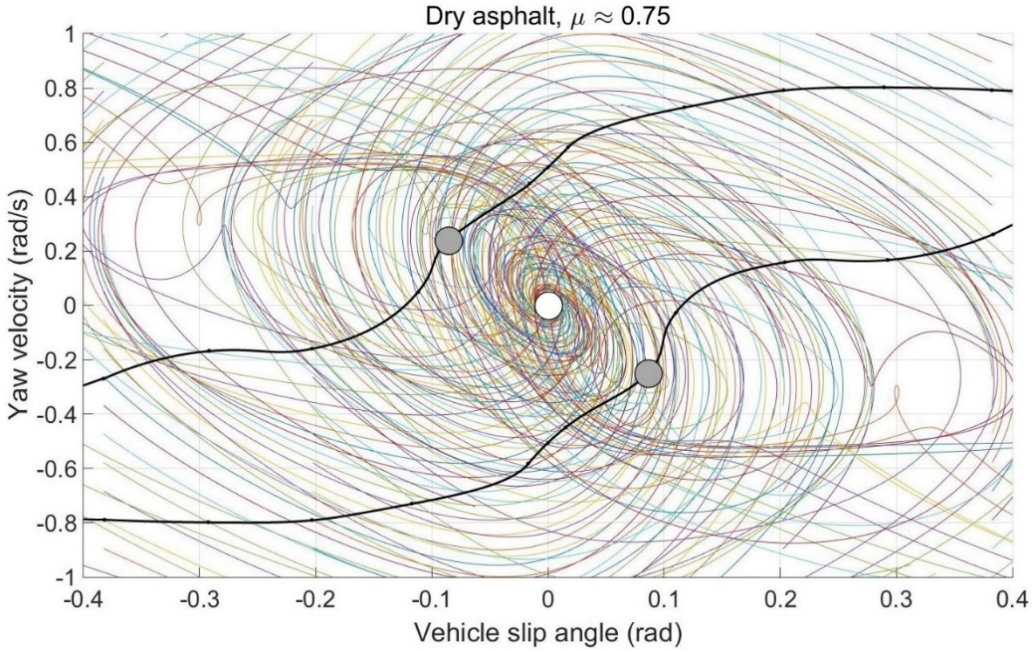

Figure 32. Dolly vehicle unit phase portrait in dry asphalt surface simulation with a forward velocity of 80 km/h

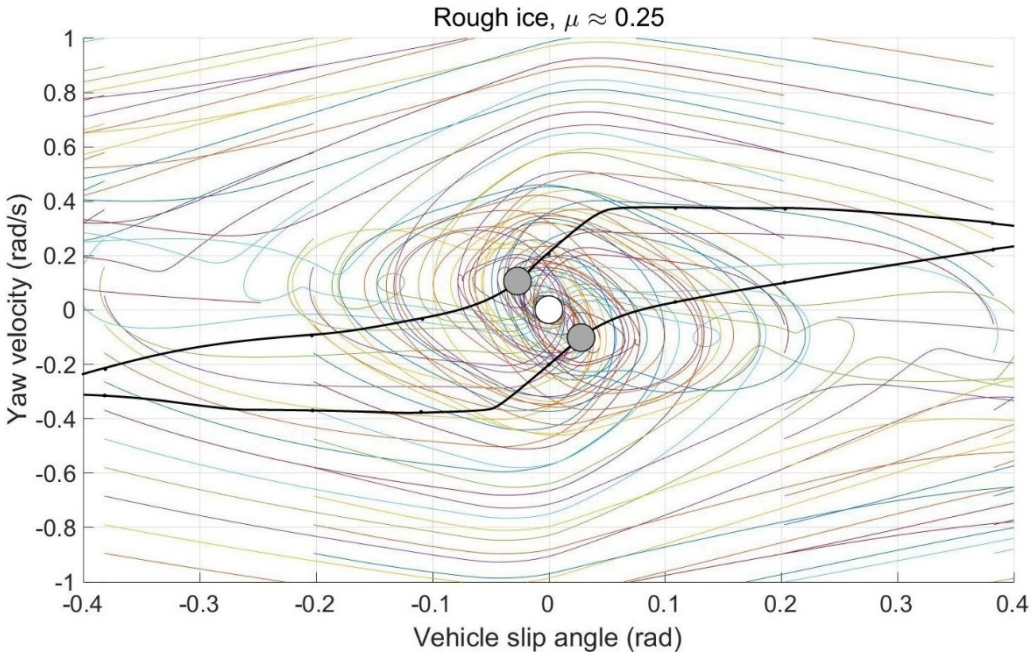

Figure 33. Dolly vehicle unit phase portrait in rough ice surface simulation with a forward velocity of 80 km/h

The stable area is objectively larger in the dry surface simulation than in the rough ice surface simulation. The vehicle combination in dry surface simulation allows much higher yaw rates and larger slip angles. The stable area yaw velocities in the dry surface simulation are between $\pm\sim 0.8\frac{rad}{s}$ and the stable area slip angles continue significantly over ± 0.4 radians. However, the MF parameters were only valid up to slip angle values

of ± 0.4 radians. The unstable saddle points locate at (-0.083, 0.25) and (0.083, -0.25). The stable area yaw velocities in the rough ice surface simulation are between $\pm \sim 0.35 \frac{rad}{s}$ and the stable area slip angles continue up to ± 0.4 radians. The unstable saddle points locate at (-0.028, 0.1) and (0.028, -0.1). The stable focuses locate at the origin in both simulations.

The vehicle combination in rough ice surface simulation tends to slide excessively and spin out due to yaw instability more easily in extreme situations, which furthermore decreases the size of the stable area. A significant observation is done regarding the shape of the curves. The curves in the rough ice surface simulation seem to be more calm and straightforward than in the dry surface simulation. This could be the result of excess wheel and vehicle unit sliding in extreme situations, which means that the vehicle unit is more or less in constant sliding motion and doesn't transmit the dynamic motions properly. The vehicle unit acts somewhat as a sledge and ignores the state and position of the wheels towards the global direction of propagation. This phenomena supports the evidence of the smaller stable area in slippery circumstances due to the vehicle sliding and spinning. Contrary to the rough ice surface, the vehicle unit in dry surface simulation transmits the dynamic motions properly as the wheel road contact is significantly better. This results in a larger area of stable states, however, the vehicle motions are also broader.

If we consider a comparison between a deviated stable state between rough ice and dry surface, one might say that the vehicle in slippery circumstances is more stable due to the lesser amount of dynamic motions. Although, one must also consider the controllability of the vehicle, which furthermore means that the vehicle unit in the slippery circumstances is difficult to control at any level due to the constant sliding phenomenon. An observation is done. In both the dry and slippery surface simulations, the situations where the vehicle unit has yaw velocity to the same direction as the slip angle results in a narrower stable area. This can be seen in the phase portrait areas where the vehicle unit has different signed yaw velocity and vehicle slip angle, which is an example of an extreme situation.

One clear difference between the simulations is that the locations of the unstable saddle points are different. The unstable saddle points of the slippery surface simulation are much closer to the stable focus, which makes the stable area even narrower in the middle area. This is the result of the different signed yaw velocity and vehicle slip angle. The vehicle combination in rough ice surface allows more narrow stable area unlike the vehicle combination in dry surface. Overall the stable area and stable states for the dolly vehicle unit in dry surface are wider and the vehicle unit is more controllable and seems to have less unstable behavior. Even though, the dynamic motions are broader in the dry surface simulation. A loss of control of the dolly vehicle unit results certainly into the loss of control of the 2nd semi-trailer. This furthermore tends to lose the control of the entire vehicle combination, so the stability of the dolly vehicle unit is crucial for the vehicle combination.

The phase portrait and double lane change maneuver can be connected. They both support the same findings of unstable vehicle behavior with excess vehicle unit and wheel sliding, uncontrollability and possible spinning in slippery circumstances. For example if the values of yaw velocity and vehicle unit slip angle in double lane change for the dolly vehicle unit are compared to the stable state area of the phase portrait. It can be seen that these yaw velocity and dolly vehicle unit slip angles have different corresponding stable

states in the phase portrait graph. This furthermore promotes the evidence of successful lane change maneuver. However, the number of possible corresponding states between the double lane change graph and the dolly phase portrait is less in the rough ice surface simulation than in the dry surface simulation. This indicates, that the vehicle is more stable in dry than in slippery circumstances. In addition, the lateral acceleration, yaw velocity and vehicle unit slip angles and the RAs of lateral acceleration, yaw velocity and vehicle unit slip angle in double lane change were over the commonly considered unstable dangerous limits in rough ice surface simulation. Unlike in the dry surface simulations, the vehicle combination seems to be relatively stable and these state variable values and RA-values under the dangerously considered limits.

5.2 Sensitivity analysis of semi-trailer wheel parameter

The four different settings for semi-trailer wheel parameter were analyzed with both the double lane change and dolly phase plane simulation types. First the double lane change maneuver results are addressed and then the dolly phase plane analysis results. In the end, the results from the two simulation types are connected to each other.

The lateral accelerations in double lane change maneuver for different semi-trailer wheel settings are presented in figure 34.

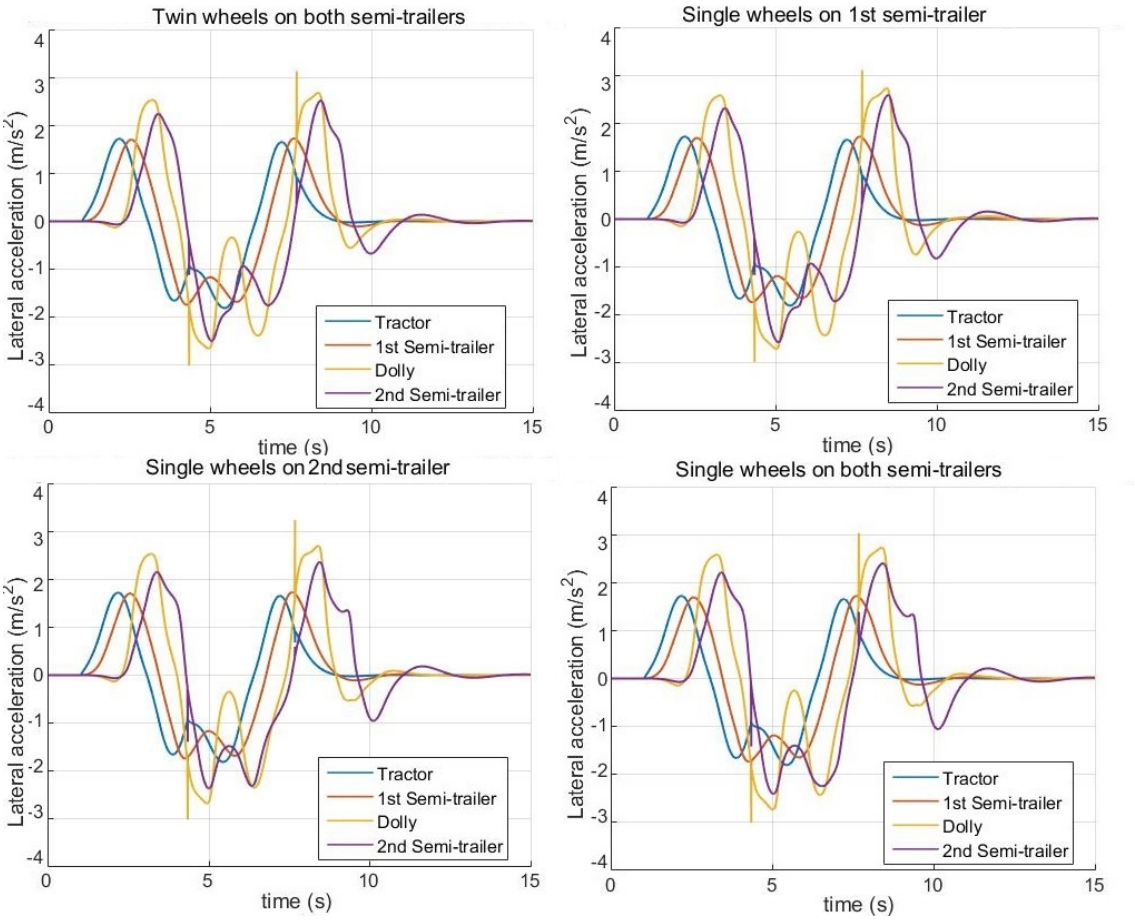

Figure 34. Lateral accelerations of different semi-trailer settings in a double lane change maneuver with a forward velocity of 80km/h

The impact of wheel parameter to the lateral accelerations is minor. It has a slight effect on the RA-values and peak values. The recovery time and motion and time delay, however, tend to stay constant. The recovery time is approximately 14 seconds and the delay from the tractor to the dolly unit is approximately 1.15 seconds in all the settings. The highest RA-values are found similarly from the tractor to dolly vehicle unit in all the settings. The highest RA-values and peak values for the different semi-trailer wheel settings are presented in the table 4 below.

Table 4. Peak values of lateral accelerations and highest RA-values

Twins on both semi − trailers	**Tractor**	**1st semi-trailer**	**Dolly**	**2nd semi-trailer**	**Highest RA-value**
$Peak\ value\left(\frac{m}{s^2}\right)$	1.82	1.740	2.697	2.533	$\frac{2.697}{1.66} = 1.62$
$Peak\ value\ (g)$	0.186	0.177	0.275	0.258	-
$Time\ (s)$	5.45	7.5	8.35	8.40	7.5
Singles on 1st semi − trailer	**Tractor**	**1st semi-trailer**	**Dolly**	**2nd semi-trailer**	**Highest RA-value**
$Peak\ value\left(\frac{m}{s^2}\right)$	1.814	1.73	2.749	2.604	$\frac{2.749}{1.664} = 1.65$
$Peak\ value\ (g)$	0.185	0.176	0.280	0.265	-
$Time\ (s)$	5.45	7.60	8.45	8.50	7.5
Singles on 2nd semi − trailer	**Tractor**	**1st semi-trailer**	**Dolly**	**2nd semi-trailer**	**Highest RA-value**
$Peak\ value\left(\frac{m}{s^2}\right)$	1.82	1.748	2.713	2.378	$\frac{2.713}{1.662} = 1.63$
$Peak\ value\ (g)$	0.186	0.178	0.277	0.242	-
$Time\ (s)$	5.45	4.25	8.40	5.00	7.5
Singles on both semi − trailers	**Tractor**	**1st semi-trailer**	**Dolly**	**2nd semi-trailer**	**Highest RA-value**
$Peak\ value\left(\frac{m}{s^2}\right)$	1.814	1.744	2.751	2.420	$\frac{2.751}{1.668} = 1.65$
$Peak\ value\ (g)$	0.185	0.178	0.280	0.247	-
$Time\ (s)$	5.45	4.25	5.00	5.00	5.00

The difference in the peak values between different settings is negligible. The biggest difference between the settings is seen in the 2nd semi-trailer peak value, between the singles only on 1st and 2nd semi-trailer settings, the percent change is $\frac{2.604-2.378}{2.604} \cdot 100\% = 9.504\%$. Other differences are around 1 to 2 %. In addition, the RA-values differ only marginally by a maximum of ± 0.03.

The RA-values change up to 9.5% between the best and worst scenario, so the impact of the semi-trailer wheel parameter on lateral acceleration is quite small. The shape of the curves are considered. The curves of the tractor, 1st semi-trailer and dolly units have almost no change, but the biggest changes are seen in the curve of the 2nd semi-trailer. The height of the peaks and the shape of the curve change visibly. Since the number of wheels on a semi-trailer rear axle change and the axle load stays constant, the single wheel

vertical load is changed. While the semi-trailer is equipped with single wheels, the height of the peaks increase due to excess RA as a result of insufficient lateral force production. The shape of the curve is smoother with the setting of twin wheels on all semi-trailer rear axles, this implies that the vehicle experiences less oscillation and promotes more stable behavior. The vehicle combination is more stable with twin wheels on all the semi-trailer rear axles. On the other hand, all the RA-values exceed the dangerously considered limit of 1.5, which means that all the settings are experiencing unstable behavior at some level. In all the settings, the lateral acceleration values of the dolly and 2nd semi-trailer units exceed the limit of 0.2 g in slippery conditions, this furthermore supports the evidence of unstable behavior, which may result in excessive vehicle or wheel sliding and a vehicle spin. The motion delay and recovery time are still relatively high if the controllability of the driver is considered. Interesting observation is found that the location of the peak value and RA-value might change between the settings. However, the value differences between the locations are also marginal. The vehicle trails in double lane change are presented in figure 35.

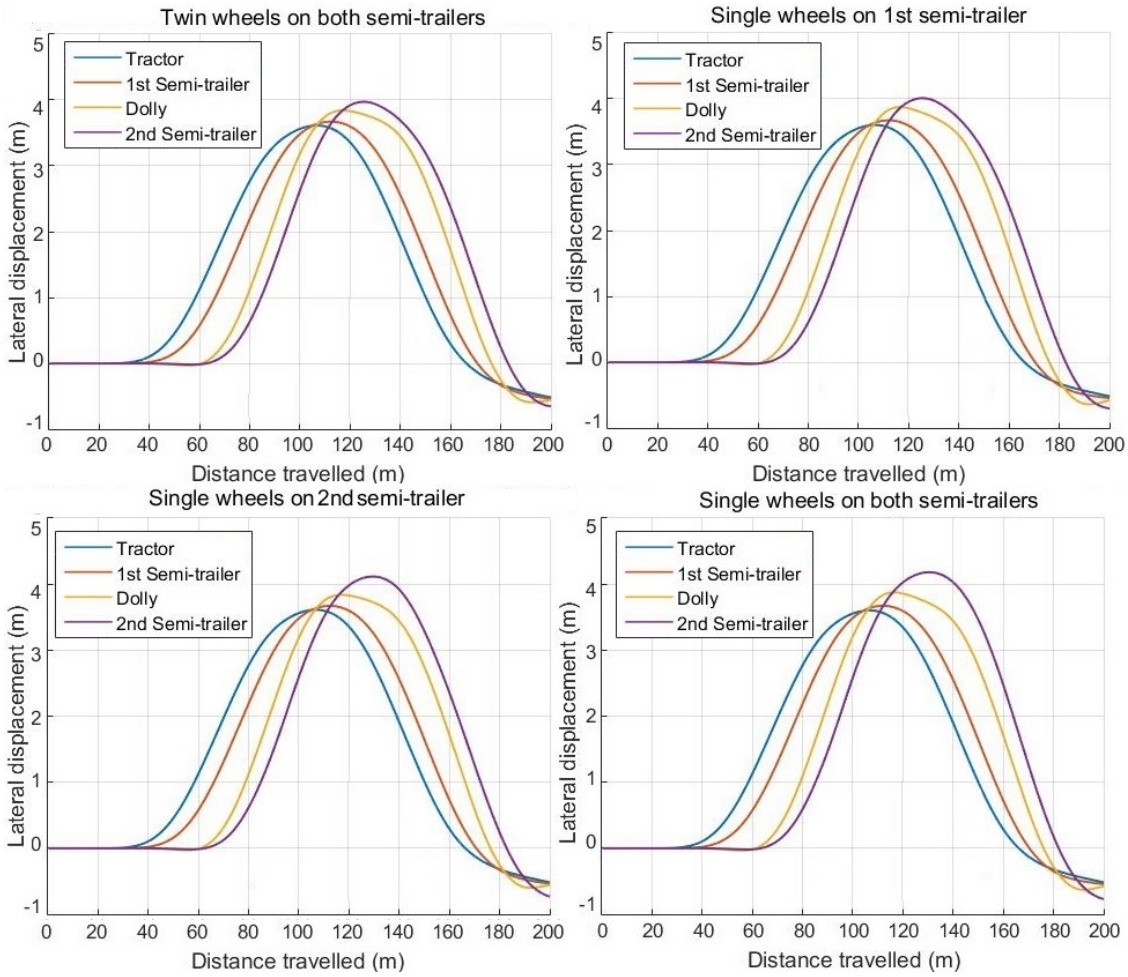

Figure 35. Vehicle unit trail graphs of different semi-trailer wheel settings in a double lane change maneuver with a forward velocity of 80km/h

The effect of the semi-trailer wheel parameter to the vehicle trails is noted. The lateral displacement of the 2nd semi-trailer increase if the semi-trailers are equipped with single wheels only. This furthermore supports the evidence of excess RA of examined state variables due to the lack of proper lateral force production, which results in an excess

wheel and 2nd semi-trailer vehicle unit sliding in lateral direction. The 2nd semi-trailer of the settings of singles on 2nd semi-trailer and singles on both semi-trailers has over 4 meters lateral displacement, which is over the tolerance level of 3.5±0.5 meters. This indicates that the 2nd semi-trailer is constantly at least in somewhat excessive sliding motion during the lane change. The motion and time delay is the same as in the lateral acceleration graphs.

The vehicle unit yaw velocities are presented in figure 36.

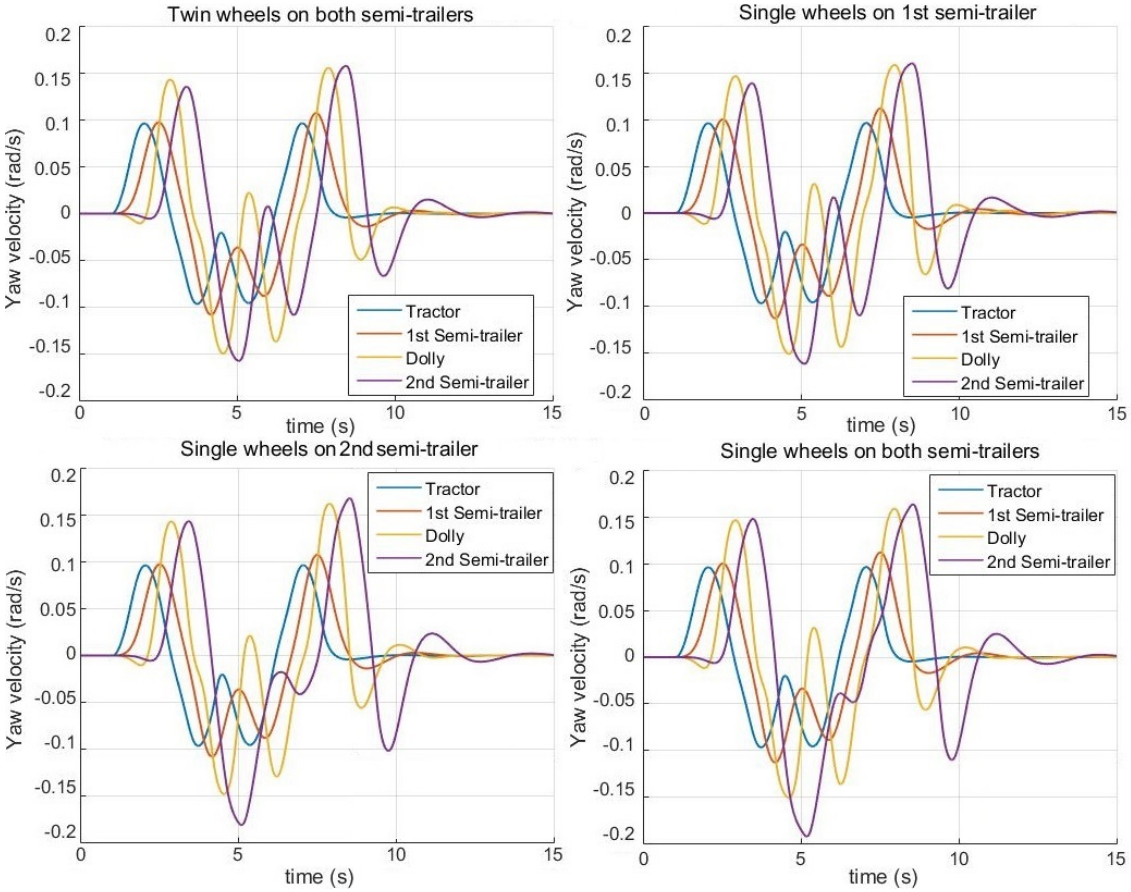

Figure 36. Yaw velocities of different semi-trailer settings in a double lane change maneuver with a forward velocity of 80km/h

The yaw velocities show similarity to the lateral accelerations. A clear effect on the RA-values and peak values can be observed. The recovery time and motion and time delay tend to stay almost unchangeable. The recovery time is approximately 14 seconds and the delay from the tractor to the 2nd semi-trailer unit is approximately 1.4 seconds in all the settings. The highest RA-values are found from the tractor unit to the 2nd semi-trailer unit. The peak values and RA-values are collected in the table 5.

Table 5. Peak values of yaw velocities and highest RA-values

Twins on both semi − trailers	**Tractor**	**1st semi-trailer**	**Dolly**	**2nd semi-trailer**	**Highest RA-value**
$Peak\ value\left(\frac{rad}{s}\right)$	0.097	0.108	0.156	0.158	$\frac{0.158}{0.097} = 1.63$
$Time\ (s)$	7.05	7.5	7.95	8.40	7.5
Singles on 1st semi − trailer	**Tractor**	**1st semi-trailer**	**Dolly**	**2nd semi-trailer**	**Highest RA-value**
$Peak\ value\left(\frac{rad}{s}\right)$	0.097	0.113	0.159	0.162	$\frac{0.162}{0.097} = 1.67$
$Time\ (s)$	7.05	4.15	7.95	5.10	4.5
Singles on 2nd semi − trailer	**Tractor**	**1st semi-trailer**	**Dolly**	**2nd semi-trailer**	**Highest RA-value**
$Peak\ value\left(\frac{rad}{s}\right)$	0.097	0.108	0.163	0.182	$\frac{0.182}{0.097} = 1.88$
$Time\ (s)$	7.05	4.15	7.90	5.10	4.5
Singles on both semi − trailers	**Tractor**	**1st semi-trailer**	**Dolly**	**2nd semi-trailer**	**Highest RA-value**
$Peak\ value\left(\frac{rad}{s}\right)$	0.097	0.113	0.160	0.193	$\frac{0.193}{0.097} = 1.99$
$Time\ (s)$	3.70	4.15	7.95	5.15	4.5

The changes in the peak values for the tractor, 1st semi-trailer and the dolly unit are under 5%. However, the 2nd semi-trailer seems to have relatively high changes in the peak values. The peak value of the 2nd semi-trailer increase up to $\frac{0.193-0.158}{0.158} \cdot 100\% = 22.152\%$ between the twin and single wheels on all semi-trailer rear axle settings. In addition, the RA-value increase up to $\frac{1.99-1.63}{1.63} \cdot 100\% = 22.086\%$. The curves also change more than in the lateral acceleration graphs. Specifically, the 2nd semi-trailer has drastic changes and the dolly unit also experience moderate changes. The tractor and 1st semi-trailer stay almost unchangeable.

The 2nd semi-trailer curve becomes more irregular and the height of the peaks increase as the semi-trailer is equipped with single wheels due to the lack of proper lateral force production. This supports the same findings as in the lateral acceleration graphs regarding the increase of unstable behavior due to the excess RA towards the end of the vehicle combination. However, all the settings have RA-values of over the dangerous limit of 1.5 and the setting of single wheels on all rear axles of semi-trailers is almost up to 2. In these conditions it is arguably clear that the vehicle combination experience unstable behavior and is difficult to control. The RA-values and peak values increase up to 22% from the best to worst scenario, which indicates clear differences in the rotational stability between the settings. This may lead into excess wheel and vehicle unit sliding, when the vehicle unit tries to rotate excessively. As a single notion, the yaw velocity peak values over 0.15 rad/s are relatively high and may indicate some unstable behavior and tendency to excess wheel and vehicle unit sliding at the peak value times. The motion delay and recovery time are still relatively high if the controllability of the driver is considered. Interesting observation is found that the location of the peak values and RA-values might change between the settings, this furthermore supports the evidence of increased RAs and

unstable behavior in the vehicle units. The vehicle combination and specifically the 2nd semi-trailer experience more unstable behavior if the semi-trailers are equipped with single wheels.

The vehicle unit slip angles in different semi-trailer settings are presented in figure 37.

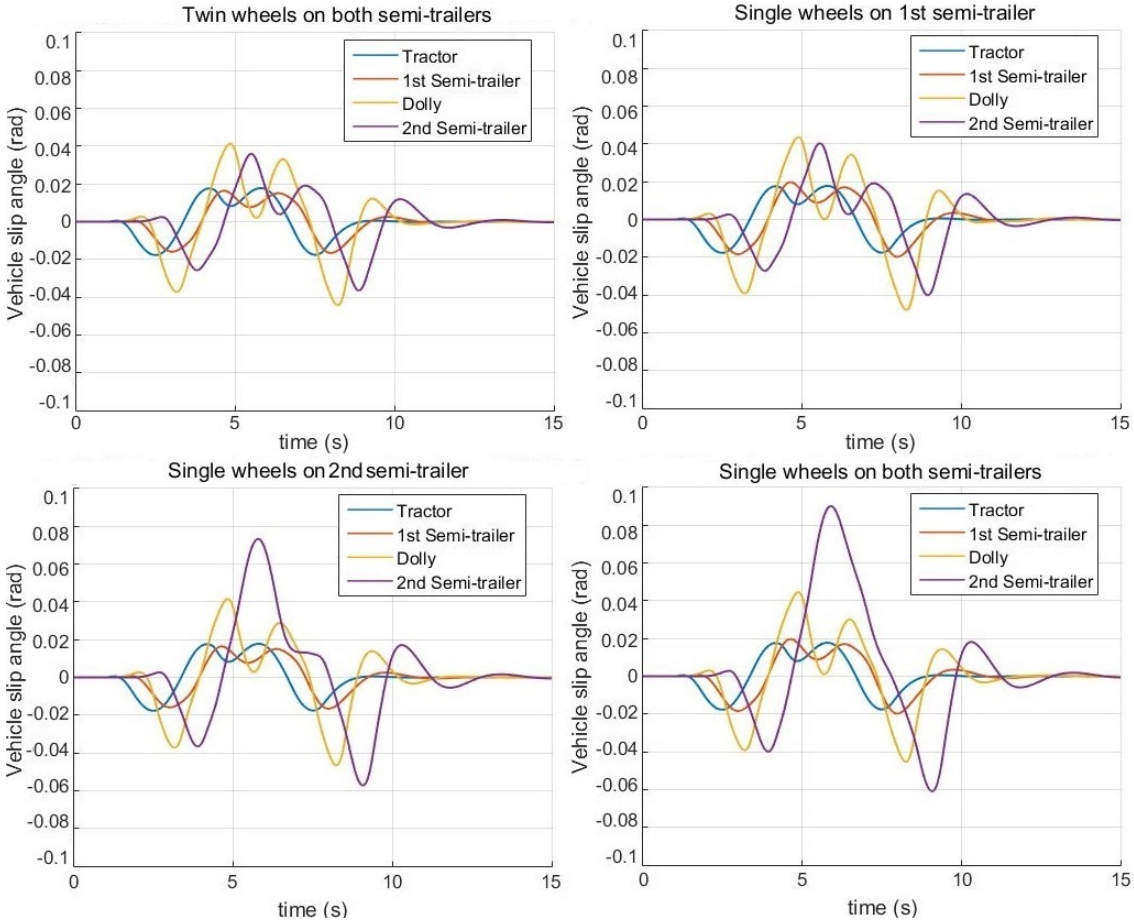

Figure 37. Vehicle unit slip angles of different semi-trailer wheel settings in a double lane change maneuver with a forward velocity of 80km/h

The vehicle unit slip angles visually indicates the same findings as the yaw velocity and lateral acceleration graphs. The recovery time and motion and time delay have almost no changes between the different semi-trailer wheel settings. The recovery time is approximately 14 seconds and the delay from the tractor to the 2nd semi-trailer unit is approximately 1.5 seconds in all the settings. The RA-values and peak values of the slip angles experience clear changes. An observation is done regarding the highest RA-value. In the two upper graphs the highest RA-value is found from the tractor unit to the dolly unit, but in the two lower graphs the highest RA-value is found from the tractor unit to the 2nd semi-trailer unit. The peak values and RA-values are gathered in the table 6.

Table 6. Peak values of vehicle slip angles and highest RA-values

Twins on both semi − trailers	**Tractor**	**1st semi-trailer**	**Dolly**	**2nd semi-trailer**	**Highest RA-value**
$Peak\ value(rad)$	0.018	0.016	0.044	0.036	$\frac{0.044}{0.018} = 2.44$
$Peak\ value\ (°)$	1.031	0.917	2.521	2.063	-
$Time\ (s)$	4.15	4.65	8.2	8.9	7.5
Singles on 1st semi − trailer	**Tractor**	**1st semi-trailer**	**Dolly**	**2nd semi-trailer**	**Highest RA-value**
$Peak\ value(rad)$	0.018	0.020	0.048	0.040	$\frac{0.048}{0.018} = 2.67$
$Peak\ value\ (°)$	1.031	1.146	2.750	2.292	-
$Time\ (s)$	4.15	4.65	8.3	5.55	7.5
Singles on 2nd semi − trailer	**Tractor**	**1st semi-trailer**	**Dolly**	**2nd semi-trailer**	**Highest RA-value**
$Peak\ value(rad)$	0.018	0.017	0.047	0.073	$\frac{0.073}{0.018} = 4.06$
$Peak\ value\ (°)$	1.031	0.974	2.693	4.183	-
$Time\ (s)$	5.80	8.0	8.25	5.8	5.8
Singles on both semi − trailers	**Tractor**	**1st semi-trailer**	**Dolly**	**2nd semi-trailer**	**Highest RA-value**
$Peak\ value(rad)$	0.018	0.020	0.045	0.090	$\frac{0.090}{0.018} = 5.00$
$Peak\ value\ (°)$	1.031	1.146	2.578	5.157	-
$Time\ (s)$	5.8	8.0	8.25	5.9	5.9

The slip angle value of the 2nd semi-trailer increases from twins on both trailers to singles on both trailers up to $\frac{0.090-0.036}{0.036} \cdot 100\% = 150\%$. The slip angles of the tractor and 1st semi-trailer unit in all the settings are considered to be moderate at this forward velocity, and not dangerous. The slip angles of dolly and 2nd semi-trailer unit are very large at this forward velocity, specifically the slip angle of the 2nd semi-trailer in the two lower graphs.

The larger slip angles are the result of excessive wheel and vehicle sliding in lateral direction, which was earlier indicated with the trail and yaw velocity graphs due to excess RA and incapability of producing enough lateral force. The large peaks of the 2nd semi-trailer slip angle in the lower graphs occur at the same time as the large peaks of the yaw velocity and lateral acceleration. In addition, the wide lateral displacement of the dolly and 2nd semi-trailer occur at the same moment of time. This finding furthermore supports the evidence of very unstable behavior and excessive wheel and vehicle sliding in lateral direction in a double lane change maneuver with single wheels equipped in the semi-trailer rear axle wheels. This indicates that the vehicle might be close to unstable behavior or difficult to control. The slip angles of the tractor and 1st semi-trailer units are generally between 1° and 2°, which is moderate at this forward velocity and the tires are functioning in the linear region, which promotes stable behavior. Most of the slip angles of the dolly and 2nd semi-trailer units are over the limit of 2.5°, which was considered large at this forward velocity and the tire lateral forces might be close to nonlinear region.

Furthermore, the 2nd semi-trailer of the single wheels on both trailers setting has over 5° slip angle. This large vehicle slip angle cannot be considered to be controllable or stable at any level on low road friction surfaces. The tire lateral forces most probably act strongly in the nonlinear region. The slip angle RA-values are very high for all the vehicle combinations in all the settings, specifically in the lower graphs. This implies that the dolly and 2nd semi-trailer units receive a high amount of RA of the examined state variables, such as lateral velocity, lateral acceleration and yaw velocity. Furthermore, this means that they are being deviated much more from the initial position. For example, as the 2nd semi-trailer unit in the singles on both semi-trailers setting has 5 times the slip angle of the first vehicle unit in the same maneuver and a peak value increase of 2.5 times compared to the most stable setting. This kind of vehicle behavior cannot be considered as stable and the vehicle unit and moreover, the vehicle combination is uncontrollable and unstable.

The sensitivity analysis of the semi-trailer wheel parameter in double lane change imply that all the vehicle combinations experience unstable behavior at some level and they would be difficult to control for the driver in slippery road circumstances. Moreover, the number of wheels on semi-trailer axles plays a decent role regarding the lateral stability. With single wheels on the rear axles of the semi-trailers, the system experiences more unstable behavior, such as excessive wheel and vehicle unit sliding and oscillation due to lack of capability of producing enough lateral force on a single tire, which is the result of increased vertical load in a single wheel. However, all the vehicle combination systems are mathematically stable, as they return back to the lane in the end and the vehicle units are recovered. On the other hand, as the excess RAs of the examined state variables and extra lateral displacements of dolly and 2nd semi-trailer units show that the vehicle is uncontrollable by the driver. Furthermore, the extra lateral displacements in the worst scenarios show that the dolly and 2nd semi-trailer units would have not staid in the standard 3.5 meters wide lane. This means that they would either be partially on the opposing lane of the traffic or on the hard shoulder of the road. If a vehicle is driven off on to the opposing lane of the traffic, it may cause extremely dangerous situations to anyone in the traffic, particularly on low road friction surfaces. Specifically a vehicle combination with such a high mass and velocity as Double-A would probably drive over everyone else. Depending on the quality of the ground outside the lane, the vehicle is highly probable to experience more unstable behavior, which may lead into a vehicle spin or roll-over.

The negative influence of twin wheels on a semi-trailer rear axle would be that it increases the vehicle mass and the fuel consumption of the vehicle combination. The increased mass and friction contact area of tires increase the requirement of more engine power in order to overcome the rolling resistance. The vehicle combination would also require more wheels, which increases the consumption of rims. In addition, the twin wheels and increased consumption factors indirectly decrease the productivity. The dolly vehicle unit phase portraits for different semi-trailer wheel settings are presented in figures 38-41.

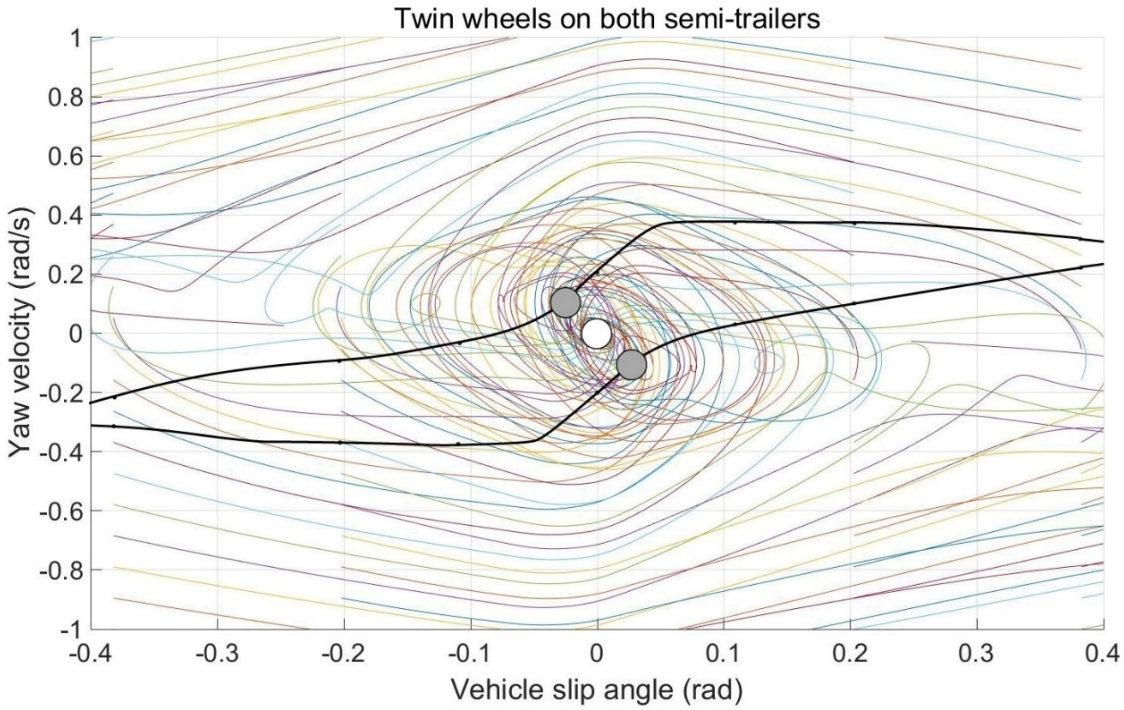

Figure 38. Dolly vehicle unit phase portrait with twin wheels on both semi-trailers simulated with a forward velocity of 80km/h

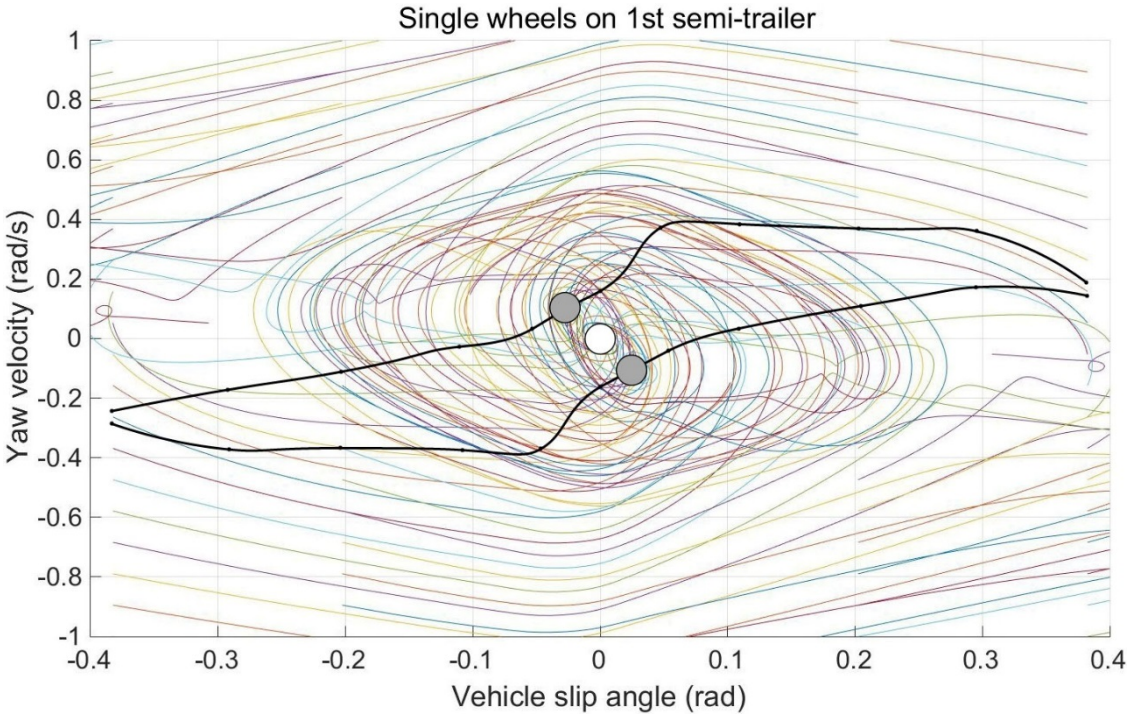

Figure 39. Dolly vehicle unit phase portrait with single wheels on 1st semi-trailer simulated with a forward velocity of 80km/h

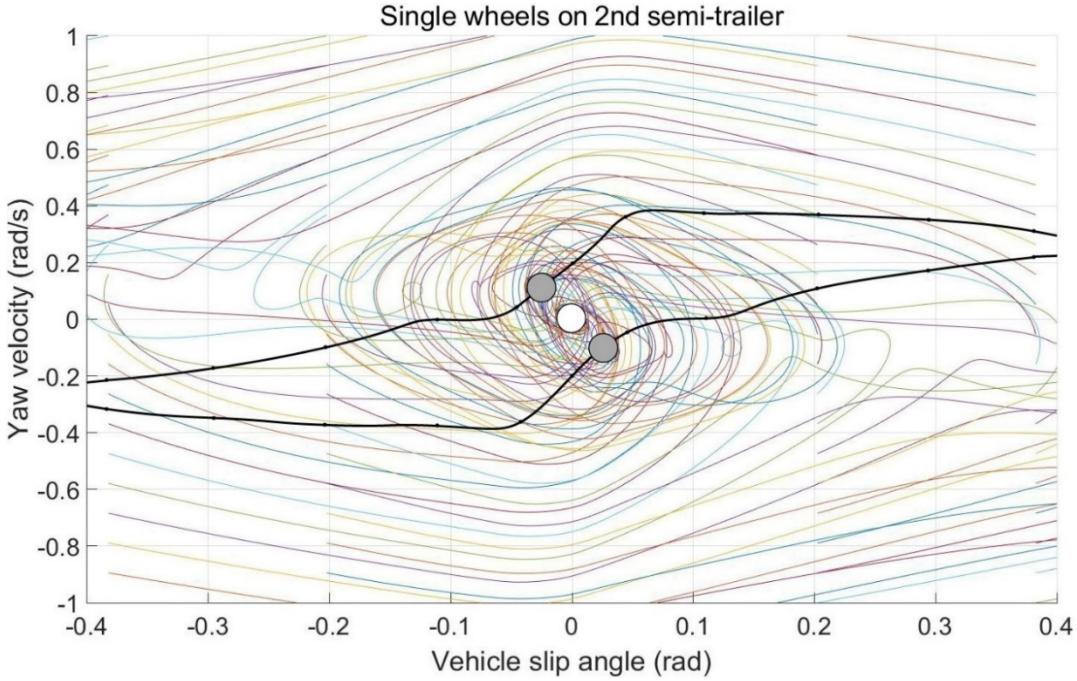

Figure 40. Dolly vehicle unit phase portrait with single wheels on 2nd semi-trailer simulated with a forward velocity of 80km/h

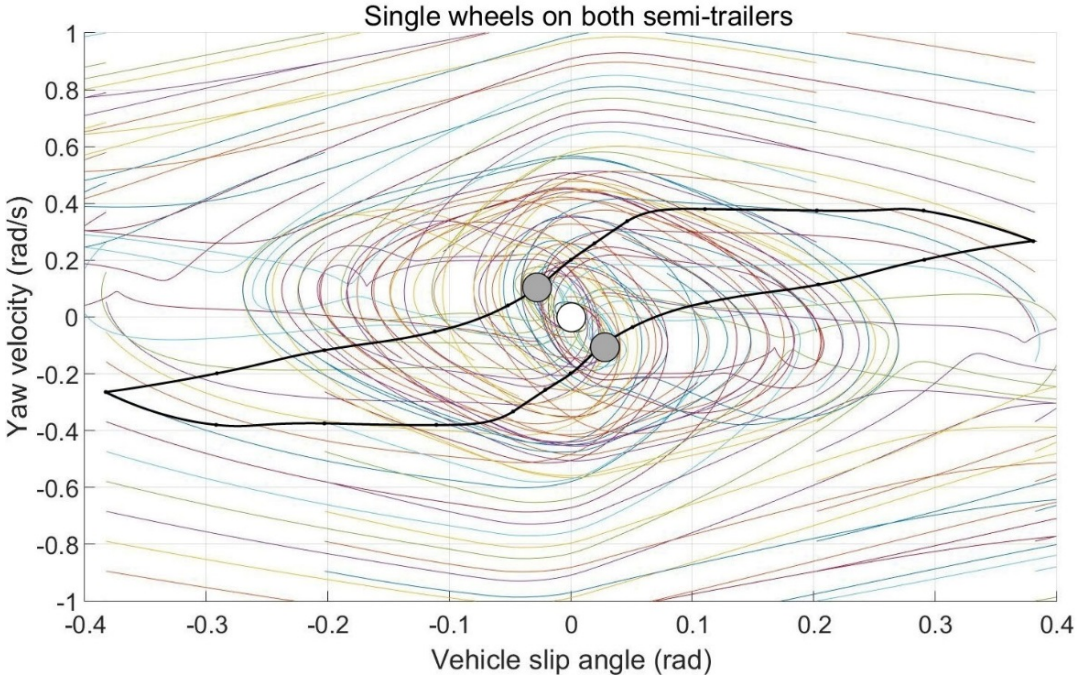

Figure 41. Dolly vehicle unit phase portrait with single wheels on both semi-trailers simulated with a forward velocity of 80km/h

The stable areas of the phase portraits of different semi-trailer wheel settings are very similar to each other. The stable focuses locate at the origin in all the settings. Additionally, the location of the unstable saddle points are equal in all the settings. The unstable saddle points locate at (-0.028, 0.1) and (0.028, -0.1). The size of the stable areas have some differences. The stable area becomes thinner with larger vehicle slip angles. Furthermore, the slip angle boundary values of the phase portraits of the graphs with

single wheels on the rear axles of the 1st semi-trailer and single wheels on the rear axles of both semi-trailers end before the slip angle reaches ± 0.4 radians. Whereas the slip angle boundary values of the phase portraits of the graphs with single wheels on the rear axles of the 2nd semi-trailer and twin wheels on the rear axles of both semi-trailers continue over the slip angle values of ± 0.4 radians. However, the MF parameters were only valid up to slip angle values of ± 0.4 radians. All the stable areas of different settings are limited by yaw velocity between $\pm 0.35 \frac{rad}{s}$.

This indicates that the dolly vehicle unit has a narrow track of stable area further for the settings of twin wheels on the rear axles of both semi-trailers and single wheels on the rear axles of the 2nd semi-trailer, which means that the dolly vehicle unit could be somewhat more stable with very large slip angles. The overall stable area shape differs between the graphs. The cases with only single wheels on either one of the rear axles of the semi-trailers have a bending in the area at the middle section. This decreases the stable area in the middle section as it becomes slightly narrower. The shapes of the curves in graphs differ. Generally, the same observation is done as in the earlier chapter, where the dry surface and slippery surface were compared. The dolly vehicle unit and it wheels seem to be sliding excessively at some level, which means that they don't transmit the dynamic motions and phenomena properly. This excessive sliding cannot be considered completely as stable behavior, because it may be uncontrollable. An observation is done that in the two settings where the rear axles of both semi-trailers are equipped with twin wheels and the rear axles of the 2nd semi-trailer is equipped with single wheels the dolly vehicle unit oscillates clearly less towards the center point. This may be the result of the vehicle unit order, because if the vehicle unit behind the dolly vehicle unit is modified, the effect is arguably lower than the effect if the vehicle unit in front of the dolly is modified. This excessive oscillation in the two other graphs can be considered as unstable behavior, because the vehicle state variables increase and decrease fast from side to side. This kind of behavior is at least uncontrollable by the driver. Not any of the settings allow different signed yaw rate and slip angle values in the stable area, similarly to the cases in the dry surface versus slippery surface comparison.

The semi-trailer wheel parameter unit has an indirect influence to the dolly vehicle, so the analysis was relatively difficult to perform. The twin wheels on the rear axles of the semi-trailers seem to promote the stability of the dolly vehicle unit slightly and the differences between the settings are relatively small. However, all the settings have relatively low stable area, which indicates that the vehicle unit and combination can easily become unstable. A more stable dolly vehicle unit promotes directly the stability of the entire system, specifically the stability of the 2nd semi-trailer unit behind it.

The phase plane analysis and double lane change maneuver can be connected. If the values of yaw velocity and vehicle unit slip angle in double lane change for the dolly vehicle unit are compared to the stable state area of the phase portrait. It can be seen that these yaw velocity and dolly vehicle unit slip angles have different corresponding stable states in the phase portrait graph. This furthermore promotes the evidence of a successful lane change maneuver. On the other hand, the modified parameter affects directly the semi-trailer units and indirectly the dolly vehicle units. This means that the stability of the vehicle combination is viewed differently, since the effect of the semi-trailer wheel parameter to the dolly vehicle unit in double lane change is relatively low, but the effect to the vehicle combination is relatively high. Furthermore, the effect is also relatively low in the dolly vehicle unit phase portraits as was discussed. The semi-trailer wheel

parameter has indirect effect on the stability of the dolly vehicle unit and it seems that the dolly vehicle unit is somewhat more stable and has less unstable behavior such as excessive oscillation and sliding when the semi-trailers have twin wheels on their rear axles. Specifically, the semi-trailers and particularly the 2nd semi-trailer becomes more stable with more wheels on their rear axles. They experience less excessive sliding, oscillation and uncontrollability. Moreover, the vehicle combination becomes more stable to control and maneuver. Both the double lane change and dolly vehicle unit phase portraits indicate the same findings that the vehicle combination is more stable with twin wheels on the rear axles of the semi-trailers when driven in slippery circumstances, particularly, in extreme situations.

5.3 Sensitivity analysis of dolly drawbar parameter

The three different dolly vehicle unit settings were simulated with both simulation types, similarly to the semi-trailer wheel parameter simulation. First the double lane change maneuver results are presented and after the dolly phase plane analysis results. Finally, the two simulation results are connected to each other.

The lateral accelerations of different dolly drawbar settings are presented in figure 42.

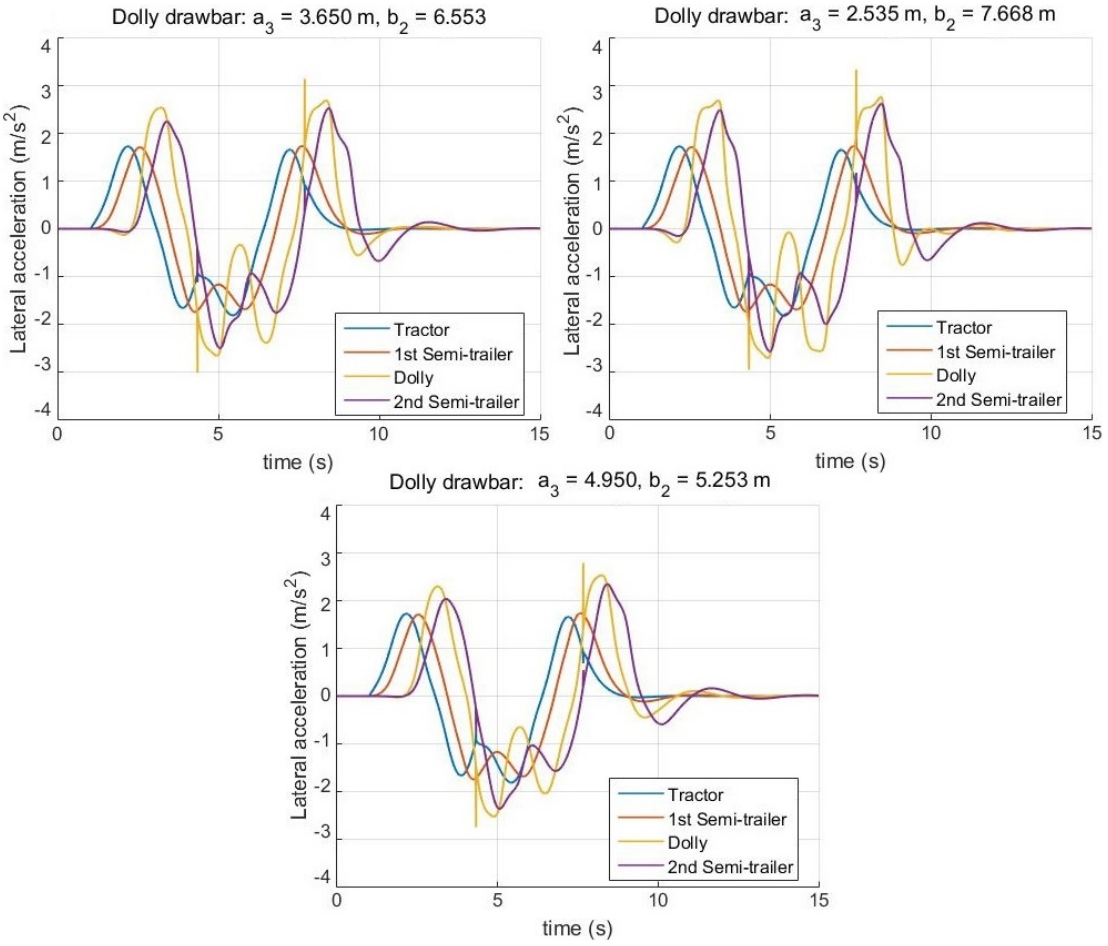

Figure 42. Lateral accelerations of different dolly drawbar parameter settings in a double lane change maneuver with a forward velocity of 80km/h

The dolly drawbar parameter has slight impact on the lateral accelerations. The peak values and RA-values have small differences. The recovery time and motion and time delay seems to stay relatively constant. The recovery time is approximately 14 seconds and the delay from the tractor to the dolly unit is approximately 1.15 seconds in all the settings. However, the oscillation of dolly vehicle unit seems to differ between the different dolly parameter settings. The highest RA-values are found from the tractor unit to the dolly vehicle unit. The peak and RA-values for different dolly drawbar parameter settings are presented in the table 7 below.

Table 7. Peak values of lateral accelerations and highest RA-values

$\boldsymbol{Default\ dolly}$ $\boldsymbol{a_3 = 3.65, b_2 = 6.553}$	**Tractor**	**1st semi-trailer**	**Dolly**	**2nd semi-trailer**	**Highest RA-value**
$Peak\ value\left(\frac{m}{s^2}\right)$	1.82	1.740	2.697	2.533	$\frac{2.697}{1.66} = 1.62$
$Peak\ value\ (g)$	0.186	0.177	0.275	0.258	-
$Time\ (s)$	5.45	7.5	8.35	8.40	7.5
$\boldsymbol{Minimum\ dolly}$ $\boldsymbol{a_3 = 2.535, b_2 = 7.668}$	**Tractor**	**1st semi-trailer**	**Dolly**	**2nd semi-trailer**	**Highest RA-value**
$Peak\ value\left(\frac{m}{s^2}\right)$	1.827	1.74	2.772	2.63	$\frac{2.772}{1.657} = 1.67$
$Peak\ value\ (g)$	0.186	0.177	0.283	0.268	-
$Time\ (s)$	5.45	4.25	8.45	8.45	7.5
$\boldsymbol{Maximum\ dolly}$ $\boldsymbol{a_3 = 4.95, b_2 = 5.253}$	**Tractor**	**1st semi-trailer**	**Dolly**	**2nd semi-trailer**	**Highest RA-value**
$Peak\ value\left(\frac{m}{s^2}\right)$	1.817	1.75	2.54	2.37	$\frac{2.54}{1.664} = 1.53$
$Peak\ value\ (g)$	0.185	0.178	0.259	0.242	-
$Time\ (s)$	5.45	4.25	8.25	5.05	7.5

The value differences between the settings are small. It can be seen, that the maximum dolly setting has the smallest peak values and RA-value. This indicates that the maximum dolly setting is more stable. The tractor and 1st semi-trailer peak values differ only marginally between the settings, but the dolly and 2nd semi-trailer units have visible differences between the settings. The largest difference between the peak values can be found from the 2nd semi-trailer between the minimum and maximum dolly settings. The percentage change is $\frac{2.63-2.37}{2.37} \cdot 100\% = 10.97\%$. The peak values of dolly units between the minimum and maximum setting has a percentage change of $\frac{2.772-2.54}{2.54} \cdot 100\% = 9.134\%$. The other differences are relatively smaller. The RA-values differ. The maximum dolly setting has slightly over 1.5 whereas the other two settings have above 1.6. All of these are considered relatively high, because they exceed the limit of 1.5. None of the peak values of the tractor or 1st semi-trailer unit exceed the limit of 0.2 g, however, all of the peak values of the dolly and 2nd semi-trailer unit exceed the limit of 0.2 g.

This indicates that the dolly and 2nd semi-trailer units might experience some unstable behavior. On the other hand, the double lane change maneuver is completed successfully in all the setting simulations. The RA-values and peak values increase up to 10% between

the best and worst scenario, so the effect is relatively small on lateral acceleration. An observation is done. The maximum setting simulation has the most calm and smoothest curve shapes among vehicle units, whereas the two other settings has more oscillation and irregularity in the curves of the dolly and 2nd semi-trailer units. Specifically the dolly vehicle unit has relatively high oscillation and amplification in the minimum dolly setting during the double lane change maneuver. This furthermore indicates that the vehicle combination with the minimum dolly drawbar setting is more unstable. The vehicle combination in minimum dolly setting is experiencing some unstable behavior, and the possibility of excess wheel and vehicle unit sliding is possible. The same phenomena might occur in the default setting. A long dolly drawbar attached close to the rear wheels of the vehicle unit in front promotes stable behavior and decreases RAs and excess oscillation. A long dolly vehicle unit drawbar doesn't transmit the dynamic motions so aggressively and it preserves the vehicle combination from high RAs, which would furthermore, promote unstable behavior. The location of the peak values might change when the dolly drawbar is adjusted. However, the differences are negligible. The motion and time delays and recovery times are relatively high in all the settings, which makes the controllability of the vehicle more difficult for a driver.

The vehicle unit trails in double lane change are presented in figure 43.

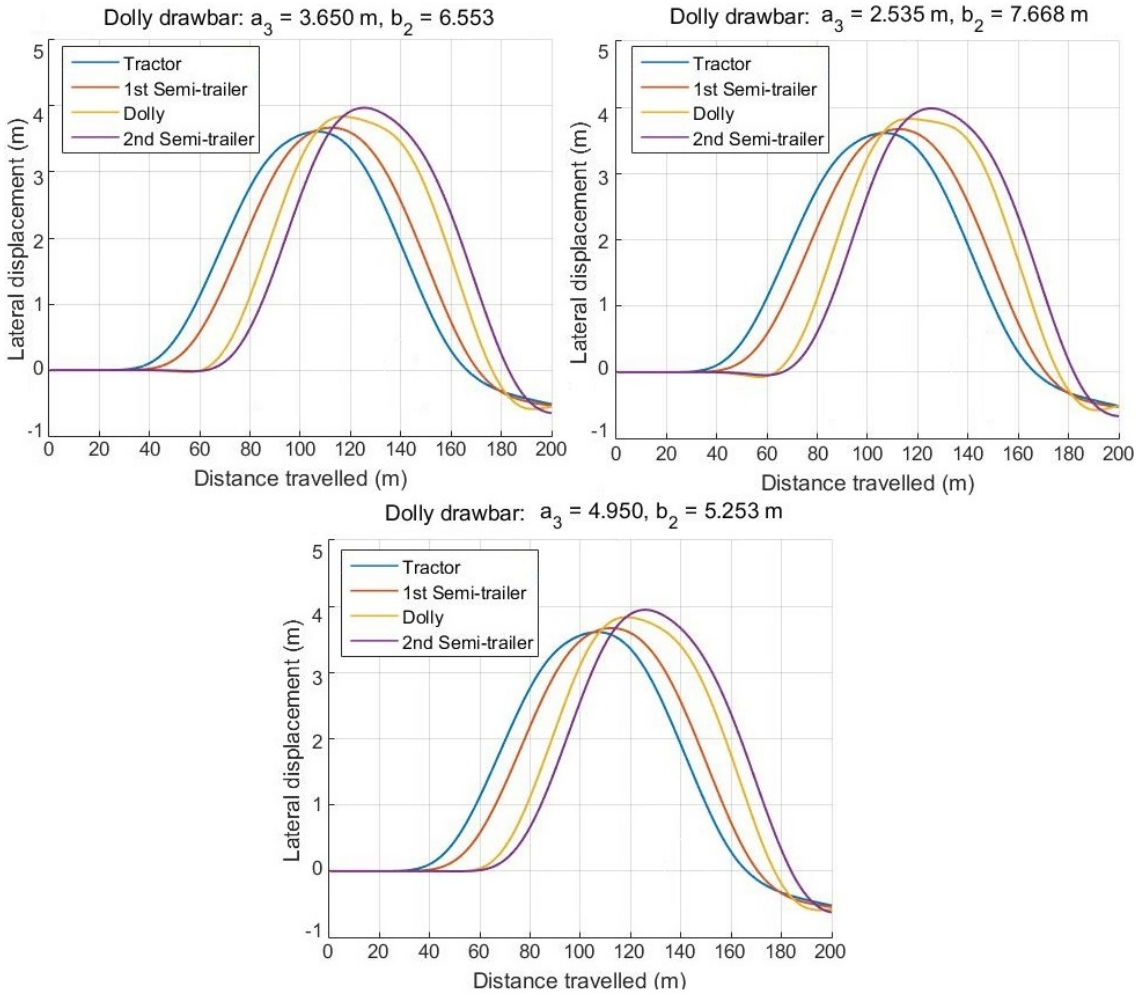

Figure 43. Vehicle unit trail graphs of different dolly drawbar settings in a double lane change maneuver with a forward velocity of 80km/h

The lateral displacement differences of the vehicle units between the different dolly setting simulations is negligible. The minimum dolly setting seems to have some irregularity in the curve of the dolly vehicle unit, compared to the two other simulations. This indicates some tendency of excessive sliding in the lateral direction, because of the sharper shape of the curve. Although, this phenomenon is very marginal and it is not enough alone to indicate unstable or stable behavior. The rest of the vehicle units seem to act similarly calm to each other. The recovery and delay times are similarly approximately 14 seconds and 1.5 seconds from the tractor to the 2nd semi-trailer unit. The dolly and 2nd semi-trailer vehicle units have up to 0.5 meters more lateral displacement in the lane change. Similarly to other simulations, the vehicle units in the returning maneuver seem to go approximately 0.5 meters off target due to the open-loop simulation and excessive sliding in lateral direction. It was indicated, that these two vehicle units slide excessively in the slippery circumstances with such a high forward velocity as the result of excess RAs of the examined state variables from the vehicle units in front. The vehicle yaw velocities are presented in figure 44.

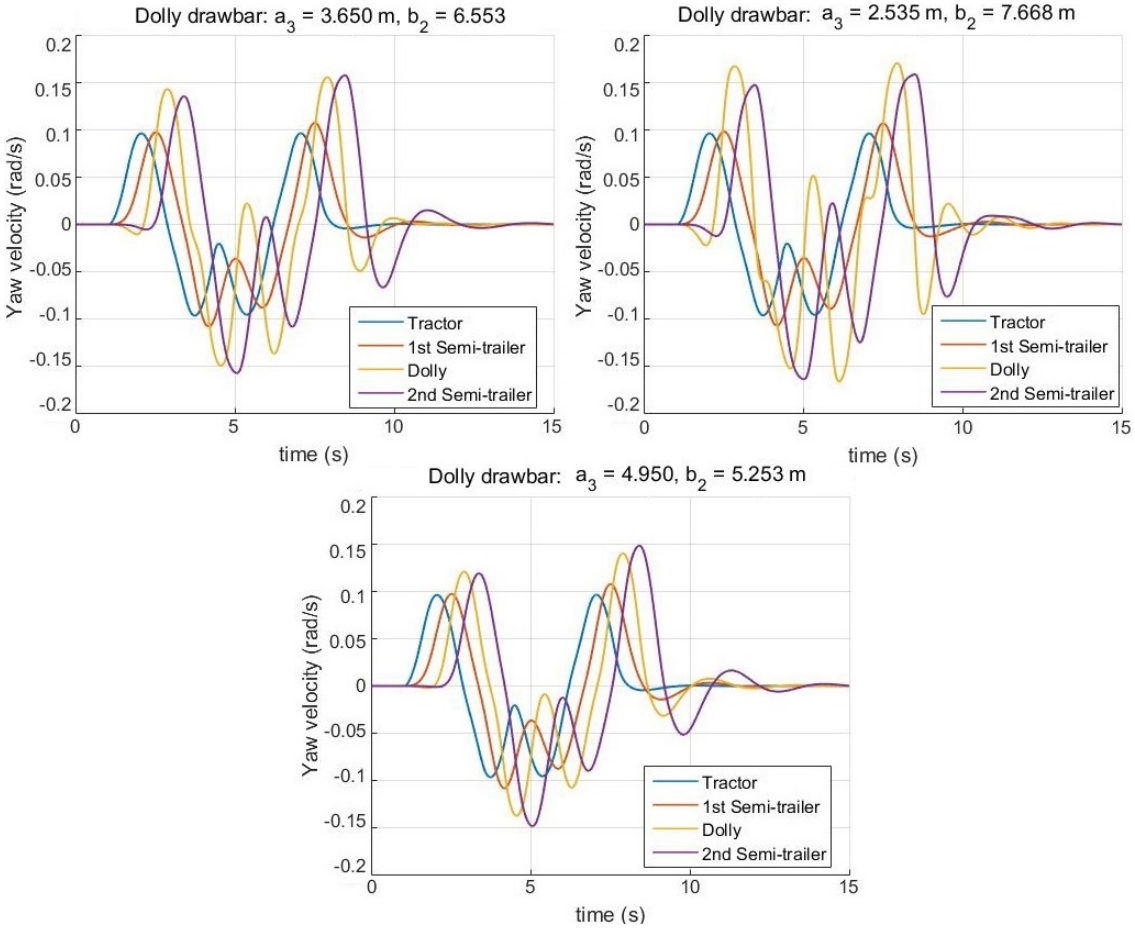

Figure 44. Yaw velocities of different dolly drawbar parameter settings in a double lane change maneuver with a forward velocity of 80km/h

The yaw velocities have relatively large differences between the dolly settings. The recovery and delay times are similar to the trail and lateral acceleration graphs. The peak values and RA-values are highest with the minimum dolly setting and lowest with the maximum dolly setting. Additionally, the oscillation and shape of the curves is calmer in the maximum dolly setting than in the two other settings. The highest RA-values are

found from the tractor unit to the 2nd semi-trailer with the default and maximum setting. The highest RA-value for the minimum setting is, however, found from the tractor unit to the dolly unit. The peak values and RA-values are presented in the table 8 below.

Table 8. Peak values of yaw velocities and highest RA-values in different dolly drawbar settings

$\boldsymbol{Default\ dolly}$ $\boldsymbol{a_3 = 3.65, b_2 = 6.553}$	**Tractor**	**1st semi-trailer**	**Dolly**	**2nd semi-trailer**	**Highest RA-value**
$Peak\ value\left(\frac{rad}{s}\right)$	0.097	0.108	0.156	0.158	$\frac{0.158}{0.097} = 1.63$
$Time\ (s)$	7.05	7.5	7.95	8.40	7.5
$\boldsymbol{Minimum\ dolly}$ $\boldsymbol{a_3 = 2.535, b_2 = 7.668}$	**Tractor**	**1st semi-trailer**	**Dolly**	**2nd semi-trailer**	**Highest RA-value**
$Peak\ value\left(\frac{rad}{s}\right)$	0.097	0.107	0.171	0.164	$\frac{0.171}{0.097} = 1.76$
$Time\ (s)$	7.05	4.15	7.95	5.0	4.5
$\boldsymbol{Maximum\ dolly}$ $\boldsymbol{a_3 = 4.95, b_2 = 5.253}$	**Tractor**	**1st semi-trailer**	**Dolly**	**2nd semi-trailer**	**Highest RA-value**
$Peak\ value\left(\frac{rad}{s}\right)$	0.097	0.109	0.141	0.149	$\frac{0.149}{0.097} = 1.54$
$Time\ (s)$	7.05	4.15	7.90	8.40	4.5

The tractor and 1st semi-trailer units tend to stay unchangeable. The dolly and 2nd semi-trailer vehicle units experience more oscillation and higher yaw velocity values when the dolly drawbar is shortened and the articulation point is further away from the rear axles of the vehicle unit in front. The percentage change of the RA-value between the minimum and maximum settings is $\frac{1.76-1.54}{1.54} \cdot 100\% = 14.3\%$. The largest percentage change between the peak values can be found from the dolly vehicle unit between the minimum and maximum settings $\frac{0.171-0.141}{0.141} \cdot 100\% = 21.3\%$. The motion and time delay and recovery time seems to stay relatively constant between the settings, however, the amount of excess oscillation changes. The minimum and default settings have more oscillation in the yaw velocity curves than the maximum setting. The shapes of the curves seem to be quite smooth in all the settings. The RA and the yaw velocity values increase when the articulation point is further away from the rear axles of the vehicle unit in front and when the dolly drawbar is shorter.

A longer dolly drawbar attached closer to the rear wheels of the vehicle unit in front promotes more stable vehicle combination and unit behavior. The yaw velocities of the vehicle units decrease, as well as the excess oscillation and RA. On the other hand, all the RA-values of different dolly settings exceed the limit of 1.5, which indicates, that all the settings might experience at least some unstable behavior. Specifically, the minimum setting is under heavy RAs, which might lead to a loss of control of the dolly and 2nd semi-trailer units. The yaw velocity peak values over 0.15 rad/s are relatively high and may indicate some unstable behavior and tendency to excessive wheel and vehicle unit sliding at the peak value times. The RA-values increase up to 15% and the yaw velocity values up to 21% from the best to worst scenario, which is a clear difference in the rotational stability. This indicates that the vehicle combination is more stable with a

longer dolly drawbar and an articulation point located closer to the rear axles of the vehicle unit in front. The slip angles of the different vehicle units with different dolly drawbar settings are presented in figure 45.

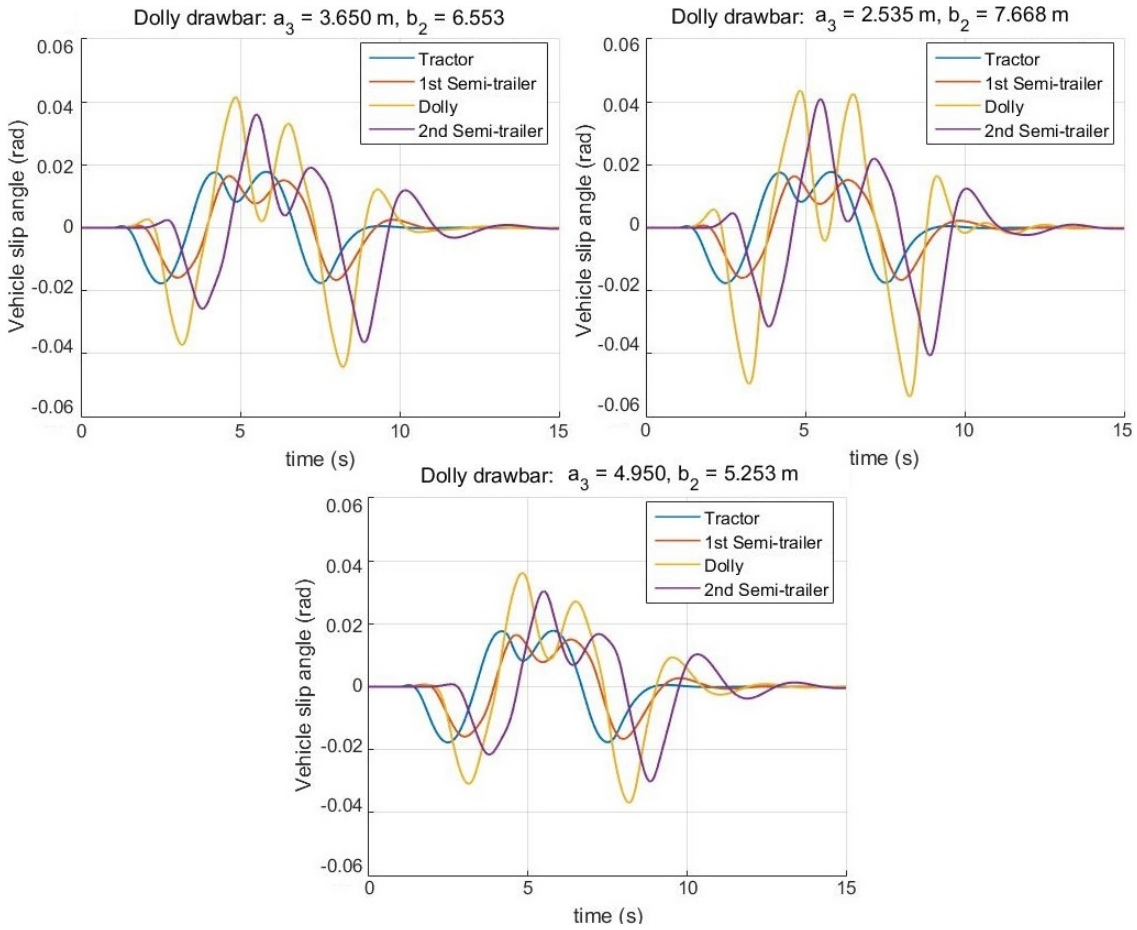

Figure 45. Vehicle unit slip angles with different dolly drawbar settings in a double lane change maneuver with a forward velocity of 80km/h

The vehicle unit slip angle graphs support the same findings as the lateral acceleration and yaw velocity graphs. The recovery time is approximately 14 seconds and the motion and time delay is approximately 1.15 seconds from the tractor to the dolly vehicle unit. They stay almost unchangeable between the different dolly drawbar settings. The RA-values and peak values of the slip angles experience visible changes. Especially, the slip angles of the dolly and 2nd semi-trailer vehicle units change noticeably. The peak values and RA-values are gathered in table 9.

Table 9. Peak values of vehicle unit slip angles and highest RA-values

$\boldsymbol{Default\ dolly}$ $\boldsymbol{a_3 = 3.65, b_2 = 6.553}$	Tractor	1st semi-trailer	Dolly	2nd semi-trailer	Highest RA-value
$Peak\ value(rad)$	0.018	0.016	0.044	0.036	$\frac{0.044}{0.018} = 2.44$
$Peak\ value\ (°)$	1.031	0.917	2.521	2.063	-
$Time\ (s)$	4.15	4.65	8.2	8.9	7.5
$\boldsymbol{Minimum\ dolly}$ $\boldsymbol{a_3 = 2.535, b_2 = 7.668}$	Tractor	1st semi-trailer	Dolly	2nd semi-trailer	Highest RA-value
$Peak\ value(rad)$	0.018	0.017	0.054	0.041	$\frac{0.054}{0.018} = 3.0$
$Peak\ value\ (°)$	1.031	0.974	3.094	2.349	-
$Time\ (s)$	5.80	8.0	8.25	5.45	7.5
$\boldsymbol{Maximum\ dolly}$ $\boldsymbol{a_3 = 4.95, b_2 = 5.253}$	Tractor	1st semi-trailer	Dolly	2nd semi-trailer	Highest RA-value
$Peak\ value(rad)$	0.018	0.017	0.037	0.030	$\frac{0.037}{0.018} = 2.06$
$Peak\ value\ (°)$	1.031	0.974	2.120	1.719	-
$Time\ (s)$	5.80	8.0	8.20	5.50	7.5

The slip angles of all the vehicle units are at least moderate in all the settings. Specifically the latter dolly and 2nd semi-trailer units have noticeably large slip angle values, particularly, in the minimum dolly setting. The peak value of the dolly vehicle unit increase up to $\frac{0.054-0.037}{0.037} \cdot 100\% = 45.9\%$. The RA-values increase up to $\frac{3-2.06}{2.06} \cdot 100\% = 45.6\%$. The other peak values change also, but not this much. This indicates that the vehicle unit slip angles of the dolly and 2nd semi-trailer units increase when the drawbar of the dolly unit is shorter and the articulation point is further away from the rear axles of the vehicle unit in front. The slip angles of the vehicle units in the front don't change noticeably between the different dolly settings.

The slip angles of the tractor and 1st semi-trailer units are generally between 1° and 2°, which is moderate at this forward velocity and the tires are functioning in the linear region. The slip angles of the dolly and 2nd semi-trailer units of the minimum and default settings are between 2° and 3° and some of the slip angles exceed the limit of 2.5°, which was considered as the limit, where the nonlinear region of the tire lateral force is close on slippery circumstances. In the maximum setting the slip angle values of the dolly and 2nd semi-trailer units are generally under 2°, which indicates that the combination in this setting is more stable than in the two other settings and the tires are probably functioning in the linear region. The larger slip angles of 3° are the result of excess wheel and vehicle sliding in lateral direction, which was earlier indicated with the trail and yaw velocity graphs due to excess RA of the examined state variables and incapability of producing enough lateral force. The peak values and RA-values increase up to 45% from best to worst scenario, which is a clear indication of the decrease of lateral stability. An observation is done regarding the oscillations in graphs. In the default and minimum settings, the dolly and 2nd semi-trailer units first turn to the opposite direction before following the first vehicle units. Unlike in the maximum setting, the dolly and 2nd semi-trailer units follow the vehicle units in front better. This is the result of the location of the

articulation point, which affects the turning radius, swept-path, off-tracking and out swing and the following motion directly. The shape of the curves in all the simulations are calm, but the amount of large oscillation is present particularly in the minimum setting. The vehicle unit slip angles indicate that the dolly and 2nd semi-trailer units follow the front vehicle units better and behave more stable when the articulation point is close to the rear axles of the vehicle unit in front and when the dolly drawbar is longer.

The sensitivity analysis of the dolly drawbar parameter in double lane change indicate that all the vehicle combinations experience unstable behavior at some level and they would be difficult to control for the driver. Moreover, the dolly drawbar length and articulation point play a focal role regarding the stability of the dolly and 2nd semi-trailer units and moreover, of the entire vehicle combination. With shorter dolly drawbar, articulated far away from the rear axles of the vehicle unit in front, the system experiences more unstable behavior. This is due to the long lever between the articulation point and the rear axles of the vehicle unit in front, which amplifies the RAs more. However, all the vehicle combination systems are mathematically stable, as they return back to the lane in the end and the vehicle units are recovered. On the other hand, as the excess RAs of the examined state variables and extra lateral displacements of the dolly and 2nd semi-trailer units show that the vehicle may be uncontrollable by the driver. These excess RAs of yaw velocities, lateral accelerations and vehicle unit slip angles may lead into a vehicle spin or roll-over, particularly on the low road friction circumstances.

The longer dolly drawbar and the closer location of an articulation point to the rear axles of the vehicle unit in front have some negative influences. A longer dolly drawbar could cost more to produce. If the drawbar is longer and the articulation point stays unchanged, the total length of the vehicle combination increase, which even more increases the delays and uncontrollability. With a longer drawbar the dolly and especially the 2nd semi-trailer units tend to be driven to the outer lane, wrong lane or out of the roadway easier, because of the increase in off-tracking, swept-path and outswing. The closer articulation point location could require some extra work and costs to be modified and it significantly affects the turning radius and capability of moving in the infrastructure via increased off-tracking, swept-path and possible out swing.

An articulation point closer to the rear axles of the vehicle unit in front, affects the dolly and 2nd semi-trailer units to turn earlier and they can be easily driven into inner lane, wrong lane or out of the lane. For example a traffic circle, traffic light turns and sharper turns would be difficult to maneuver for the vehicle combination and they could cause serious accidents or dangerous situations in the traffic. However, these kinds of situations and maneuvers are usually driven with low vehicle speeds. On the other hand, if the control and stability of the vehicle combination is lost in regular driving with higher vehicle forward velocities due to bad vehicle structure designing, it will cause more serious accidents and dangerous situations than the possible low vehicle velocity accidents in traffic circles and traffic light turns. These HCT combinations are driven in special routes and for special purposes, so the route could be planned that it excludes all the possible problematic traffic circles and turns. On the other hand, if these HCT combinations are wanted to be approved by the law for commercial use and not just with derogations of law restrictions, it would then require modifications to the infrastructure in any case. Particularly, if more possible routes were needed to be able to be driven. A compromise between the infrastructural planning and vehicle combination planning should be obtained. It should be able to be driven through most of the regular traffic

situations without creating dangerous situations, but on the other hand it should be able to perform maneuvers with higher vehicle velocities without losing its stability and creating even more dangerous situations.

The dolly vehicle unit phase portraits for different dolly drawbar settings are presented in figures 46-48.

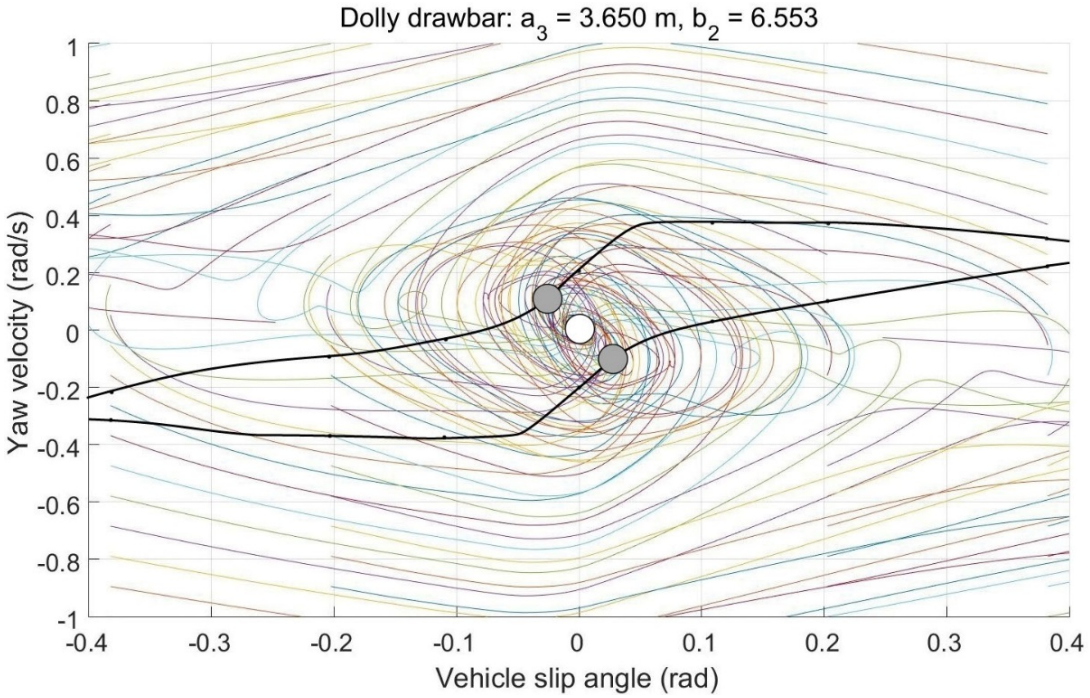

Figure 46. Dolly phase portrait with default dolly drawbar setting simulated with a forward velocity of 80km/h

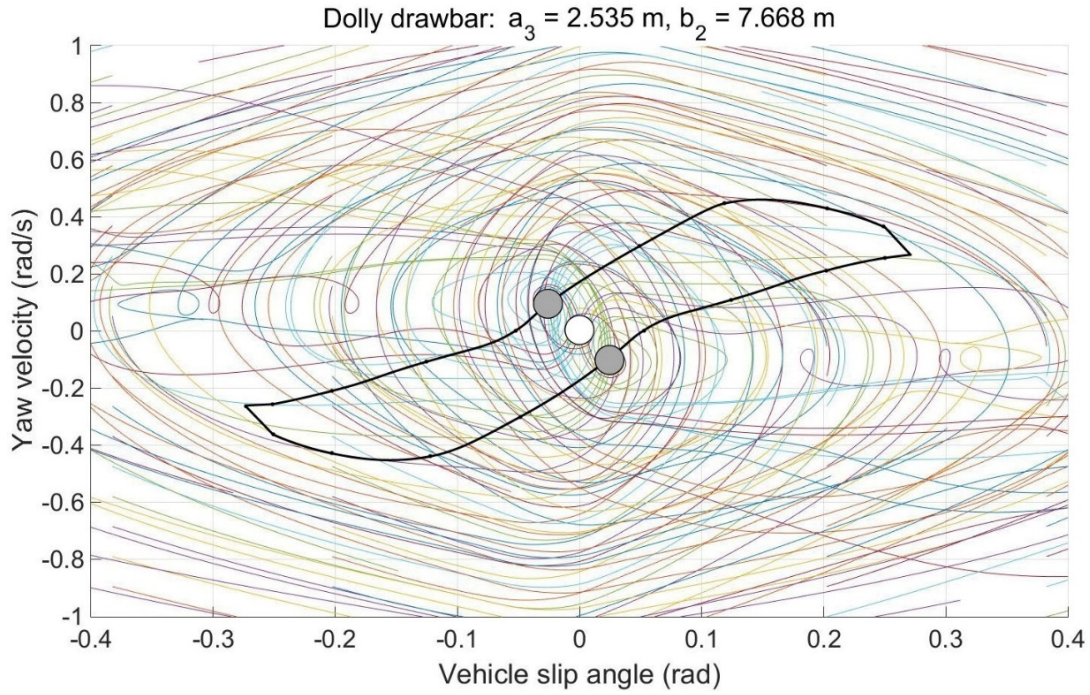

Figure 47. Dolly phase portrait with minimum dolly drawbar setting simulated with a forward velocity of 80km/h

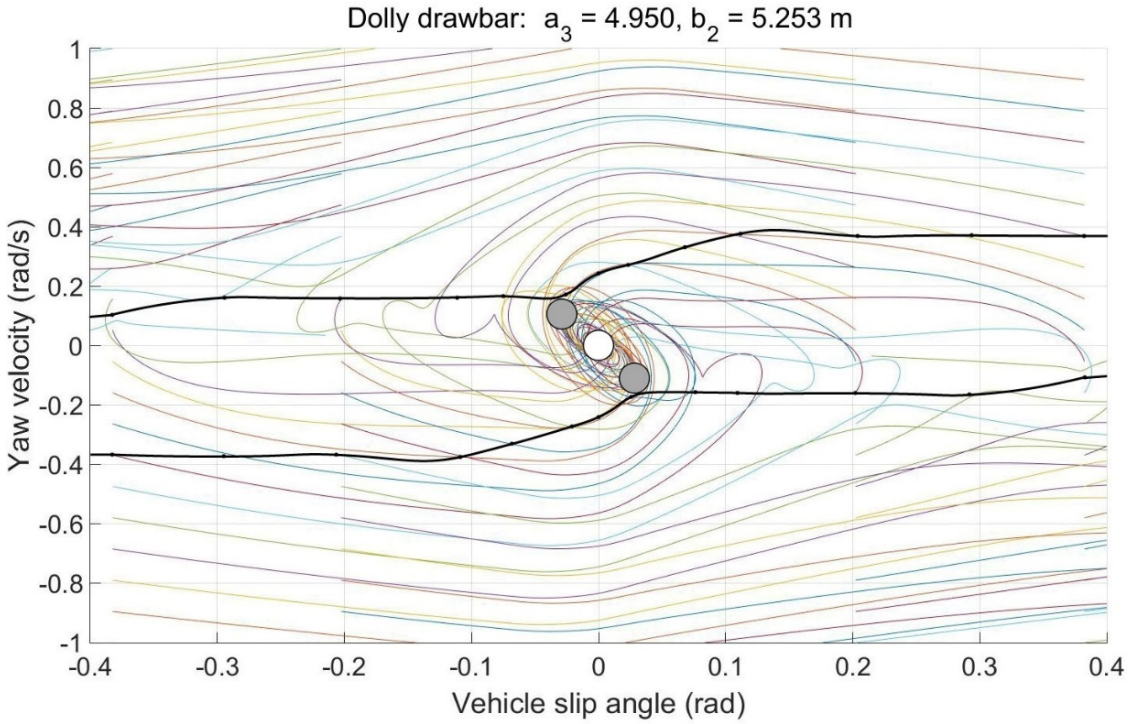

Figure 48. Dolly phase portrait with maximum dolly drawbar setting simulated with a forward velocity of 80km/h

The dolly phase portraits between the different dolly settings are very different. The size of the stable area experiences visible changes between the settings. Additionally, the shape of the curves and the amount of oscillation change certainly between the settings. The maximum dolly setting has the largest stable area and the minimum dolly setting has the smallest area. The stable area of the minimum dolly setting is limited to $\pm 0.275\ rad$ and $\pm 0.45 \frac{rad}{s}$. The stable area of the maximum dolly setting is not limited to certain vehicle slip angles, the area continues relatively long and it allows large slip angle values. However, the stable area is limited to $\pm 0.4 \frac{rad}{s}$. The default dolly setting area is limited to $\pm 0.425\ rad$ and $\pm 0.35 \frac{rad}{s}$. Although, the MF parameters were only valid up to slip angle values of ± 0.4 radians.

The curves in the default setting have some oscillation towards the stable focus, specifically they first go away from the origin and then they turn towards it. The minimum dolly setting has high amount of oscillation around the center area and the curves go further away from the origin compared to the two other settings before turning towards it. The maximum dolly setting curves don't turn away from the origin first and they oscillate only very little in the center area. This results in a much faster recovery time for the maximum dolly setting. The stable focus points locate in the origin in all the settings. The unstable saddle points seem to stay unchangeable, and they locate at (-0.028, 0.1) and (0.028, -0.1) in every setting. The stable area of the maximum dolly setting allows arguably more different signed yaw velocity and vehicle slip angle values than the two other settings. The minimum dolly setting and default setting stable areas disallow different signed yaw velocity and vehicle slip angle, only close to the center area there are very small areas for different signed yaw velocity and vehicle slip angle values.

It is clear that the maximum dolly setting results in the largest stable area. When a vehicle unit is more stable, this usually promotes the overall stability of the entire vehicle combination. However, the cross-influences of different parameters are not under examination. This indicates that the maximum dolly setting is the most stable setting for the dolly vehicle unit and furthermore, for the vehicle combination. Particularly for the 2nd semi-trailer, which receives high RA-values of different examined state variables based on the behavior of the dolly vehicle unit. The amount of excess oscillation in the default and minimum settings indicate that the dolly vehicle unit is sliding excessively at some level and this cannot be considered as stable behavior, or at least it is uncontrollable by the driver, which could lead into the loss of control of the 2nd semi-trailer and furthermore of the entire vehicle combination. In the maximum dolly setting the oscillation is certainly calmer, which indicates lesser amount of excessive sliding and uncontrollability. This could result in a more stable and controllable vehicle combination, particularly in a more stable 2nd semi-trailer. The observation that the maximum dolly setting allows quite large stable area of different signed yaw velocity and vehicle slip angle indicates that the dolly vehicle unit and furthermore the vehicle combination in this setting has better recovery capability and becomes stable and controllable even from very difficult states. Whereas the default and minimum settings can't allow these difficult different signed states to be stable, controllable and recovered in a reasonable time. The dolly phase plane analysis in this parameter sensitivity analysis indicates that the dolly vehicle unit becomes clearly more stable with longer drawbar attached closer to the rear axles of the vehicle unit in front. This can furthermore promote the overall stability of the entire vehicle combination.

The double lane change simulation and phase plane analysis can be connected. They both support the same findings of more stable dolly vehicle unit and vehicle combination behavior with longer drawbar attached closer to the rear axles of the vehicle unit in front. The double lane change maneuver also shows and supports the implication from phase plane analysis that the entire vehicle combination becomes more stable in this kind of dolly setting. The RA-values and peak values of the different examined state variables decrease in the dolly and 2nd semi-trailer units with longer dolly drawbar and closer articulation point to the rear axles of the vehicle unit in front. In addition, the stable area of the dolly vehicle unit in the phase portrait increase both in yaw velocity and vehicle slip angle with the maximum dolly drawbar setting. The excess sliding of wheels and vehicle units in lateral direction and oscillation decrease in both the double lane change maneuver and in the dolly phase portraits. Moreover, the dolly vehicle unit allows more difficult plane states to be stable and more controllable, which may lead to overall more stable and controllable behavior of the vehicle combination. The vehicle combination and dolly vehicle unit experience noticeably more stable behavior and are controllable with the maximum dolly drawbar setting.

5.4 Error analysis of the simulations

A quantitative error analysis is difficult to perform for the nonlinear simulation model. However, some relevant qualitative points regarding the possible errors and inaccuracy of the results is presented and discussed.

The MATLAB numeric integration informed warnings about inaccurate simulation loop results as in the form of simulation tolerances in few single simulations. Although, the inaccuracy of the tolerances are only approximately 10^{-7}. This is an indication of simulation inaccuracy and some of the results are slightly inaccurate.

The second notion is that the time domain approach of RA calculations doesn't contain the phase information, and it had to be considered separately. The use of the frequency response functions in the calculation of RA-values would have given different and possibly more suitable results due to the long time and motion delays in the vehicle combination. The use of time domain approach indicates some inaccuracy of the results, however, the general trend of the results between the sensitivity analysis parameter settings would have been the same. Only the RA-values would have changed but their relative value compared to others should have stayed the same.

The third possible error in the simulation model is that it doesn't take into account the active roll-over prevention system and its functioning. On the other hand, the simulations were performed mostly on the rough ice road surface and all the lateral acceleration values stayed under the dangerously considered roll-over limits in all the simulations. This indicates that the roll-over prevention system probably would not have been functioning in those situations, because the vehicle units and the vehicle combination would have probably span before rolling over. The roll-over prevention system doesn't control the pitch and yaw motions at all. Only the roll-over motions regarding certain lateral acceleration values is being controlled, so it is of no use in controlling the spinning motions. The dry asphalt simulations also stayed under the roll-over limits, so the relevance of this system in the sensitivity analysis is low. Although, it is possible that the lack of roll-over prevention system created some inaccuracy to the results.

The fourth possible error in the simulation is the lack of proper vehicle body and suspension stiffness factors. These stiffnesses have great influence on the wheel load transfers as well as the roll-over events. However, as the simulation results indicated, the vehicle combination is far away from the roll-over limits, because of the slippery circumstances and tendency to spin before rolling over. The amount of wheel load transfers with low lateral acceleration values is also low, so the influence is marginal whether the wheel load transfers consider the body and suspension stiffnesses or not. Additionally, HVCs are relatively stiff compared to other vehicle types (Sampson & Cebon 2005; Tabatabaei Oreh et al. 2014). These stiffness factors are considered not to have great influence on the results of simulations on low road friction surfaces. Although, the lack of stiffness factors has some influence on the accuracy of the results, but the inaccuracy should only be related marginally to the values and not to the prevalent phenomena at all with these lateral acceleration values.

If the results of this thesis are compared to similar results, similarities can be found. P. Rahkola simulated few simulations in his research study on low road friction surface with a two articulated HVC (Rahkola 2006). Additionally, in the University of Oulu some simulations with a different HCT combination have been performed with ADAMS simulation program (Venäläinen & Korpilahti 2015). M. Lehessaari simulated comparable double lane change simulations with ADAMS simulation program (Lehessaari 2007). The results of this thesis show clear similarity in the RA-values and peak values of the examined state variables and general phenomena in a double lane change maneuver compared to these three research studies. This furthermore supports the results, implications and conclusions of this thesis. Additionally, the parameters and

results of the Double-B HCT combination used in the different MATLAB simulations by Volvo Sweden are comparable and indicate that the vehicle structural parameters and results of this thesis are valid (Raatikainen 2015).

After all, the simulation model is sufficiently accurate and gives very decent results for the analysis of lateral dynamic behavior of the HCT vehicle combination in an open loop examination.

6 Conclusions

Based on the theory and existing studies of the lateral dynamics of HVCs, analytical simulation model, simulation results, discussion and the error analysis the following conclusions are drawn.

Any kind of Double-A vehicle combination setting is clearly more unstable on slippery road conditions than on dry road conditions. All the Double-A combinations with different semi-trailer and dolly settings experience more RAs of the examined state variables. The examined state variables of the latter dolly and 2nd semi-trailer units in an open-loop double lane change maneuver exceed the limits that are considered dangerous and unstable. The stable area in dolly vehicle unit phase portrait decreases significantly in slippery road conditions, which indicates that the dolly and 2nd semi-trailer units and furthermore the vehicle combination loses its stability and controllability easier. It is difficult to justify that if the vehicle combination is suitable with any kind of settings to be driven on slippery road circumstances at all. The possibility of traffic accidents due to loss of control and vehicle stability in regular maneuvers with higher vehicle velocities would have disastrous consequences, which could be both human casualties and commercial losses.

The 1st sensitivity analysis parameter, the semi-trailer rear axle wheel setting indicates following conclusions:

- Twin wheels on a semi-trailer axle improve the stability and controllability of the semi-trailer vehicle unit in slippery road conditions, because the individual wheel load is lower (figures 5, 8, 9, 15, 26, 27)
    - The RAs and peak values of the examined state variables in the dolly and 2nd semi-trailer units decrease in a double lane change maneuver
    - The excess vehicle sliding of the dolly and 2nd semi-trailer units in lateral direction and oscillation of vehicle units is decreased in a double lane change maneuver
    - The dolly vehicle unit phase portrait stable area experience only marginal differences, however, a trend is that the stable area is increased
- The stability and controllability of the entire vehicle combination is increased with twin wheels on semi-trailers
- The fuel and rim consumption, as well as the resistive forces might increase, which could increase the vehicle combination costs

The 2nd sensitivity analysis parameter, the dolly drawbar length and the location of the articulation point in front indicate following conclusions:

- A longer dolly drawbar with an articulation point located closer to the rear axles of the vehicle unit in front increase the stability of the dolly vehicle unit significantly (list on pages 35 to 36)
    - The RAs and peak values of the examined state variables in the dolly and 2nd semi-trailer units decrease significantly in a double lane change maneuver
    - The excessive vehicle unit sliding in lateral direction and oscillation of vehicle units is decreased, particularly in the dolly and 2nd semi-trailer units in a double lane change maneuver

    - The phase plane stability of the dolly vehicle unit is increased significantly, and it allows more difficult states to be stable
        - Decreases RAs and instability of the 2nd semi-trailer significantly, which leads to a more controllable vehicle combination
- The stability and controllability of the entire Double-A combination is increased with a longer dolly drawbar and articulation point located closer to the rear axles of the vehicle unit in front
- The turn radius and sharp turns and low speed maneuvers become slightly more problematic, because the swept-path, possible outswing and off-tracking are increased. The vehicle costs might increase with a longer drawbar and articulation point located closer to the rear axles of the vehicle unit in front

Similar results and findings appear in the many other studies of lateral dynamics of HVCs and HCT combinations as was indicated in the error analysis of this thesis. It was indicated in the chapter of 2.3 articulated vehicle dynamics that the dolly drawbar length, articulation locations and number of wheels affect significantly the lateral stability of the vehicle combination. These other studies and similar findings support the findings of this research study and vice versa. Although, the research methods and simulation models differ significantly between this study and the other studies, they have much in common regarding the theory, results, parameters and furthermore findings.

The analytical model doesn't take into account the driver model or active safety systems, however, it gives evidence of the handling behavior of the Double-A vehicle combination on slippery road conditions. The error analysis indicates that the nonlinear simulation model is sufficiently accurate and the results can be qualified. The Double-A combination should be driven with twin wheels on all non-steering axles and with a longer dolly unit drawbar attached as close as possible to the rear axles of the semi-trailer unit in front. These modifications improve the stable behavior and increase the stability and overall controllability of the vehicle combination, particularly in slippery road conditions with higher vehicle velocities. Although, it is difficult to justify that if the vehicle combination is suitable and stable enough to be driven in slippery road conditions at all. The use of an active safety system regarding the yaw and pitch motions would be of great benefit for the vehicle combination. The disadvantages of these improvements would be that the vehicle costs and fuel and rim consumptions may increase. In addition, the low speed maneuvers and sharp turns such as traffic lights and traffic circles become more problematic, because of the increased outswing, off-tracking and swept-path.

For further research the phase plane analysis of other vehicle units are suggested and more possible sensitivity analysis parameters to be tested. The influence of the roll-over prevention system to the lateral dynamic behavior should be examined. Additionally, a driver model and closed-loop simulations would be of great interest to furthermore justify the drivability of the Double-A combination and the permission to drive in the public traffic in slippery circumstances.

Bibliography

Aurell, J. & Edlund, S., 1989. The Influence of Steered Axles on the Dynamic Stability of Heavy Vehicles. In *Truck and Bus Meeting and Exposition*. Charlotte, North Carolina: SAE, pp. 1–18.

Bosch, 2011. *Automotive Handbook* 8th ed., Robert Bosch GmbH.

Bosch, 2004. *Automotive Handbook* 6th ed., Robert Bosch GmbH.

Bucko, A., Germanchev, A. & Arredondo, J., 2013. Modular AB-triples: Australia's next generation of very high productivity freight vehicles. In *Heavy Vehicle Transport Technology*. p. 10.

Christidis, P. & Leduc, G., 2009. Longer and Heavier Vehicles for freight transport. *Institute for Prospective Technology Studies (IPTS), Joined Research Centre (JCR), European Commission. Seville*. Available at: http://ec.europa.eu/transport/road/events/doc/2009_06_24/2009_jrc52005.pdf.

Dukkipati, R. et al., 2008. *Road Vehicle Dynamics*, SAE International.

European Commision, 2012. *Commission clarifies existing rules on cross-border use of longer trucks, Directive 96/53*, Available at: http://europa.eu/rapid/press-release_IP-12-611_en.htm.

Fancher, P., 1989. Directional Dynamics Considerations for Multi-Articulated, Multi-axled Heavy Vehicles. In *Truck and Bus Meeting and Exposition*. Charlotte, North Carolina: SAE, pp. 19–30.

Fancher, P., 1985. The Static Stability of Articulatd Commercial Vehicles. *Vehicle System Dynamics: International Journal of Vehicle Mechanics and mobility*, 14(Issues 4-6), pp.201–227.

Fancher, P. et al., 1998. Using Braking To Control the Lateral Motions of Full Trailers. *Vehicle System Dynamics: International Journal of Vehicle Mechanics and Mobility*, Vol. 29(Issue 1), pp.462–478.

Fancher, P.S. & Mathew, A., 1987. *A vehicle dynamics handbook for single-unit and articulated heavy trucks*, The University of Michigan Transportation Research Institute.

Genta, G., 1997. *Motor Vehicle Dynamics*, World Scientific Publishing Co. Pte. Ltd.

Giangiulio, E. (VTI), 2005a. *HGV High Friction VTI, MF-Tyre fitting report, Volvo Vertec Project*,

Giangiulio, E. (VTI), 2005b. *HGV Rough & Smooth Ice VTI, MF-Tyre fitting report, Volvo Vertec Project*,

Gillespie, T.D., 1992. *Fundamentals of Vehicle Dynamics*, Society of Automotive Engineerings, Inc.

Göhring, E., von Galsner, E.C. & Bremer, C., 1989. The Impact of Different ABS-Philosophies on the Directional Behavior of Commercial Vehicles. In *Truck and Bus Meeting and Exposition*. Charlotte, North Carolina: SAE, pp. 31–42.

Hac, A., Fulk, D. & Chen, H., 2008. *Stability and Control Considerations of Vehicle-Trailer Combination*, Detroit, Michigan.

Inagaki, S., Kshiro, I. & Yamamoto, M., 1994. Analysis of vehicle stability in critical cornering using phase-plane method. In *International Symposium on Advanced Vehicle Control*. Tokyo, Japan: SAE International, pp. 287–292.

Islam, M., 2013. *Parallel Design Optimization of Multi-Trailer Articulated Heavy Vehicles with Active Safety Systems Md . Manjurul Islam*. University of Ontario Institute of Technology.

Kamnik, R., Boettiger, F. & Hunt, K., 2003a. Roll dynamics and lateral load transfer estimation in articulated heavy freight vehicles. *Journal of Automobile Engineering*, 217(11), pp.985–998. Available at: http://eprints.gla.ac.uk/15156/.

Kamnik, R., Boettiger, F. & Hunt, K., 2003b. *Roll dynamics and lateral load transfer estimation in articulated heavy freight vehicles*, Ljubljana, Slovenia. Available at: http://eprints.gla.ac.uk/15156/.

Karlsson, R. et al., 2015. Performance based standards for high capacity transports in Sweden FIFFI project 2013-03881 - Report 1, Review of existing regulations and literature. , p.76.

Kati, M.S. et al., 2013. Performance improvement for A-double combination by introducing a smart dolly. In *Heavy Vehicle Transport Technology*. p. 10.

Lehessaari, M., 2007. *Development stability of vehicle combinations based on the modular cnocept by tires*. Helsinki University of Technology.

Luijten, M.F.J. et al., 2012. Analysis of the lateral dynamic behaviour of articulated commercial vehicles. *Vehicle System Dynamics: International Journal of Vehicle Mechanics and Mobility*, Vol. 50(Issue 1), pp.169–189.

Luijten, M.F.J., 2010. *Lateral Dynamic Behaviour of Articulated Commercial Vehicles*. Eindhoven University of Technology.

Milliken, W.F. & Milliken, D.L., 1995. *Race car Vehicle Dynamics*, SAE International.

Nordström, O. (VTI), 1989. Heavy Duty Vehicle Dynamics Related to Braking, Steering and Tires. In *Truck and Bus Meeting and Exposition*. Charlotte, North Carolina: SAE, pp. 43–58.

Otto Lahti (Trafi), 2015. Volvo DUO2. [E-mail] message to Jere Lehtinen.

Pacejka, H.B., 2006. *Tyre and Vehicle Dynamics* 2nd ed., Oxford: Elsevier Ltd.

Pauwelussen, J., 2015. *Essentials of Vehicle Dynamics*, Oxford: Elsevier Ltd.

Raatikainen, J.-M. (juha-matti. raatikainen@volvo. com., 2015. HCT Thesis in Finland. [E-mail] message to Jere Lehtinen.

Rahkola, P., 2006. *Raskaan ajoneuvoyhdistelmän ajodynamiikka*. University of Oulu.

Sampson, D.J.M. & Cebon, D., 2005. Achievable roll stability of heavy road vehicles. *Journal of Automobile Engineering*, 217(4), pp.269–287.

Sandin, J. & Nilsson, P., 2013. Drivers' assessment of driving a 32 meter a-double with and without full automation in a moving base simulator. In *Heavy Vehicle Transport Technology*. p. 10.

Shen, S. et al., 2007. Nonlinear dynamics and stability analysis of vehicle plane motions. *Vehicle System Dynamics*, 45(1), pp.15–35.

Smakman, H., 2000. *Functional Integration of Slip Control with Active Suspension for Improved Lateral Vehicle Dynamics*, Munich: Herbert Utz Verlag GmbH.

Tabatabaei Oreh, S.H., Kazemi, R. & Azadi, S., 2014. A sliding-mode controller for directional control of articulated heavy vehicles. *Journal of Automobile Engineering*, 228(3), pp.245–262.

Torkkeli, M. (Liikennevirasto) & Lindström, J. (Keslog oy), 2015. HCT-Foorumi.

Trafi, 2015. HCT-rekat. Available at: http://www.trafi.fi/tieliikenne/luvat_ja_hyvaksynnat/hct-rekat [Accessed June 16, 2015].

Tuononen, A. & Koisaari, T., 2014. *Ajoneuvojen dynamiikka*, Espoo: Autoalan Koulutuskeskus.

United Nations (UNECE), 2008. *Uniform Provisions Concerning Approval of Vehicle of Categories M, N and O with Regard to Braking. ECE-R13*, Available at: http://www.unece.org/fileadmin/DAM/trans/main/wp29/wp29regs/r013r6a1e.pdf.

Welsh, K., Driscoll, O. & Hassall, K., 2013. What are the safety benefits of Australian high productivity vehicles when compared to the conventional heavy vehicle fleet? In *Heavy Vehicle Transport Technology*. p. 12.

Venäläinen, P. & Korpilahti, A., 2015. *HCT-ajoneuvoyhdistelmien vaikutus puutavarakuljetusten tehostamisessa*, Ministry of employment and the economy.

Wong, J.Y., 2001. *Theory of ground Vehicles* 3rd ed., New York: John Wiley & Sons, Inc.

Appendix A1: Magic Formula coefficients in rough ice road simulation
(Giangiulio 2005b)

[COEFFICIENT]	[FHN]	[THN]	[STN]	[DESCRIPTION]
PCY1	1.3895	1.5097	1.4564	$Shape factor Cfy for lateral forces
PDY1	0.28167	0.023265	0.24716	$Lateral friction Muy
PDY2	-0.057945	-0.059437	-0.071813	$Variation of friction Muy with load
PDY3	0	0	0	$Variation of friction Muy with squared camber
PEY1	-53.923	-54.1378	-44.1601	$Lateral curvature Efy at Fznom
PEY2	-5.0893	-28.3816	-25.1564	$Variation of curvature Efy with load
PEY3	0	0	0	$Zero order camber dependency of curvature Efy
PEY4	0	0	0	$Variation of curvature Efy with camber
PKY1	-4.0742	-3.519	-4.1692	$Maximum value of stiffness Kfy/Fznom
PKY2	1.706	1.3181	1.6175	$Load at which Kfy reaches maximum value
PKY3	0	0	0	$Variation of Kfy/Fznom with camber
PHY1	-0.0055616	-0.005591	-0.0065636	$Horizontal shift Shy at Fznom
PHY2	-0.0017721	-0.0022331	-0.0039954	$Variation of shift Shy with load
PHY3	0	0	0	$Variation of shift Shy with camber
PVY1	0	0	0	$Vertical shift in Svy/Fz at Fznom
PVY2	0	0	0	$Variation of shift Svy/Fz with load
PVY3	0	0	0	$Variation of shift Svy/Fz with camber
PVY4	0	0	0	$Variation of shift Svy/Fz with camber and load
RBY1	20.8885	10.0715	23.0432	$Slope factor for combined Fy reduction
RBY2	33.0521	18.017	23.2384	$Variation of slope Fy reduction with alpha
RBY3	0.090705	0.071229	0.088651	$Shift term for alpha in slope Fy reduction
RCY1	0.97206	1.0083	1.0345	$Shape factor for combined Fy reduction
REY1	0.59571	0.10348	0.73634	$Curvature factor of combined Fy
REY2	0.15224	0.24308	0.031968	$Curvature factor of combined Fy with load
RHY1	0	0	0	$Shift factor for combined Fy reduction
RHY2	0	0	0	$Shift factor for combined Fy reduction with load
RVY1	0	0	0	$Kappa induced side force Svyk/Muy*Fz at Fznom
RVY2	0	0	0	$Variation of Svyk/Muy*Fz with load
RVY3	0	0	0	$Variation of Svyk/Muy*Fz with camber
RVY4	0	0	0	$Variation of Svyk/Muy*Fz with alpha
RVY5	0	0	0	$Variation of Svyk/Muy*Fz with kappa
RVY6	0	0	0	$Variation of Svyk/Muy*Fz with atan(kappa)
PTY1	0	0	0	$Peak value of relaxation length SigAlp0/R0
PTY2	0	0	0	$Value of Fz/Fznom where SigAlp0 is extreme

Appendix A2: Magic Formula coefficients in dry asphalt road simulation (Giangiulio 2005a)

[COEFFICIENT]	[FHN]	[THN]	[STN]	[DESCRIPTION]
PCY1	1.5968	1.7722	1.5351	$Shape factor Cfy for lateral forces
PDY1	0.67266	0.66722	0.73067	$Lateral friction Muy
PDY2	-0.21588	-0.10961	-0.19216	$Variation of friction Muy with load
PDY3	0	0	0	$Variation of friction Muy with squared camber
PEY1	0.013241	-0.080508	-0.83249	$Lateral curvature Efy at Fznom
PEY2	-0.53203	-1.8385	-1.0293	$Variation of curvature Efy with load
PEY3	0	0	0	$Zero order camber dependency of curvature Efy
PEY4	0	0	0	$Variation of curvature Efy with camber
PKY1	-8.358	-8.1829	-10.1051	$Maximum value of stiffness Kfy/Fznom
PKY2	1.9297	1.7164	2.3501	$Load at which Kfy reaches maximum value
PKY3	0	0	0	$Variation of Kfy/Fznom with camber
PHY1	-0.011707	-0.012878	-0.001178	$Horizontal shift Shy at Fznom
PHY2	-0.00049819	-0.0064475	-0.0063766	$Variation of shift Shy with load
PHY3	0	0	0	$Variation of shift Shy with camber
PVY1	0	0	0	$Vertical shift in Svy/Fz at Fznom
PVY2	0	0	0	$Variation of shift Svy/Fz with load
PVY3	0	0	0	$Variation of shift Svy/Fz with camber
PVY4	0	0	0	$Variation of shift Svy/Fz with camber and load
RBY1	14.517	9.5569	6.4669	$Slope factor for combined Fy reduction
RBY2	12.7825	8.3288	15.7373	$Variation of slope Fy reduction with alpha
RBY3	-0.15387	-0.19481	0.0034935	$Shift term for alpha in slope Fy reduction
RCY1	1.1847	1.1928	1.255	$Shape factor for combined Fy reduction
REY1	0.60999	0.41204	0.75643	$Curvature factor of combined Fy
REY2	0.1024	0.083567	0.37508	$Curvature factor of combined Fy with load
RHY1	0	0	0	$Shift factor for combined Fy reduction
RHY2	0	0	0	$Shift factor for combined Fy reduction with load
RVY1	0	0	0	$Kappa induced side force Svyk/Muy*Fz at Fznom
RVY2	0	0	0	$Variation of Svyk/Muy*Fz with load
RVY3	0	0	0	$Variation of Svyk/Muy*Fz with camber
RVY4	0	0	0	$Variation of Svyk/Muy*Fz with alpha
RVY5	0	0	0	$Variation of Svyk/Muy*Fz with kappa
RVY6	0	0	0	$Variation of Svyk/Muy*Fz with atan(kappa)
PTY1	0	0	0	$Peak value of relaxation length SigAlp0/R0
PTY2	0	0	0	$Value of Fz/Fznom where SigAlp0 is extreme